Study on Chaotic Behavior of Human Photoplethysmogram by Comprehensive Nonlinear Time Series Analysis

2015.9

Agricultural and Environmental Engineering Department
United Graduated School of Agricultural Science
Tokyo University of Agriculture and Technology

Nina Vladimirovna Sviridova
(Нина Владимировна Свиридова)

Abstract

Significant effort in the area of health monitoring has been made over the last few decades. Many studies have investigated the correlation between biological signals produced by the cardiovascular system (CVS) and patient health conditions, and obtained indexes identifying various diseases or their states. The photoplethysmogram (PPG) is one of the widely used techniques in medical settings and sports equipment to measure biological signals. It is recognized that the PPG, which can be defined as the continuous recording of the light intensity scattered from a given source by the tissues and collected by a suitable photodetector, can provide valuable information about CVS performance [Allen, 2007]. However, PPG dynamics is not yet fully understood. The PPG is measured noninvasively by inexpensive and simple to use pulse oximeters, and this makes it quite useful for health monitoring applications.

This study sought to investigate the underlying dynamics of the PPG signals from healthy young human subjects. In previous studies the PPG was claimed to be driven by deterministic chaos [Tsuda, 1992, Sumida and Arimiru, 2000]; however, the methods applied for chaos detection were noise sensitive and inconclusive. Therefore, to reach a consistent conclusion it is important to employ additional nonlinear time series analysis tools that can test different features of the signal's underlying dynamics. In this thesis, a comprehensive set of nonlinear time series analysis methods, including time-delay embedding, embedding dimension, largest Lyapunov exponent, deterministic nonlinear prediction, Poincaré section, the Wayland test and the method of surrogate data were applied to the PPG time series to identify the unique characteristics of the PPG as a dynamical system. Results demonstrated that PPG dynamics is consistent with the definition of chaotic movement, and its chaotic properties showed some similarity to Rössler's single band chaos with induced dynamical noise. Additionally, it was found that deterministic nonlinear prediction, Poincaré section and the Wayland test can reveal important characteristics about the PPG signal and therefore these methods will be important tools for theoretical and applied studies on the PPG.

Despite the topological similarities between Rössler's single band chaos and the PPG, the declining trend of their short-term deterministic nonlinear prediction was considerably different, which gave rise to new questions. One of them is related to the rapid decline of

predictability performance in the very short range, although in the longer range high performance was sustained; another question is connected with the considerable fluctuations of prediction performance indexes. Therefore, particularly careful attention was paid to the short-term prediction properties of the PPG. Global (related to overall trajectory) and local (in a fixed region on the reconstructed trajectory) predictions were conducted and found to be significantly different. These findings illustrated the variation of the dynamic properties between the local and global levels. Additionally, similarities in the short-term prediction properties were found between the PPG and Duffing's forced oscillator in the chaotic regime. These results emphasized the importance of comparative investigation of the PPG; in addition it identified a new approach for local dynamics investigation that may be promising for further application studies.

Nowadays numerous advantages of wireless and wearable sensor technology have made it extremely useful and promising for various applications in the agriculture and food industries. However, there is still a shortage of techniques to deal with farm workers' health monitoring in the agricultural industry. Therefore, the last part of this study sought to investigate the effect of tractor noise on the CVS of farm workers by the PPG technique. Fourier transform and nonlinear time-series analysis methods, such as time-delay embedding and the Wayland test, were applied to the PPG signal to analyze differences in CVS performance arising upon exposure to levels of tractor noise corresponding to low, medium, and high tractor engine speeds. Results showed that the ratio of two significant component frequencies obtained by Fourier analysis and the Wayland test translation error can distinguish differences in the PPG signal that arise under noise exposure. Additionally, the translation error was less dependent on the subject than the frequency ratio, which may make it a useful index for application to real-time health monitoring of farmers.

This study demonstrated that comprehensive nonlinear time series analysis has high potential for effective and reliable PPG dynamics investigation and its application to the PPG can not only improve one's understanding of PPG dynamics, but also stimulate the development of new PPG signal based applications related to health monitoring in general and particularly in the agriculture industry.

Contents

Chapter 1. Introduction

1.1. Background and Review

1.1.1 Cardiovascular system and its signals

The cardiovascular system (CVS) and blood circulation have been subjects of numerous studies over the last decades. Although the first attempts to understand processes in the CVS were made centuries ago, the recent dramatic increase of cardiovascular diseases (CVDs) among the aged as well as young people have made investigation of the CVS and its processes more important than ever. Thus, according to statistical data published by The Heart Foundation organizations, CVDs are the leading cause of hospitalizations and death cases in Australia [National Heart Foundation of Australia], USA [The Heart Foundation of U.S.] and New Zealand [The National Heart Foundation of New Zealand]. Similar situations have been observed in many other developed countries. Although in Japan mortality from CVDs is lower than in other developed countries [Hiroyasu, 2008], it is the second most frequent cause of death [Japanese Ministry of Health, Labour and Welfare; Hiroyasu, 2008], and there is concern about a possible increase in mortality from CVDs due to changes in Japanese daily life towards a more Western lifestyle [Hiroyasu, 2008]. According to annual data published by the Japanese Ministry of Health, Labour and Welfare for the period from 2006 to 2013, the percentage of total deaths caused by CVDs was in the range from 15.5 to 16%. Besides lifestyle reasons, some of these fatal cases were caused by unbalanced work loads or work in difficult environmental conditions; thus workers in construction and agricultural field, power machinery operators, etc. regularly experience exposure to heat, noise, high vibration, etc. Occupational safety of workers whose profession involves high risks of health damage could benefit significantly from continuous health monitoring. This makes a deeper understanding of CVS processes not only necessary but also promising as it can provide one with valuable information about the CVS dynamics, which might lead to the development of effective and reliable CVS condition monitoring systems, methods for evaluation patients' recovery etc.

The development of modern equipment and various technologies that allow biological signal (BS) measurements have made BSs quite an attractive subject for studies. The combination of new measurement techniques, advanced equipment and continuously increasing computer computational power makes the process of data collection and analysis easier, faster and less expensive. These factors have contributed to the increased variety of health monitoring devices, and nowadays BS analysis based devices are an integral part of the equipment used in clinical settings [Allen, 2007; Fedotov and Akulov, 2013; Tamura et al., 2014]. Thus, heart rate variability (HRV), blood pressure (BP) and oxygen saturation monitors are routinely used in hospitals as well as in daily life.

Over the last few decades, a significant effort has been made to understand the correlation between different BSs and patient health conditions by obtaining indexes that identify diseases or their states [Borlotto et al., 2000; Elgendi, 2012; Elgendi et al., 2011; Gil et al., 2008; Hashimoto et al., 2002; Iokibe et al.., 2003; Kohjitani et al., 2015; Komatsu et al., 2003; Pilt et al., 2013; Sato et al., 2013; Shelley, 2007; Shi et al., 2009; Theiler, 1995; Tsuda, 1992; Usman et al., 2012]. Some studies have attempted to estimate occupational physical and mental burden through indexes obtained from BSs [Yamada et al., 2009; Miao et al., 2008; Thiyagarajan et al., 2013]; however only a small number of these studies have dealt specifically with BS dynamics. The development of new applications for advanced health monitoring and disease identification based on BS analysis requires an in depth understanding of the underlying dynamics.

1.1.2. Electrocardiogram and photoplethysmogram

A significant breakthrough was made in the last century in the field of bio-medical signal recording. Nowadays by using simple and relatively inexpensive equipment one can easily obtain extended and high resolution time series, as real-time monitoring systems have become widely available. Among various signals produced by the CVS that are commonly measured by modern sensors for medical applications the most widely used non-invasive signals are electrocardiogram (ECG or EKG), BP and photoplethysmogram (PPG) from which information regarding patient's health can be extracted, for example HRV, oxygen saturation, etc. Although

they are produced by the same, rather complex system, these signals can register different aspects of CVS dynamical properties.

The electrocardiogram is defined as a continuous recording of the bioelectrical activity of the heart. An ECG is a simple, noninvasive procedure. To obtain ECG electrodes need to be placed on the skin of the chest and connected to a device that measures electrical activity all over the heart. ECG is widely used for visual and counter analysis in diagnosis of heart rhythm dysfunction and HRV monitoring [Fedotov and Akulov, 2013]. A wide range of studies have been conducted on the ECG signal [Ende et al., 1998; Maniwa et al., 2004; Perc, 2005; Small et al., 2001; Shelhamer, 2007], in which along with direct visual and contour analysis, methods of nonlinear time series analysis were applied to investigate the dynamic properties of the ECG.

The PPG is another widely used technique to measure BS for medical applications. The PPG technique was established in 1937 by Alrick Hertzman who produced a 'photoelectric plethysmograph', which he described as a device that "takes advantages of the fact that the absorption of light by a transilluminated tissue varies with its blood contents". Subsequently the need for a small, reliable, low-cost and simple to use noninvasive cardiovascular assessment technique stimulated the reestablishment of photoplethysmography [Allen, 2007; Millasseau et al., 2006; Higgins and Froner, 1986].

Unlike the ECG signal, which is usually measured with bulky equipment that is not easily moved, modern PPG sensors, commonly called pulse oximeters, are very small, light and usually wireless. Although the ECG is one of the most widely and well-studied BSs, besides equipment limitations such as cost and size, it also has the disadvantage of being sensitive to the sensor placement. In contrast PPG sensors can generally be placed on almost any area of open skin, which makes them applicable for various studies and suitable for occupational health monitoring, where sensor placement has crucial importance. Additionally, the most important physiological indexes such as peak to peak intervals and heart rate obtained from the PPG and the ECG show significant correlation [Schäfer and Vagedes, 2013]. These factors, along with sensor's inexpensive cost have made the PPG quite attractive as a BS for applications in many fields. Although the PPG is widely used and it is recognized that the PPG can provide valuable

information about the CVS, the PPG signal is still not fully understood [Allen, 2007; Kamal et al., 1989]. As the PPG contains rich and valuable information about the CVS processes it is expected that understanding of PPG dynamical properties could lead to the development of new types of monitoring devices and methods for health condition estimation. Considering the above mentioned advantages of the PPG, it appears to be quite promising for investigation and was chosen as the subject of investigation in this study.

The PPG can be defined as the continuous recording of the light intensity scattered from a given source by the tissues and collected by a suitable photodetector [Bernardi and Leuzzi, 1995]. The apparatus consists of a transducer that shines infrared light onto the skin. The light is absorbed by hemoglobin, and the backscattered radiation is detected and recorded. The backscattered light will depend on the amount of hemoglobin in the skin, and the result obtained will therefore reflect the cutaneous blood flow [Wahlberg and Lindberg, 1995]. Modern PPG sensors usually utilize low cost semiconductor technology with LED and matched photodetector devices working at the near infrared (NIR) wavelengths (NIR band 0.8 to 1 μm), which allows measurement of deep-tissue blood flow [Allen, 2007; Tamura et al., 2014].

PPG detectors have two operational configurations: transmission and reflectance modes. In the transmission configuration, the tissue sample is placed between the source and detector, so light from the LED is transmitted through the tissue and detected on the opposite side from the source by the photodetector. In the reflectance mode the emitter and detector are positioned adjacent to each other [Allen, 2007; Bernardi and Leuzzi, 1995; Tamura et al., 2014]. Transmission mode PPG imposes more restrictions on the body locations available for study than the reflection mode [Allen, 2007]. However it was found that the significance of the signals obtained by the two methods is the same: in both cases it depends on the superficial circulation [Bernardi and Leuzzi, 1995].

1.1.3. Applications of the photoplethysmography

The PPG technique has been widely used in commercially available sports and medical devices measuring heart rate, oxygen saturation and blood pressure that can be directly used for

health assessment and monitoring of patients in medical settings or for exercising individuals [Allen, 2007; Han and Kim, 2012; Nakajima et al., 1996; Perez-Martin et al., 2010]. Besides these the PPG has been applied in clinical settings for detecting peripheral vascular decease, assessment of autonomic function, such as vasomotor function, thermoregulation, neurology and other cardiovascular variability assessment [Allen, 2007], and for studies of dermatological disorders and systemic disease, for skin experimental purposes [Wahlberg and Lindberg, 1995].

Nowadays the advantages of wireless and wearable sensor technology have made the PPG extremely useful and promising for applications in many fields including the agriculture and food industries [Kawakura and Shibasaki, 2014; Wang et al., 2005]. However, there is still a significant difference in the number of techniques, equipment and methods that are actually applied to farm workers' health monitoring in the agricultural industry compared with the number of medical and sports applications.

1.1.4. Analysis methodologies applied to the photoplethysmogram

As mentioned above, the various advantages of the PPG have made it the subject of many studies in different fields, and various approaches have been applied to analyze the PPG. Among them conventional methods such as contour analysis, analysis of the 1st and 2nd derivatives of the PPG, Fourier transform, and rather advanced methods of nonlinear time series analysis can be distinguished.

Contour analysis. Analysis of PPG waveform was initiated in the 1940s by A. Hertzman, who introduced first pulse oximeter [Millasseau et al., 2006] this was probably one of the first attempts to analyze the PPG.

The appearance of the pulse waveform is defined by anacrotic and catacrotic phases. The anacrotoc phase being the rising edge of the pulse, and the catacrotic phase is the falling edge of the pulse wave. The first one is primary concerned with systole and the second one with diastole and wave reflection from the periphery. A dicrotic notch is usually seen in catacrotic phase of subjects with healthy compliant arteries Fig. 1.1 [Allen, 2007; Millasseau et al., 2006].

The pulsatile component of the PPG waveform that related to the cardiac pulsation is usually called the 'AC' (alternative current) component and its fundamental frequency depends on the heart rate and typically varies around 1-1.4 Hz. This AC component is superimposed onto a large 'DC' (direct current) components that depends on the structure of the tissue and the average blood volume of both arterial and venous blood. DC component varies slowly due to the respiration, vasomotor activity, vasoconstrictor waves, thermoregulation and other slow circulatory changes [Allen, 2007; Tamura et al., 2014; Bernardi and Leuzzi, 1995].

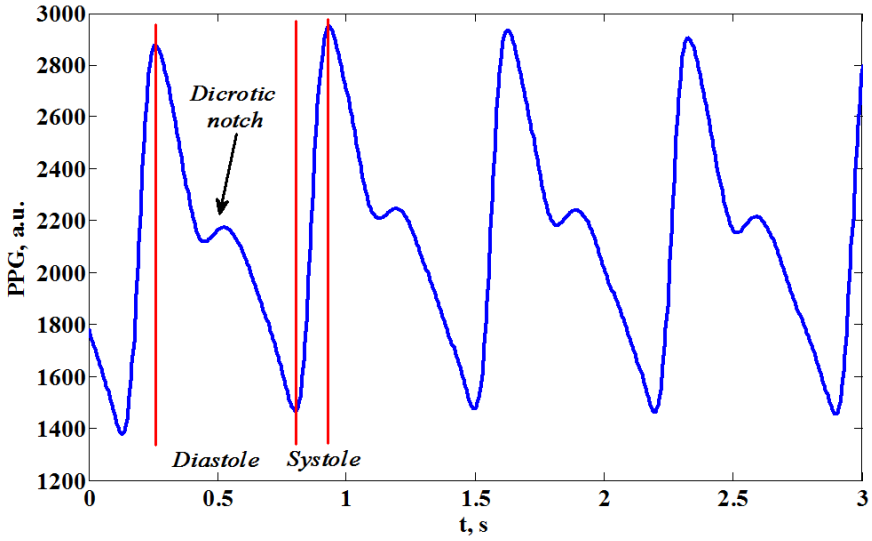

Fig. 1.1 *Components of the PPG signal waveform for healthy young subjects.*

Despite the amplitude variations from person to person and various factors that influence local perfusion, the contour or shape of the PPG remains approximately same. While it was found that a well-defined dicrotic notch is usually observed in data from healthy subjects, in atherosclerosis patients the dicrotic notch is generally missing or diminished; another study showed sensitivity of the dicrotic notch shape to alcohol and nitrates [Millasseau et al., 2006]. Various patterns of PPG contour, such as the systolic amplitude, pulse width peak to peak interval, measure of reflected wave contribution to systolic pressure, and others were used in attempts to classify results according to patient age and the presence of coronary artery diseases

[Elgendi, 2012; Millasseau et al., 2006]. Later contour analysis was expanded on the acceleration PPG (APG) data, which are obtained as the 2nd derivative of the PPG, and correlations of different indexes derived from APG shape with age, arterial distensibility in adolescence, mental stress, arteriosclerosis, arterial stiffness, and other factors were found [Bortolotto et al., 2000; Elgendi et al., 2011; Elgendi et al., 2014; Elgendi, 2014; Fujimoto and Yamaguchi, 2008; Iokibe et al., 2003; Maniwa et al., 2004].

Although contour analysis appeared to be quite useful and can provide valuable information for medical applications, it does not reveal the true dynamics of the PPG.

Nonlinear time series analysis. Development of the theory of deterministic chaos and methods of nonlinear time series analysis became an inspiration for new studies on many BSs such as ECG, HRV as well as PPG. Many studies have investigated ECG, HRV and PPG signals obtained from healthy human subjects, as well as from patients with mental or heart illnesses [Glass, 2009; Goldenberg et al., 1990; Ivanov et al., 1999; Letellier, 2013; McClintock and Stefanovska, 2002; Miao et al., 2008; Miao et al., 2012; Poon and Merrill, 1997; Phamet et al., 2013; Shelhamer, 2007]. For example, two studies [Tsuda, 1992; Sumida and Arimitu, 2000] attempted to use the geometric pattern of the PPG time-delay reconstructed trajectories for qualitative measurement of mental disease. The Lyapunov exponent (LE), which gives a measure of the rate of divergence of neighboring trajectories [Bezruchko and Smirnov, 2010], was used as measure of mental load during the performance of particular tasks, such as talking, reading or driving a car on a simulator [Sato et al., 2013]. Additionally, method of surrogate data [Sumida and Arimitu, 2000], sample entropy [Pham et al., 2013] and the trajectory parallel measure method [Fujimoto and Yamaguchi, 2008] were applied to the PPG. Although a limited number of nonlinear time series analysis methods were applied to the PPG data, the results appeared to be valuable and promising for medical health monitoring applications.

Besides applying methods of nonlinear time series analysis for obtaining practical measurements of mental and physical health conditions in early studies, the PPG, as well as the ECG and HRV, were claimed to be chaotic. These conclusions were generally drawn based on results of time-delay reconstructed trajectories, correlation dimension (CD) and LE. Later, with

further investigation of methods of nonlinear time series analysis for real world data, evidence for the chaotic nature of many BSs was questioned [Glass, 2009; Paluš, 1998; Shelhamer, 2007]. Many tools that were previously thought to provide explicit evidence of chaotic motion were discovered to be noise sensitive and could produce misleading results. In addition, these tools did not take into account all of the important properties of the PPG signal needed for positive identification of chaos. Thus it is still quite controversial whether the dynamics of these signals involve chaotic motion or not [Glass, 2009; Shelhamer, 2007]. Signals like HRV and ECG, which were believed to be driven by deterministic chaos, have been subjected to detailed reinvestigation [Glass, 2009; Shelhamer, 2007]. Similarly the PPG signal was claimed to be chaotic in the early 1990s; however, past evidence of chaos has been found to be necessary rather than sufficient, especially in biological studies [Glass, 2009; Shelhamer, 2007]. In general, positive identification of chaotic motion is not straightforward and evaluation of results obtained by methods of nonlinear time series analysis is often empirical and relies on the researcher's experience. Therefore, it is still not known whether the PPG signal is chaotic or not. In addition, many of its characteristics are not yet well studied. Therefore, to reach a consistent conclusion on the nature of the PPG dynamics, it is important to employ additional nonlinear time series analysis tools that can test different features of the signal's underlying process. Also, it is expected that extracting new information from the PPG by using an expanded nonlinear time series toolkit might lead to the discovery of new features of the PPG that would be valuable for the development of new applications.

1.2. Constructive approach

In mathematical modeling, the creation of the model as a rule is supported by experimental data representing the process for which the model is to be built. Accordingly, model validation is not possible without relevant real world data, which can confirm the appropriateness of the model or lead to further model modification. Therefore, the importance of real world data in modelling is apparent. However in studies of real-world signals, for which dynamics are under investigation and are not yet described by any model, models do not usually contribute

significantly to the study of data dynamics. One of the obvious problems in the reverse relationship (model-data) for utilizing first one for the sake of the second is that in an assumed case the dynamics of the real world data is unknown. In some specific cases researcher can assume that one or another model for a similar process may demonstrate similar behavior; however, one can hardly expect to have the same variables in the model as in the investigated signal. On the other hand, positive identification of the dynamics in the case of complex systems is not straightforward and often may cause confusion due to highly empirical interpretation of results.

To overcome above-mentioned difficulties and find a way to utilize well-known models for obtaining reliable results of the study on dynamics and chaotic behavior of the PPG, methodology called the "constructive approach" is introduced in this thesis. The constructive approach is shown schematically in Fig. 1.2.

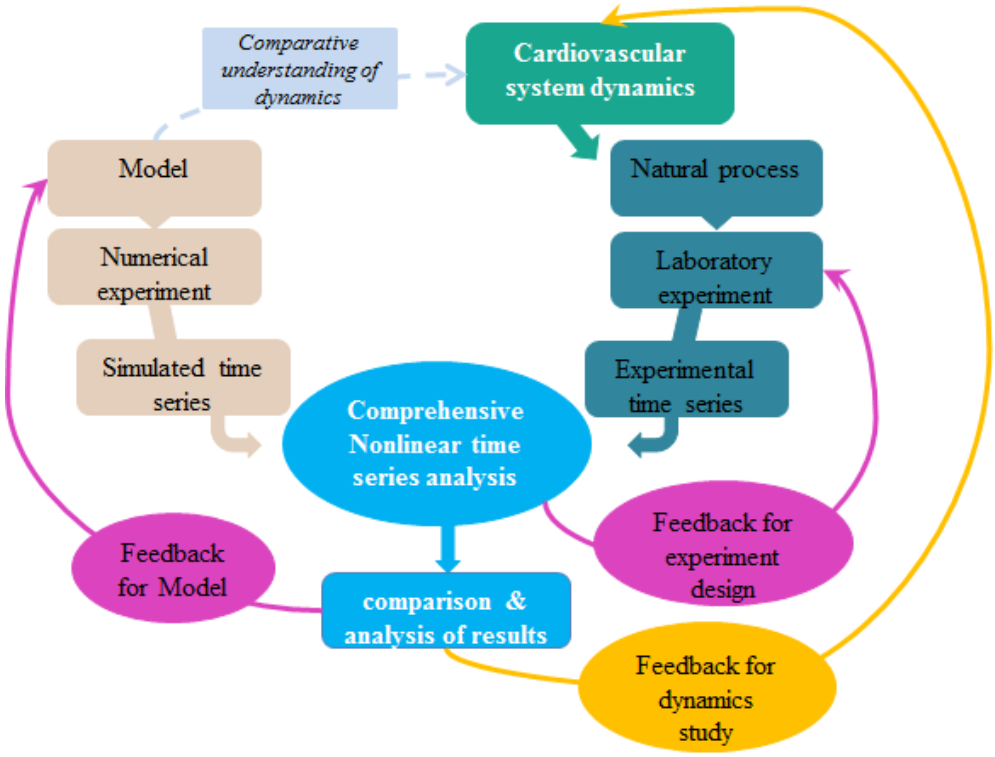

Fig. 1.2 *Constructive approach scheme.*

Since in many cases direct comparison of model output and real data is impossible, comprehensive nonlinear time series analysis, which includes an expanded toolkit, was chosen as a core of the constructive approach as seen in the Fig. 1.2. Unlike traditional approaches, nonlinear time series analysis allows not only direct comparison of signals, but comparison of the underlying signal characteristics. Based on results of nonlinear time series analysis, similarities in dynamics that define core properties can be found. Although identifying a dynamical system that has properties resembling those of PPG dynamics would not mean that the dynamics are identical, it would provide an opportunity for comparative dynamics investigation, so that features of the PPG can be evaluated on the basis of comparison with dynamics of a system that possesses similar characteristics.

In the constructive approach scheme, the use of nonlinear time series analysis serves not only as a tool for comparing data, but it can also indicate the necessity for experiment design improvement. As seen in Fig. 1.2, after conducting nonlinear time series analysis for real-world data, depending on the results the experimental design may be changed or analysis can be proceeded to the next step, to compare analysis results for simulated and real-world data. After comparison of data characteristics, according to the results one may be able to proceed to comparative study and obtaining dynamical characteristics of signal under investigation, which is the main step of the constructive approach, or if results were not comparable model can be changed to the model that may have properties more similar to those of the PPG. As seen from this scheme, the constructive approach has a recursive structure and therefore this sequence of steps can be repeated until enough information about signal dynamics can be obtained.

1.3. Objectives of the thesis

The PPG appears to be quite a useful and promising BS for various medical and daily health care applications; as well it might be promising for developing advanced applications related to occupational safety and health. However, even though nowadays it is widely used for routine health monitoring in medical and sports devices, the PPG dynamics is still not completely

understood. Therefore this study was designed to fulfill the following objectives. The main objective of this thesis is to investigate dynamics of the PPG time series as a nonlinear dynamical system by applying comprehensive nonlinear time series analysis and provide solid evidence of the PPG signal's dynamics consistence with the definition of chaotic motion as "recurrent motion in simple systems or low-dimensional behavior that has some random aspects as well as certain order" [Thompson and Stewart, 1991]. Another goal of this thesis is the detailed study of the PPG properties and determining important indexes that are obtained by methods of nonlinear time series analysis and reflecting chaotic characteristics of PPG dynamics, which can contribute to the development of PPG applications. Another goal is to demonstrate that methods of nonlinear time series analysis and indexes obtained from them can be used for occupational health monitoring. As a case study, the physiological condition of agricultural workers under exposure to noise from agricultural machinery will be investigated by conventional time series analysis methods and methods of nonlinear time series analysis.

Additionally this thesis aims to demonstrate a methodological approach of comparative and comprehensive nonlinear time series analysis in combination with a constructive approach for investigation of chaotic behavior of BSs with the PPG as an example, which can be applied for investigation of other BSs demonstrating complex behavior.

Chapter 2. Detection of Chaotic Motion in Human Photoplethysmogram

2.1. Introduction

In studies dealing with the investigation of real-world biological data, which are measured from the studied subject, the dynamical process underlying the obtained signal is usually unknown. Although the identification of dynamics is highly desired, it is rarely achieved due to the intricacy of biological processes, presence of noise, experimental design, etc.

Many studies have investigated ECG, BP, HRV and PPG signals obtained from healthy human subjects, as well as from patients with mental or heart illnesses [Ivanov et al., 1999; Mascro et al., 2001; McClintock et al., 2002; Poon et al., 1997; Pham et al., 2013; Millasseaua et al., 2006; Miao et al., 2012; Glass, 2009; Shelhamer, 2007]. In early studies, the PPG as well as ECG and HRV were claimed to be chaotic primarily based on results of time-delay reconstructed trajectories, CD and largest Lyapunov exponent (LLE). Subsequently, however, with the development of methods of nonlinear time series analysis for real world data, evidence for the chaotic nature of many BSs has been questioned [Glass, 2009; Shelhamer, 2007]. Indeed, positive identification of dynamical processes in the case of real-world signals is not straightforward. Various tools that intend to test dynamics have reliable performance in the case of model-generated data; however, noise inevitably present in the BSs can mislead tests and produce results that cannot be unambiguously interpreted. In this case, the final conclusion is often based entirely on the investigator's personal judgment and experience. Thus, many tools that were previously thought to provide explicit evidence of chaotic motion, which were applied for the analysis of the PPG, were discovered to be noise-sensitive and could produce ambiguous results. Therefore it is still quite controversial whether PPG signals' dynamics involves chaotic motion or not [Glass, 2009; Shelhamer, 2007]. Signals like HRV and ECG that were believed to be driven by deterministic chaos have been subjected to detailed reinvestigation [Glass, 2009; Shelhamer, 2007]. Similarly PPG signal was claimed to be chaotic in the early 90s [Tsuda, 1992], however nowadays past evidence of chaos was found to be necessary rather than sufficient,

especially in biological studies [Glass, 2009; Shelhamer, 2007]. Therefore it is also still not known whether the PPG signal is chaotic or not. In addition, many of its characteristics are not yet well studied.

Claims of the chaotic nature of the PPG in normal subjects were mostly based only on the application of classical methods such as time-delay reconstructed trajectories, power spectrum, correlation dimension (CD) and Lyapunov exponent (LE) and surrogation that were applied to characterize PPG time series [Pham et al., 2013; Tsuda, 1992; Sumida et al., 2000]. Positive Lyapunov exponent was believed to provide strong evidence of chaotic behavior. However, these tests (CD and LE) are inconclusive since as it was found in recent studies that they may indicate chaos even in systems that are not driven by chaos [Shelhamer, 2007; Paluš, 1998]. Therefore, a clear answer regarding the nature of the PPG signal dynamics cannot be obtained by only applying these types of classical measurements, although they may provide useful results for medical applications.

Various definitions of chaos can be found in the literature; this study abides by the following quite broad, so called "positive" definition of chaos as "recurrent motion in simple systems or low-dimensional behavior that has some random aspects as well as certain order" provided by Thompson and Stewart. It covers a wide range of systems that produce chaos and yet have significantly different properties, as for example chaotic Lorenz, Rössler, and Duffing systems. In order to test whether the PPG is consistent with this definition, a comprehensive set of nonlinear time series analysis tools is required; such a toolkit must cover all significant characteristics of chaotic motion as well as perform well with noise-contaminated data.

In this chapter a time-delay embedding method, the power spectrum, embedding dimension, largest Lyapunov exponent (LLE), deterministic nonlinear prediction's (DNP) correlation coefficient (CC) and relative route mean square error (RRMSE), Poincaré section, Wayland test translation error and the method of surrogate data were applied to investigate whether the underlying dynamics of the PPG signal involves motion on a strange attractor and to study the chaotic motion characteristics of the PPG signal. This expanded toolkit was designed to cover most of the defining characteristics of chaotic motion and is expected to help in this study to

investigate a wider range of PPG signal characteristics, compared with previous studies, and thus to extract its underlying properties. Additionally, in an effort to analyze the PPG signal not only quantitatively, but qualitatively a comparative analysis of the PPG signal and Rösser's single band chaos was conducted.

2.2. Materials and Methods

The PPG signal was recorded using a finger PPG recorder by detecting the near infrared light reflected by vascular tissue following illumination with a LED. Data were collected from ten 19- to 27-year old volunteers among Tokyo University of Agriculture and Technology (TUAT) students in a good health condition. Experimental data collection was approved by TUAT authorities. Written informed consent was obtained from participants prior the experiment. All participants were surveyed about their age, health condition and life style; at the time of the study all subjects were healthy non-smokers, physically active to similar levels, were not taking any medication, and nine of them declare no history of heart disease, while one has minor heart disorder.

For each subject five measurement repeats were done. The measured period was 5 min with 5 msec sampling steps. For all data collection sessions, a BACS (Computer Convenience, Inc.) transmission-mode PPG sensor (Fig. 2.1) was located on the right forefinger. The experiment was designed taking into account the factors affecting cutaneous blood flow as described in appendix section A.1. Every measurement was preceded by a blood pressure check and was done with the subject in a relaxed sitting position in a room with temperature, noise and vibration control. Each test subject was asked to rest for 5 min under quiet conditions in the laboratory room in the same sitting position in which the recordings were obtained, and with the test site uncovered. An example of a 30-second long portion of the obtained PPG signal is shown in Fig. 2.2. Time series of all collected data are shown in appendix Fig. A.1-2.

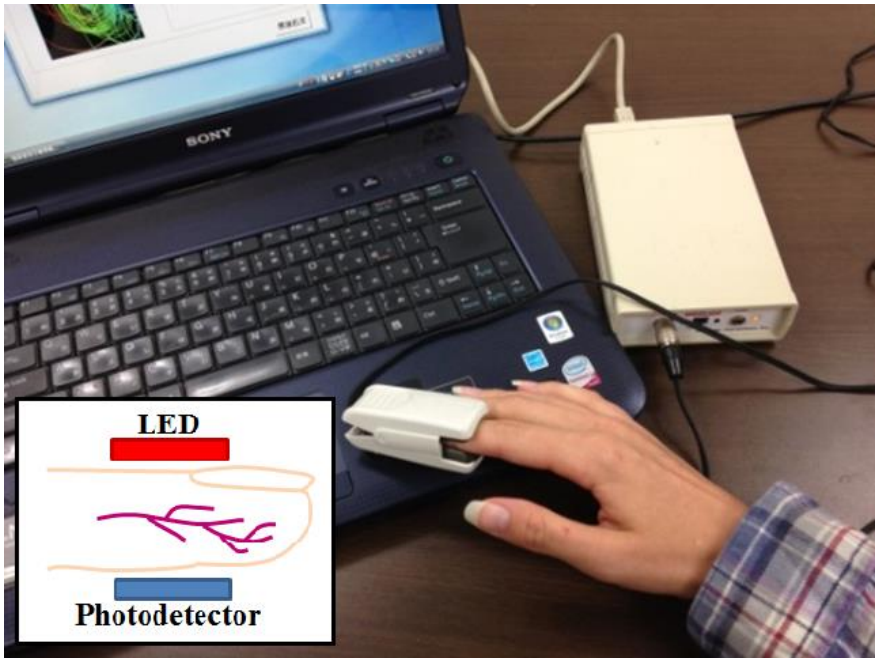

Fig. 2.1 *Finger PPG recorder.*

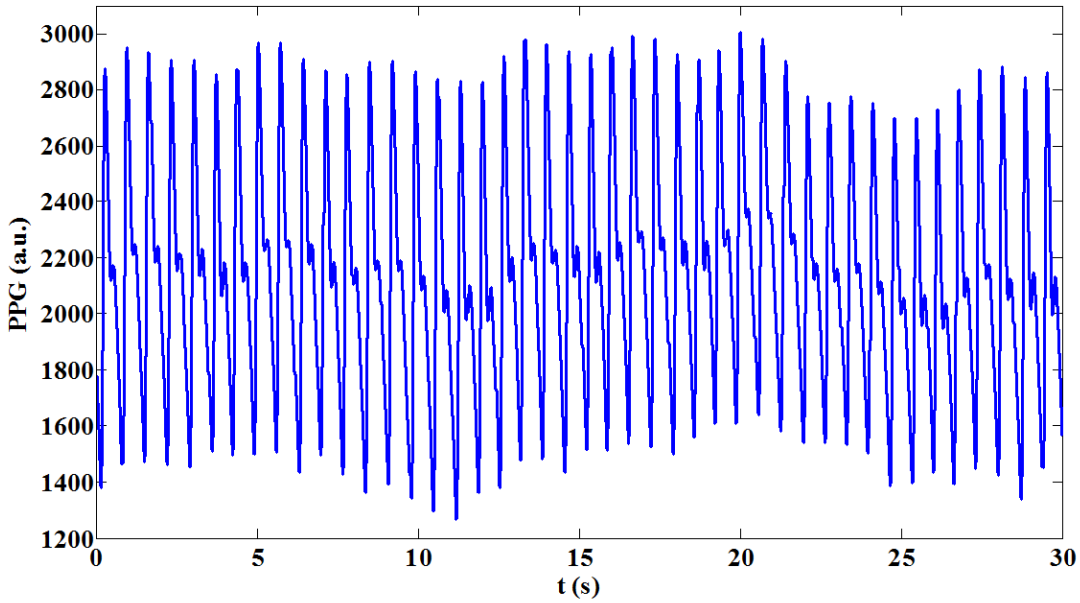

Fig. 2.2 *Example of 30-second long portion of the healthy young subject PPG signal (10th subject's 2nd measurement).*

2.3. Comprehensive Nonlinear time series analysis

To analyze data sets obtained in the experiments described in section 2.2 and to investigate whether the PPG signal is consistent with the above definition by Thompson and Stewart and study its chaotic characteristics in details, a complex of nonlinear time series analysis tools was applied. Orbital instability was tested with LLE, determinism with DNP, WTE, recurrence of motion with time-delay embedding and Poincaré section; additionally phase randomized surrogation was applied.

2.3.1. Spectral analysis

An example of typical plot of the Fourier spectrum in the studied time series after smoothing by moving average method is shown in Fig. 2.3; Fourier transform for all collected data is shown in appendix Fig. A.3-4. In Fig. 2.3, small fluctuations, which indicate environmental noise, can be distinguished around the high frequency predominant component (HF), which period is approximately equal to the heart cycle period. Lower frequency (LF) components correspond to respiration and other effects, such as thermoregulation and nervous system activity. Table 2.1 shows values of amplitude and frequency corresponding to the predominant component obtained by Fourier transform. As seen from Table 2.1, while amplitude (|FT|) demonstrates significant variations among subjects, all predominant frequencies (HF) are changing in the range 1.02-1.52 Hz, which is the range of normal heart beat frequencies.

2.3.2. Time-Delay Embedding

By using the time-delay embedding technique the possible dynamics of time series can be reconstructed in phase space. Many of the nonlinear time series analysis tools are applied on the reconstructed dynamics. The structure of reconstructed trajectories is considered to be an important characteristic of time series [Shelhamer, 2007l West, 2013]; the obtained geometric pattern of the trajectories may provide valuable information about the PPG signal properties, for example, it can reflect the level of physical or mental activity or the level of maturity [Tsuda, 1992; Sumida et al., 2000].

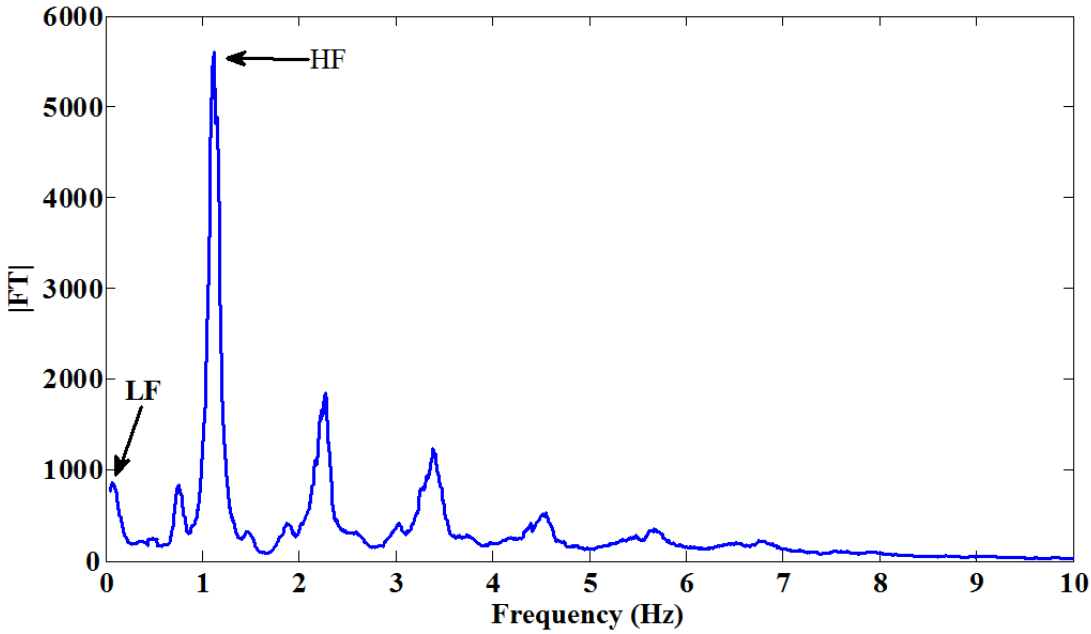

Fig. 2.3 *Example of typical spectra obtained by Fourier analysis, where LF is low frequency and HF is predominant frequency components (data correspond to the 1st measurement for the 1st subject).*

TABLE 2.1 Amplitude (|FT|) and frequency (HF) of the PPG predominant component.

Repeat	Subject									
	1		2		3		4		5	
	|FT|	HF	|FT|	HF	|FT|	HF	|FT|	HF	|FT|	HF
1	5339.0	1.20	5608.5	1.12	5057.4	1.09	4185.4	1.04	1814.5	1.02
2	1877.5	1.24	2063.1	1.21	2906.8	1.21	2276.4	1.12	1839.4	1.22
3	876	1.08	799.9	1.09	545.7	1.12	326.1	1.16	711.4	1.08
4	6198.9	1.16	6960.6	1.15	5438.9	1.11	5765.3	1.03	2947.3	1.19
5	1057.7	1.40	3475.7	1.28	2384.0	1.24	4018.1	1.29	3792.7	1.34
6	7843.4	1.07	6379.4	1.09	7048.2	1.05	4945.1	1.03	2784.6	1.05
7	4382.0	1.17	5915.2	1.19	7298.9	1.12	5763.3	1.14	4100.3	1.15
8	7085.3	1.17	6758.1	1.12	5449.0	1.15	4378.1	1.07	4711.1	1.13
9	3028.2	1.09	2557.6	1.10	2451.6	1.11	3563.0	1.12	3006.1	1.06
10	5324.7	1.52	7062.0	1.47	8937.0	1.43	5444.2	1.41	3658.1	1.39

If data points of the original time series are denoted as $X(t)$ ($t \in [1, N]$) and m is the embedding dimension, then trajectories can be reconstructed in m-dimensional phase space. Each point on the reconstructed trajectory is defined as $Z(t)=(X(t)\ X(t+\tau)\ ..\ X(t+(m-1)\tau))$, where τ defines the separation between points of the original time series. For time-delay reconstruction, the time-delay lag τ needs to be sufficiently large to ensure that the resulting individual coordinates are relatively independent; however, it should not be too large to make it completely independent statistically [Abarbanel, 1993]. In this study the time lag for further calculations have been defined as a quarter of the period of the predominant component [Packard, Crutchfield, 1980] obtained by Fourier analysis (Table 2.1).

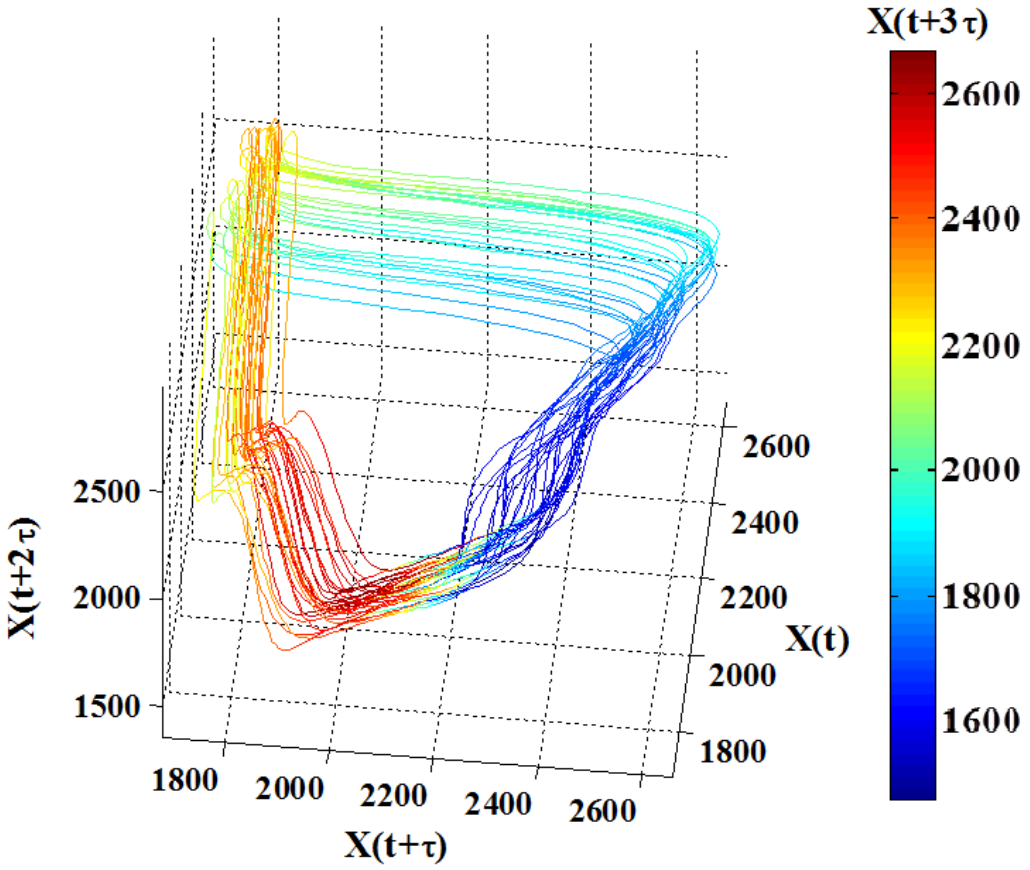

Fig. 2.4 *Trajectory reconstructed in 4-dimensional phase space by time-delay embedding.*

Following previous studies [Miao et al., 2012; Tsuda, 1992; Sumida et al., 2000] in which it was shown that at least 4 dimensions need to be used for the PPG signal and results of minimum embedding dimension calculation shown in the next section, time-delay embedding technique was performed with 4 dimensions to obtain the reconstructed trajectories in phase-space. An example (corresponding to the 1st subject's 1st measurement) of the typical data for a time-delay reconstruction is shown in Fig. 2.4, where the 4th dimension is represented by color. As seen in Fig. 2.4, the reconstructed trajectory has well-defined structure. Reconstructed trajectories for all data are shown in Fig. A.5-6. According to Fig. A.5-6, most of the data have reconstruction with clear structure, except for data corresponding to all measurements of the 3rd subject and several measurements corresponding to subjects 2 and 9, for which reconstructed trajectories do not demonstrate well-defined structure.

2.3.3 Embedding dimension

Attractor dimension has been the most intensely studied quantity for dynamical systems [Ivanov et al., 1999]. The dimension can be an indicator of the degree of "complexity" of a system [Shelhamer, 2007]. In many early studies the correlation dimension (CD) was applied in an attempt to prove that the underlying system exhibits chaotic behavior. However CD can be observed for certain types of filter noise, or random processes with power-law frequency spectra. Therefore, by itself it cannot be considered as sufficient proof of the chaotic nature of a signal, but it is an important index for nonlinear time series analysis for investigated signals. In some cases, the dimension value obtained under different stimulus conditions or health versus pathology can be useful [Shelhamer, 2007].

In this study the embedding dimension was estimated. One efficient method to determine the embedding dimension is the method of false nearest neighbors (FNN) [Kennel et al., 1992; Cao, 1997], which is based on the idea that if m is a perfect embedding dimension then any two points that are close in m-dimensional phase-space will remain close in $(m+1)$-dimensional phase-space. In this study the embedding dimension for collected PPG data was calculated by the modified method of FNN [Cao, 1997]. This method is based on calculation of the following quantity

$$E(m) = \frac{1}{N - m\tau} \sum_{i=1}^{N-m\tau} \frac{\left\| Z_i(m+1) - Z_{n(i,m)}(m+1) \right\|}{\left\| Z_i(m) - Z_{n(i,m)}(m) \right\|},$$

where $Z_i(m) = (X(i)\ X(i+\tau)\ ..\ X(i+(m-1)\tau))$ is the i^{th} reconstructed vector in m dimensional phase-space; $Z_{n(i,m)}(m)$ is the nearest neighbor of $Z_i(m)$ in the m-dimensional reconstructed phase-space [Cao, 1997]. The vector norm $\|\bullet\|$ is calculated as a Euclidian distance. The value $E(m)$ depends only on dimension m and time lag τ. To find an appropriate embedding dimension according to the suggested method [Cao, 1997], the value $E1(m)=E(m+1)/E(m)$ must be calculated. The minimum embedding dimension can be defined as $m = (m_0+1)$, where m_0 is the dimension starting from which the value $E1$ saturates.

Fig. 2.5 shows results of $E1(m)$ calculation for $m=1,..,10$. As seen in Fig. 2.5, the minimum embedding dimension can be defined as 4; therefore, in all further calculations the embedding dimension was chosen as 4. Results of $E1(m)$ calculation for all data are shown in Fig. A.7-8.

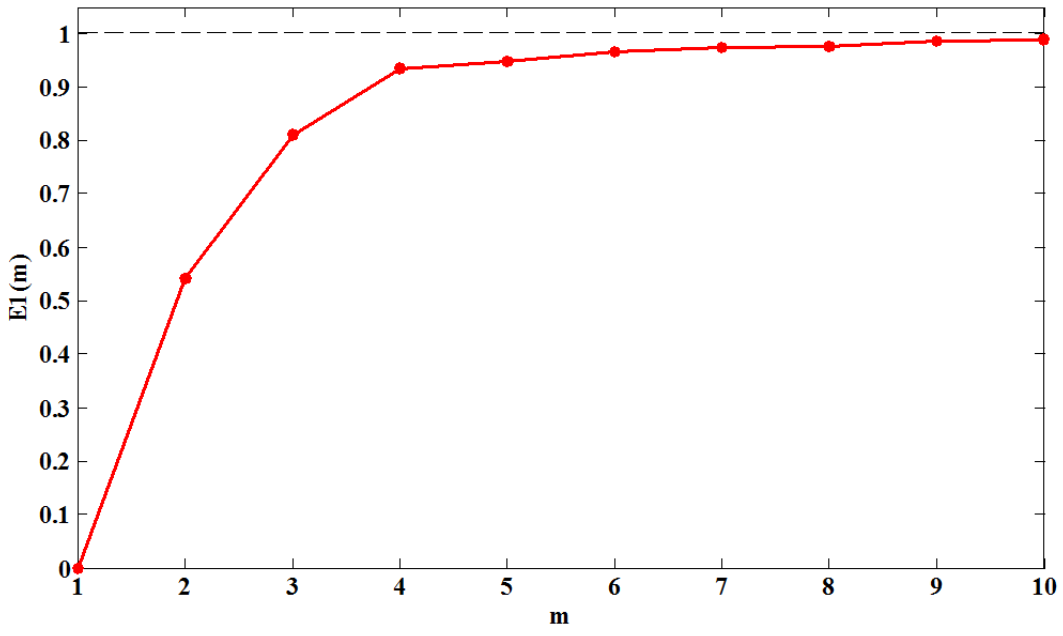

Fig. 2.5 *Determining the minimum embedding dimension by the modified method of false nearest neighbors.*

2.3.4. Largest Lyapunov exponent

Sensitive dependence to initial conditions is one of the most important properties of the chaotic system. Any chaotic system should have at least one positive Lyapunov exponent, with the magnitude reflecting the time scale on which system dynamics become unpredictable [Wolf et al., 1985; Bezruchko and Smirnov, 2010]. Lyapunov exponent, which provides a qualitative and quantitative characterization of dynamical behavior, is a useful dynamical diagnostic for chaotic systems since it gives a measure of the rate of divergence of neighboring trajectories [Wolf et al., 1985; Bezruchko and Smirnov, 2010].

In this study LLE was calculated with Wolf's method [Wolf et al., 1985], which allows the estimation of LLE from an experimental time series. As many studies have mentioned [Glass, 2009; Shelhamer, 2007; Skinner et al., 1998] most computational methods for estimating LLE have limitations and can produce positive LLE even for non-chaotic systems [Shelhamer, 2007] or can overestimate its value [Skinner et al., 1998].

LLE was calculated for all measured PPG data, and in all cases resulted in a positive LLE as shown in Table 2.2. However, LLEs corresponding to the 3rd subject's measurements 1, and 3-5 are at least one order of magnitude smaller than LLEs for other subjects. These significantly smaller values are highlighted.

TABLE 2.2 Largest Lyapunov exponents for all collected PPG time series (calculated by Wolf's method).

Repeat	Subject									
	1	2	3	4	5	6	7	8	9	10
1	1.041	0.731	0.097	1.143	1.100	1.279	1.206	1.250	1.079	1.014
2	0.961	0.810	0.117	1.565	0.968	1.020	1.692	1.010	1.150	0.938
3	1.145	1.099	0.051	1.398	0.861	1.209	0.937	1.121	1.194	1.182
4	0.744	0.902	0.039	1.303	1.019	1.167	1.621	1.157	1.040	1.119
5	0.787	0.754	0.063	0.968	1.274	0.766	1.242	0.929	1.000	1.008

2.3.5. Deterministic Nonlinear Prediction

As it is widely known, chaotic systems show predictability in the short-term that should decay rapidly, however different systems demonstrate different predictabilities, like for example prediction performance for the Lorenz system in chaotic regime and Rössler's single band chaos differs (as shown in Fig. 2.6 (a) and (b)).

Rössler's system is described by the following equations [Thompson and Stewart, 1991]:

$$\begin{cases} \dot{x} = -y - z, \\ \dot{y} = x + ay, \\ \dot{z} = b + z(x - c); \end{cases}$$

and Lorenz system by equations [Lorenz, 1963; Thompson and Stewart, 1991]:

$$\begin{cases} \dot{x} = -\sigma(x - y), \\ \dot{y} = \rho x - y - xz, \\ \dot{z} = xy - \beta z. \end{cases}$$

For calculation of Rösseler's data, the system coefficients chosen were a= 0.398, b= 2, c=4 which corresponds to single-band chaos [Thompson and Stewart, 1991; Small et al., 2001; Small et al., 2005], and for the Lorenz system σ=10, ρ=28, β=8/3; numerical simulation was done by the 4th order Runge-Kutta method with time step 0.01.

Information about predictability can be used to distinguish different behaviors. Additionally, the presence of short-term prediction indicates the determinism of the system under investigation [Shelhamer, 2007]. To examine whether PPG time series are predictable in the short-term and investigate how forecasting quality changes with increasing prediction time, direct (non-recurrent) deterministic nonlinear prediction (DNP) was conducted in this study. Prediction performance conventionally can be characterized by CC and RRMSE as functions of p - prediction time step. CC(p) and RRMSE(p) can be calculated as

$$CC(p) = \frac{\sum_{t=1}^{N-m\tau}(Z(t+p) - \bar{Z}(t+p))\left(Z^*(t+p) - \overline{Z^*}(t+p)\right)}{\sqrt{\sum_{t=1}^{N-m\tau}(Z(t+p) - \bar{Z}(t+p))^2}\sqrt{\sum_{t=1}^{N-m\tau}\left(Z^*(t+p) - \overline{Z^*}(t+p)\right)^2}}, \quad (2.1)$$

$$RRMSE(p) = \sqrt{\frac{\sum_{t=1}^{N-m\tau}\left(Z(t+p) - Z^*(t+p)\right)^2}{\sum_{t=1}^{N-m\tau}(Z(t+p) - \bar{Z}(t+p))^2}}\,. \qquad (2.2)$$

$Z^*(t+p)$ is p steps forward prediction of the predictee $Z(p)$, which can be defined as

$$Z^*(t+p) = Z(p) + \frac{1}{n}\sum_{i=1}^{n}\left(Z^i(t+p) - Z(t)\right),$$

where $Z^i(t)$ ($i=1,..,n$) is n nearest neighbors of $Z(p)$. Fig. 2.6 (a) shows an example of typical data of CC and Fig. 2.6 (b) RRMSE between real and predicted signals with increasing prediction time.

While short-time predictability can be easily identified, conclusions regarding long-term prediction are not straightforward, and in many cases are rather empirical and might be based on researcher experience. The prediction quality's "gold standard" is rapid and apparent decay of CC for chaotic Lorenz data, which is actually cannot be always observed for other well-known systems generating chaos. For example, in Fig. 2.6 Rössler's single band chaos shows high CC (higher than 0.96) over more than 400 steps, while CC corresponding to Lorenz reaches zero. It is important to notice in Fig. 2.6 (a) and (b) that CC and RRMSE curves corresponding to chaotic Rössler band initially demonstrate decay, as would be expected, and later both curves stabilize at a high CC value (CC > 0.96) and a low RRMSE value (RRMSE < 0.28) over a long period, however, it is known that chaotic systems do not have long-term prediction and therefore despite the stable high CC value and low value of RRMSE these results should not be recognized as a sign of long-term prediction.

As discussed later in Fig. 2.12, PPG trajectories have some topological similarity to Rössler's single band chaos; in accordance with the constructive approach, to illustrate changes in the PPG's CC and RRMSE curves it was compared with the CC and RRMSE curves of the corresponding Rössler's data. In addition, since the PPG data were obtained experimentally, it inevitably contains noise, so PPG prediction results were also compared with the same Rössler's system with 7 percent additive (dynamical) noise; results are shown in Fig. 2.6 (a) and (b). DNP results for all time series are shown in Fig. A.9-10 and Fig. A.11-12 for the CC and RRMSE respectively.

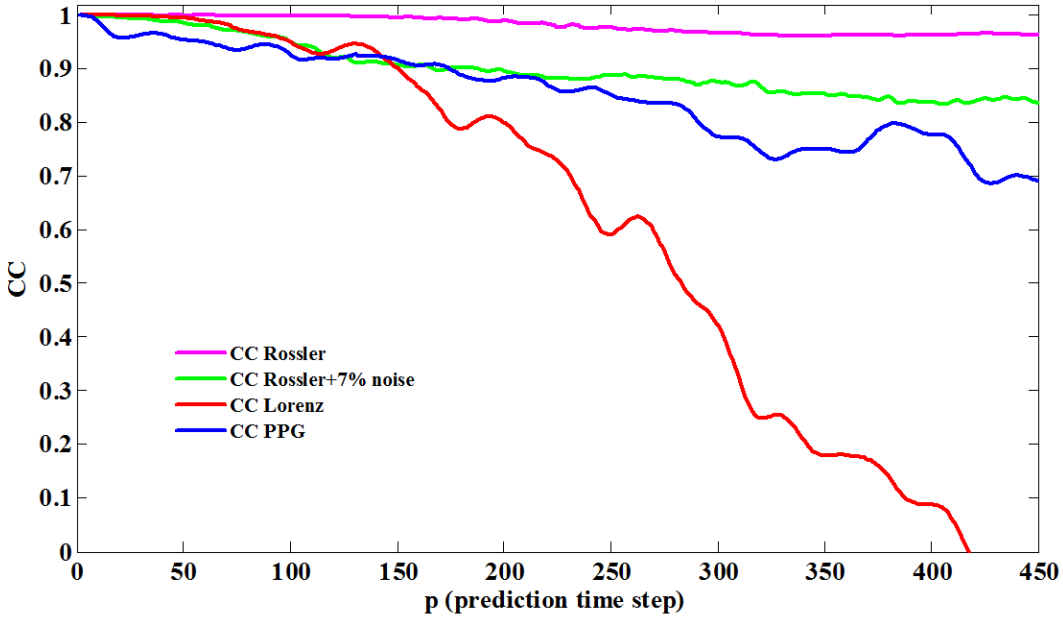

(a)

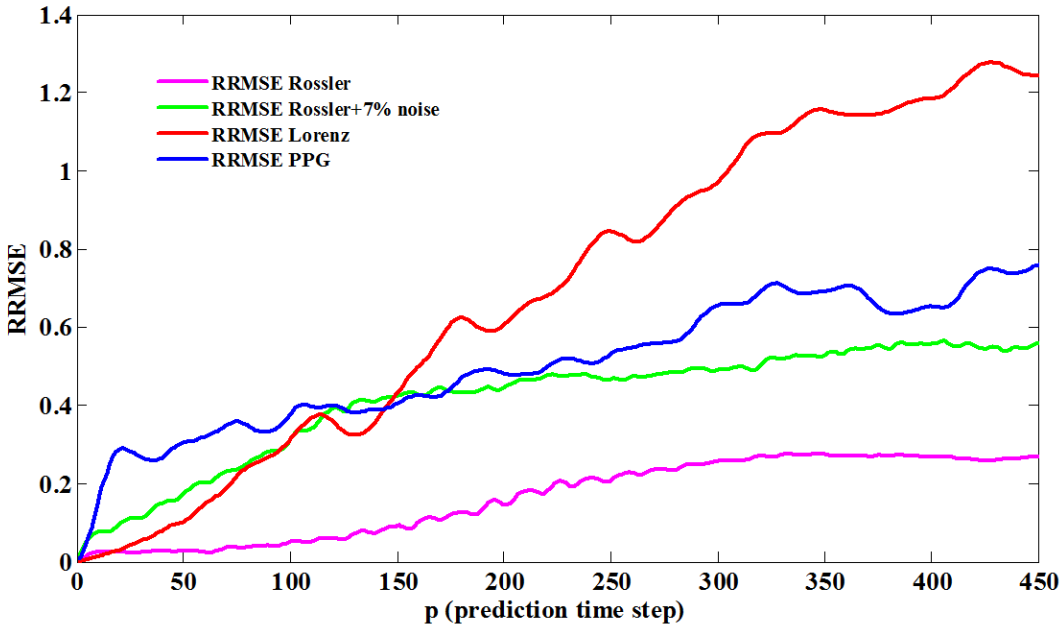

(b)

Fig. 2.6 *(a) Correlation coefficient (CC) and (b) relative root mean squared error (RRMSE) curves for nonlinear deterministic prediction of Rössler's single band chaos, Rössler's single band chaos data with 7% additive noise, chaotic Lorenz and PPG.*

Fig. 2.7 shows example of actual vs. 0.8s (160 time steps) predicted PPG, even after 160 steps forecast still resemble original time series with sufficiently high quality to reproduce not only the general trend of the PPG waveform, but also smaller details such as the dicrotic notch.

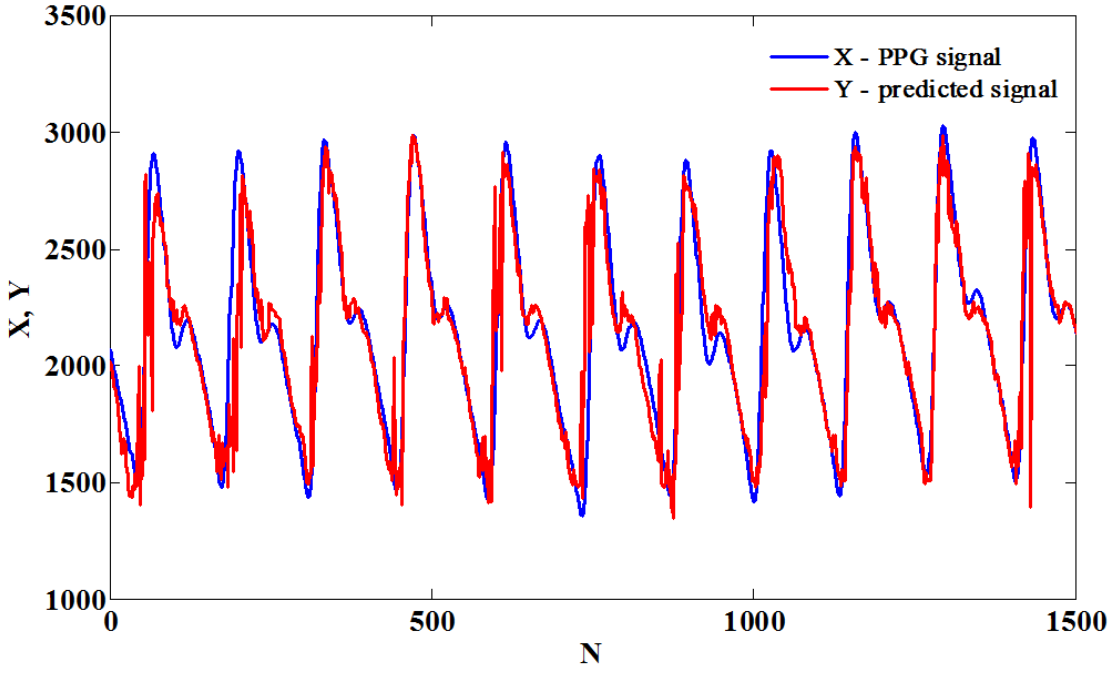

Fig. 2.7 *Performance of deterministic nonlinear prediction. Original signal vs. 160 steps (0.8s) forward prediction.*

As seen from Fig. 2.6 and Fig. 2.7, time series clearly demonstrated the presence of short-term prediction, which is indicative of underlying determinism. The chosen coefficients for the Rössler system correspond to a chaotic regime, and therefore the obtained Rössler's data should not have long-term prediction. Thus comparison between CC and RRMSE curves corresponding to PPG, Rössler and noise induced Rössler data in Fig. 2.6 demonstrate the absence of long-term forecasting in the PPG signal, which is typical for chaotic motion. Besides finding that PPG's CC and RRMSE curves showed similar trends with CC and RRMSE corresponding to 7% noise induced Rössler's data, these results have demonstrated that it might be misleading to compare

results obtained from PPG with chaotic Lorenz data, which played a role of one of the classical examples of chaos over decades, but actually demonstrates only one of many other possible chaotic behaviors.

In this study DNP became an important method for testing the predictability properties of the PPG signal. In several studies it was claimed that PPG time series of young healthy subjects are deterministic chaos, based mostly on results of the Lyapunov exponent, CD and time-delay trajectory reconstruction, which as it is nowadays known, may produce misleading results for noise contaminated real-world signals. Results of DNP (Fig. 2.6, 2.7) and its comparison with chaotic Rössler's data provided not only substantial support for the claim of the chaotic nature of the PPG, but more importantly, it provides one with quantitative (CC and RRMSE) as well as qualitative (similarity of prediction performance with noise induced chaotic Rössler's data) characteristics of PPG dynamics.

2.3.6. Poincaré section

The Poincaré section is one of the most powerful tools for qualitative exploration of the dynamics of a system [Shelhamer, 2007], as it enables a demonstration of the process generating chaos in the phase space. The Poincaré section was obtained from a three-dimensional time-delay reconstructed attractor by a clock-wise rotating slicing two-dimensional plane. Fig. 2.8 demonstrates areas on trajectory sliced by the plane; in Fig. 2.9, an example of Poincaré sections for the 1st subject's 1st measurement is shown.

As seen from Fig. 2.8 and Fig. 2.9 dense trajectories ($\alpha=75^{o}$) tend to expand ($\alpha=150^{o}$), bend ($\alpha=225^{o}$) and stretch ($\alpha=300^{o}$) and then fold back ($\alpha=0^{o}$, $\alpha=75^{o}$) along the reconstructed attractor. This stretch-and-fold behavior generates sensitive dependence on the initial conditions, which is recognized as an important property of chaotic dynamics.

The areas sliced by rotating plane on reconstructed trajectory of all PPG time series and corresponding to it Poincaré sections are shown in Fig. A.13-14 and Fig. A.15-24, respectively.

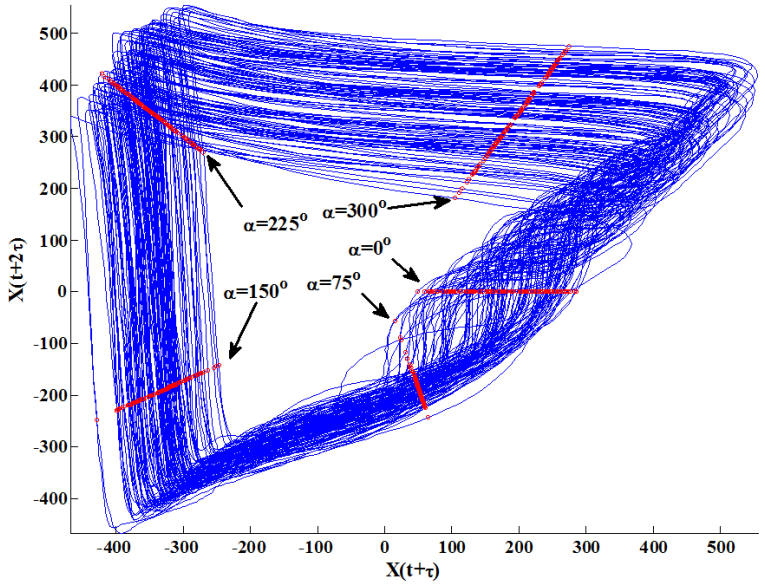

Fig. 2.8 *The reconstructed trajectory sliced by the rotating plane for the PPG (for the 1st subject's 1st measurement).*

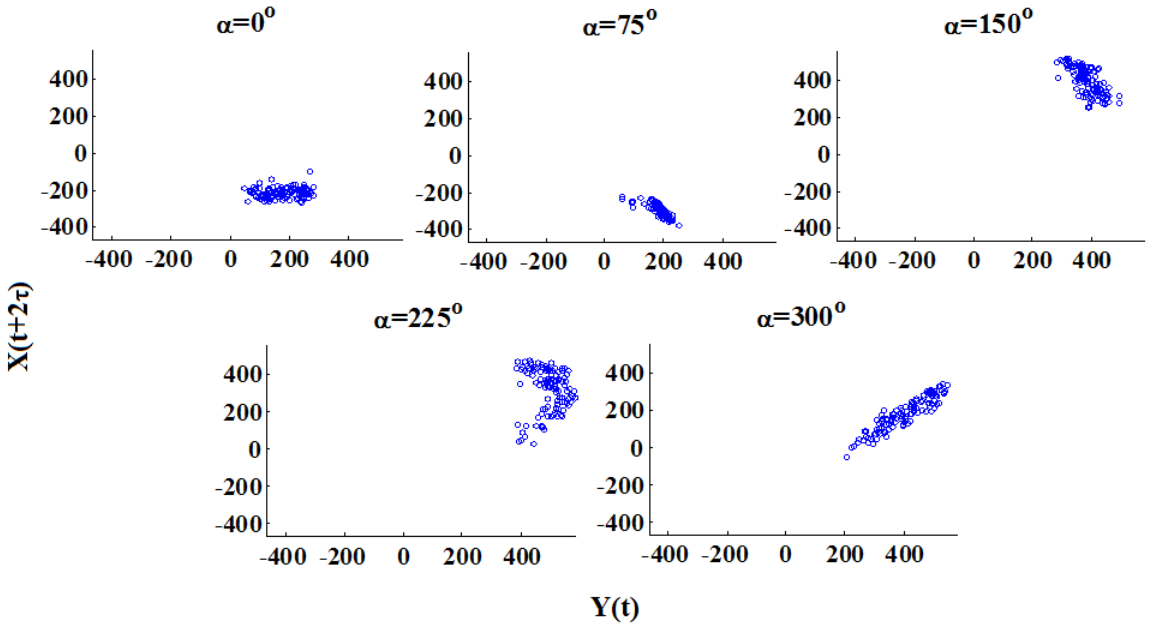

Fig. 2.9 *Poincaré section for the PPG (for the 1st subject's 1st measurement), where Y(t) =* $\sqrt{x(t)^2 + x(t+\tau)^2}$.

2.3.7. Wayland test

In order to explain the variability observed in complex time series and distinguish whether it is due to external stochastic noise, internal deterministic dynamics, or a combination of both, the Wayland test, which is a computationally simple variation of the Kaplan-Glass method and uses the phase space continuity observed in time series to measure determinism, was applied [Wayland et al, 1993].

The Wayland test Translation Error (WTE), which can quantify smoothness of the flow reconstructed in the phase space, was calculated in this study. It is defined as median of local translation errors that are defined as follows:

$$e_{trans} = \frac{1}{k+1}\sum_{j=0}^{k}\frac{\|v_j - \langle v\rangle\|^2}{\|\langle v\rangle\|^2},$$

where $v_j=y_j-x_j$ are translation vectors, $\langle v\rangle$ is the average of v_j, x_j ($j=1,2,\ldots,k$) are k nearest neighbors to the fixed and arbitrary chosen point x_0 on the reconstructed trajectory and y_j are projections of x_j as shown in Fig. 2.10.

The WTE performs well in high levels of uncorrelated noise and provides a robust measure of the determinism in the trajectories reconstructed in the phase space [Wayland et al, 1993] and it is insensitive to an overall scaling of the original time series. If the time series is deterministic, then vectors v_j will be nearly equal and therefore the WTE will be small [Wayland et al, 1993]. For instance, for chaotic Rössler time series (dataset containing 60 000 points) with parameters as described in section 2.3.5, the WTE is 0.0002, for Rössler with 7% induced noise the WTE is 0.0045, WTE for chaotic Lorenz is 0.0004 and for white noise is 1.08 (60 000 points). Table 2.3 shows the results of WTE calculations for the PPG (time series size is 60 000 points).

According to Table 2.3, most of the WTE values are small, except for those of the 3rd subject, which is an indication of determinism in the PPG data. Most the WTE values corresponding to the 3rd subject are higher than white noise; therefore, the 3rd subject's data cannot be concluded to be deterministic. However it is still an open question whether this difference in WTE values between the 3rd subject and other subjects comes from the 3rd subject's

heart disorder, which was declared in the questionnaire during data collection, from other individual features, or the presence of significantly high noise in the measured signal.

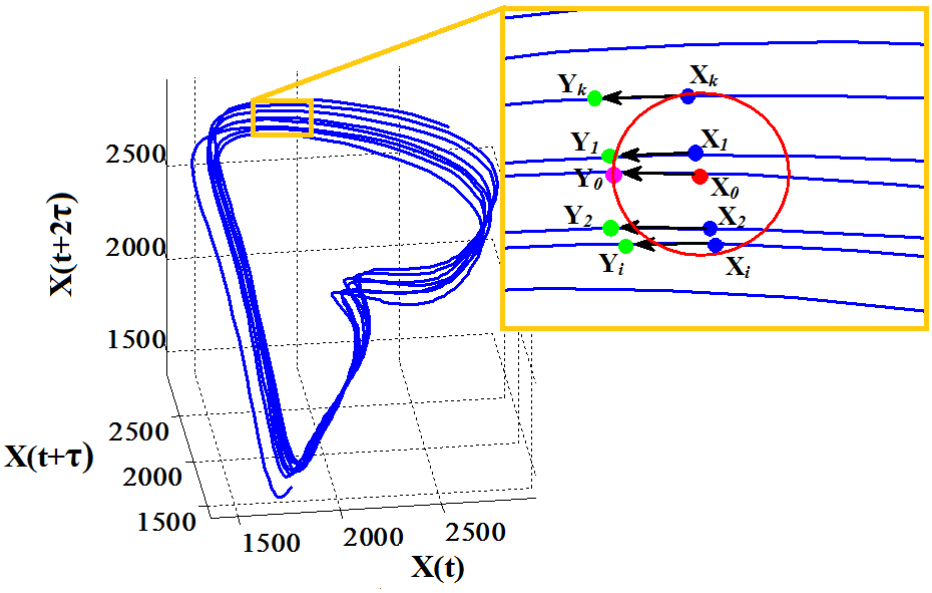

Fig. 2.10 *The nearest neighbors of an arbitrarily chosen point and its projections on a reconstructed trajectory for translation error calculation in the Wayland test.*

TABLE 2.3 Results of the Wayland test translation error (WTE) calculation for all collected PPG time series.

Repeat	Subject									
	1	2	3	4	5	6	7	8	9	10
1	0.007	0.041	1.046	0.023	0.016	0.092	0.015	0.012	0.031	0.018
2	0.006	0.041	1.06	0.012	0.024	0.024	0.01	0.017	0.03	0.019
3	0.005	0.045	1.351	0.013	0.02	0.059	0.019	0.016	0.015	0.027
4	0.01	0.023	3.148	0.015	0.034	0.027	0.019	0.026	0.039	0.045
5	0.024	0.048	1.197	0.05	0.085	0.017	0.037	0.035	0.048	0.024

2.3.8. Surrogation

The surrogation approach is to specify a defined null hypothesis and generate set of surrogate signals that embody a hypothesis about the time series. Then by determining the distribution of the index under investigation obtained from surrogates, empirical statistical boundaries can be found. By comparing the index of the original time series with the distribution of the index from surrogates, the null hypothesis under which surrogates were generated can either be rejected if the value from the original signal does not overlap with the distribution from surrogates, or fail to be rejected if the original index is within distribution with high significance [Shelhamer, 2007; Theiler et al., 1992].

One of the typical applications of surrogate data is to check for determinism and whether data are a realization of a specific random process. In this study the null hypothesis is that the signal is a realization of a linear Gaussian stochastic process. Surrogate time series were created by phase randomization of Fourier transforms for the original PPG data and following inverse Fourier transform. As a result, the obtained surrogates are stochastic, but have the same power spectrum as the original data. Applying this type of surrogates allows one not only to place empirical boundaries, but also to test for nonlinearity of PPG.

DNP was applied to 100 surrogate datasets. Fig. 2.11 (a) demonstrates the results of DNP for surrogate time series generated under the null hypothesis from the original data. As seen from the CC curves, the original signal is clearly distinct and does not overlap with curves corresponding to surrogates. Fig. 2.11 (b) shows frequency distribution of the 20 steps forward prediction CC for surrogates and CC value for the original PPG data; *CC(20)* values for surrogates and the PPG are corresponding to the values at the intersection of orange vertical line and CC curves in Fig. 2.11 (a). Results of DNP applied to 50 surrogate datasets for all PPG time series are shown in Fig. A.25-26. Since for most of the data in Fig. A.25-26 the PPG CC and surrogates CC are clearly distinguishable, the null hypothesis of a linear Gaussian stochastic process should be rejected. Additionally, it may be suggest that there is no significant effect of Gaussian noise, which PPG may contain, based on results of DNP.

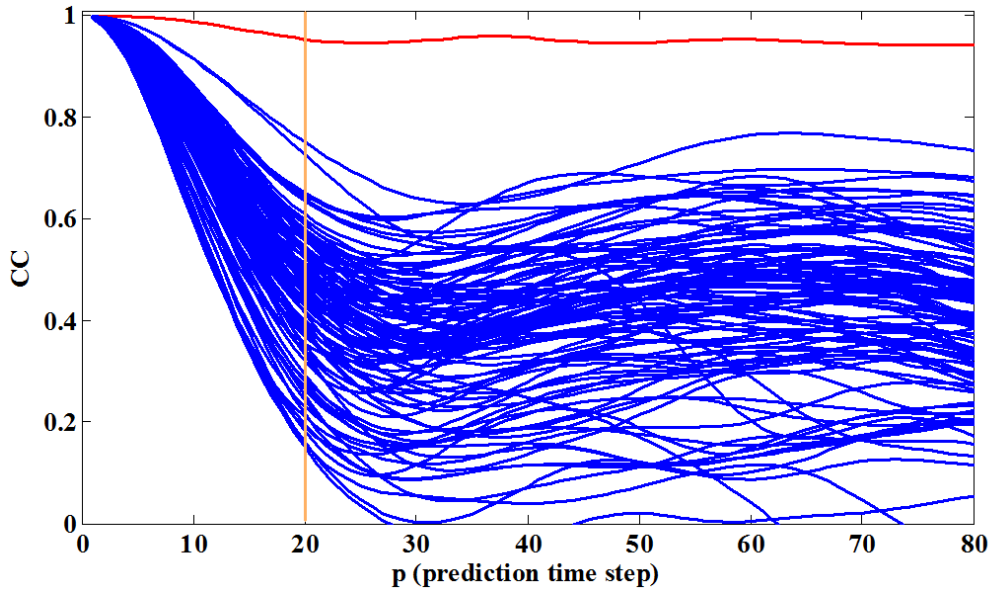

(a)

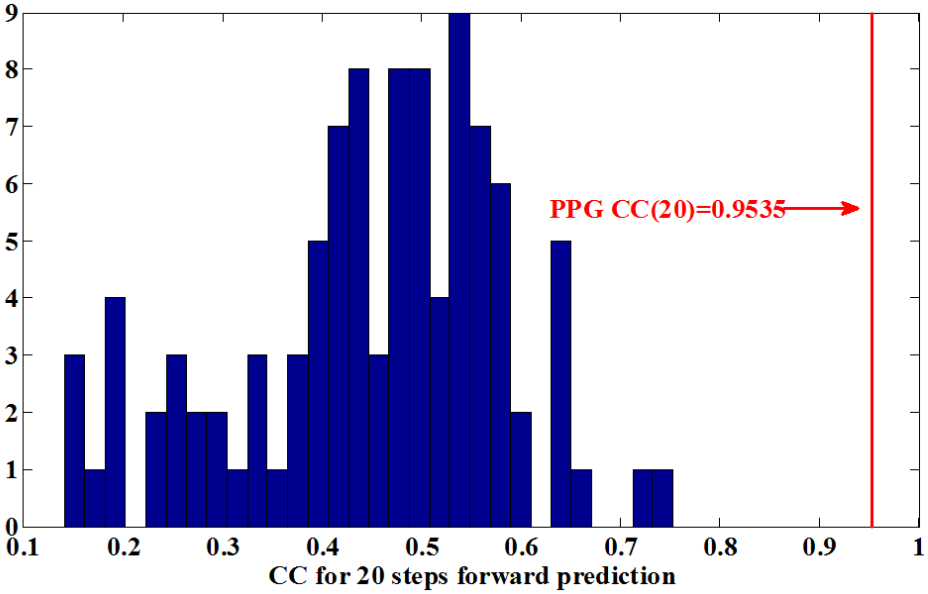

(b)

Fig. 2.11 *(a) Deterministic nonlinear prediction for the PPG (red line) and 100 surrogate datasets (blue lines), orange line indicates correlation coefficient values corresponding to the 20 steps forward prediction; (b) frequency distribution of correlation coefficients for 100 surrogate datasets (blue bars) and correlation coefficient for original PPG (red line).*

2.4. Discussion

The objective of this study was to provide evidence that the PPG signal, obtained from healthy human subjects, is consistent with the definition of chaotic motion given by Thompson and Stewart and conduct a comprehensive study of the chaotic characteristics of PPG dynamics. Produced by sophisticated mechanisms of the cardiovascular system, the PPG signal is still not fully understood. In the in early 90s PPG was claimed to be chaotic based on time-delay reconstruction, LLE and CD results [Tsuda, 1992; Sumida and Arimitu, 2000], which were previously believed to be sufficient to identify chaos. However, many studies subsequently showed that these measures can be misleading and provide false evidence of chaos in the case of, for example, noise contaminated experimental data [Glass, 2009; Shelhamer, 2007; Skinner et al., 1998]. In addition, it is well known that physiological data are inevitably contaminated by environmental noise and movement artifacts. And the same measures were used in application studies investigating the dependence of PPG characteristics from human subject's mental and physiological conditions [Pham et al., 2013; Tsuda, 1992; Sumida and Arimitu, 2000].

In an attempt to obtain reliable results, various methods of NTSA, including classical and widely used ones – power spectrum, time-delay embedding, and largest Lyapunov exponent have been applied and deterministic nonlinear prediction, Poincaré section, Wayland test and surrogation have been conducted. These results are not only considered to be more reliable in the case of noise-contaminated data, but can also provide new insights into the chaotic properties of PPG dynamics.

Additionally, to study in more detail trajectories' evolving process, trajectories spreading in phase-space have been directly investigated. An arbitrary chosen fixed point on an attractor and its nearest neighbor were selected as the starting points of two trajectories. Fig. 2.12 shows the separation of these two trajectories based on the example of 140 and 300-step long segment for PPG time series (left side) and for Rössler's single band chaos with 7 percent additive noise (right side), in both cases the trajectories evolve clock-wise. Star and circle markers are corresponding to trajectories originating from an arbitrarily chosen fixed point on an attractor and its neighboring trajectory, respectively, where red color indicates the starting and black color

the ending points of the segment. The distance between trajectories increases immediately with increasing evolution time step, however later trajectories are getting closer and remain in the bounded region. Obtained PPG trajectories are continuously bending due to that folding is realized. In this sense PPG's attractor seems to belong to the same folded band topological group as Rössel's single band chaotic attractor, rather than the Lorenz group, in which folding is produced by splitting and layering [Thompson and Stewart, 1991].

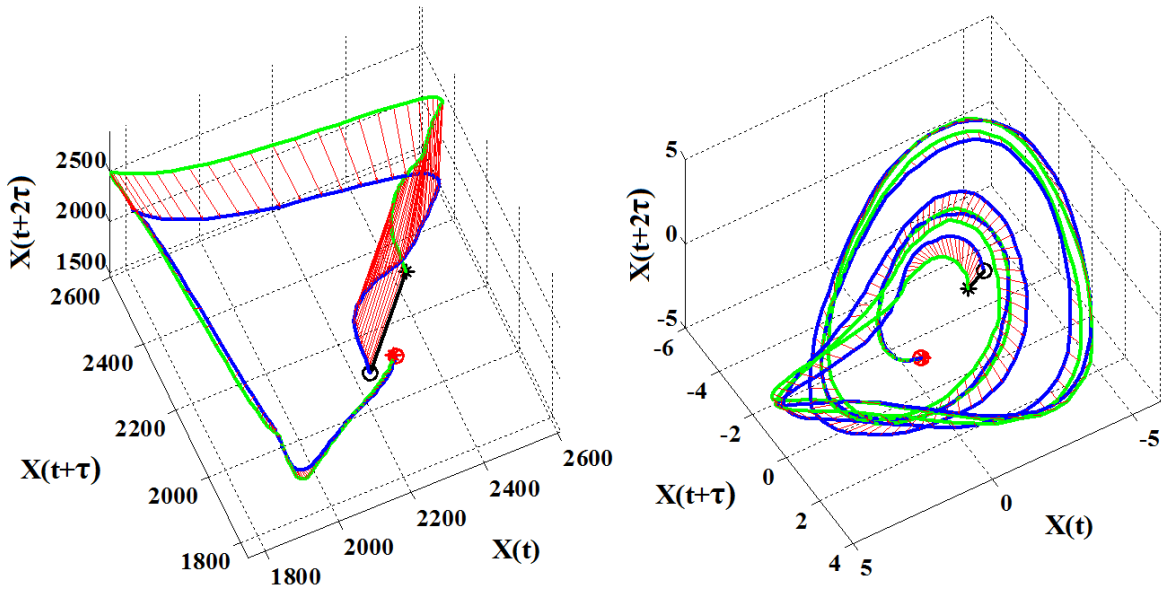

Fig. 2.12 *Trajectory tracings for PPG data (left) and Rössler's single band chaos data with 7% additive noise (right).*

The investigated data primarily demonstrated the presence of an experimental attractor with clear structure, which is necessary for a deterministic process. As shown, the time-delay reconstructed PPG attractor had some topological similarity to the attractor obtained from Rössler's single band chaotic data, in which folding is achieved by continuous bending [Thompson and Stewart, 1991]. All of the PPG time series had positive LLE that along with Poincaré section reflects the sensitive dependence on initial conditions. As shown in Fig. 2.6, Fig. 2.7 and Fig. A.9-12 all of the data had short-term predictability. The CC curve tends to decline

slowly with an increase of the prediction step. To reach a conclusion on the existence of long-term predictability, results of DNP for PPG were compared with DNP for chaotic Rössler's data. Results of the comparison explicitly illustrated that PPG data should not have long-term predictability and that prediction performance of the PPG signal is similar to noise induced chaotic Rössler data. The method of surrogate data applied to DNP confirmed the obtained results and demonstrated that there is no significant effect of Gaussian noise that may be contained the in signal on the results of DNP.

To test determinism of the PPG underlying process the Wayland test was applied. Most of the data had a small WTE that clearly indicates strong determinism of the process generating PPG data.

These results are consistent with the so-called "positive" definition of chaos by Thompson and Stewart [Thompson and Stewart, 1991] as "recurrent motion in simple systems or low-dimensional behavior that has some random aspects as well as certain order". Therefore healthy, young human subjects' PPG dynamics could be concluded as chaotic motion, with chaotic characteristics, such as bending structure of the attractor, predictability properties similar to noise induced Rössler's single-band chaos.

2.5. Conclusion

In this chapter nonlinear time series analysis was conducted to investigate the nature of finger PPG data obtained from healthy, young human subjects under resting conditions in a controlled environment. Spectral analysis, time-delay embedding, embedding dimension, nonlinear deterministic prediction, Poincaré section calculation, Wayland test and the method of surrogate data were applied to the data to obtain evidence that the studied PPG data are consistent with the definition of chaotic motion. Applied methods aimed to test the chaotic characteristics of PPG dynamics, such as dependence on initial conditions, predictability and determinism. The obtained results provided strong evidence that studied PPG signal dynamics is consistent with chaotic motion. Additionally, the similarity of PPG predictability properties and attractor's topological structure to Rössler's single band chaos was demonstrated.

These results provide new insights into the PPG signal characteristics and demonstrate the usefulness of deterministic nonlinear prediction, Poincaré section and the Wayland test in extracting the underlying chaotic characteristics of the PPG signal. It is expected that application of the above mentioned methods of nonlinear time series analysis may contribute to future applied studies on the PPG signal to detect mental and physiological conditions of human subjects.

Chapter 3. Short-term predictability of human photoplethysmogram

3.1. Introduction

As discussed in Chapter 2, DNP as well as WTE and other methods of nonlinear time series analysis can provide important information about the characteristics of chaotic systems. While most of the tests are rather quantitative, prediction also allows one to make qualitative estimation, thus the quality of prediction performance may provide useful information for distinguishing the type of process underlying the signal. Although prediction per se cannot be used for dynamics identification, its results can be valuable for dynamics distinction.

In the previous chapter, the comparison of prediction results between Rössler's single band chaos and the PPG provided an answer to the question of long-term prediction existence. Results explicitly demonstrated that long-term prediction is impossible. Additionally, certain similarities between PPG and Rössler's reconstructed trajectory were found. However, these DNP results of the PPG data in comparison with Rössler and Lorenz in Chapter 2 gave rise to two new questions concerning PPG predictability properties. First of all, as shown in Fig. 2.6 and Fig. 3.1, the short-term prediction performance for the PPG significantly differs from Rössler, Rössler with noise and Lorenz models, though for all of the curves in Fig. 2.6 and Fig. 3.1 short-term prediction is quite high in quality, and CC and RRMSE curves corresponding to the PPG have noticeably different shapes. The short-term DNP's performance for Lorenz and Rössler forms a plateau region for CC before it starts to decay and remains high significantly longer than for PPG data. Although this difference does not put into question the prediction properties stated in Chapter 2, as the existence of short-term prediction is indisputable, this indicates that in very short-term evolution, Rössler's single band chaos and the PPG underlying processes have considerable differences, which cannot be explained by simple matters such as noise induction. Understanding the PPG short-term prediction behavior is expected to provide one with a deeper understanding of PPG dynamics in general, which is one of the main objectives of this research. Therefore, one question originating from the results of Chapter 2, which will be investigated in this chapter, is

whether predictability similar to the PPG in the short-term can be observed in other systems, or in other words what type of dynamics exhibits similar prediction properties.

As shown in Chapter 2, PPG signal dynamics is consistent with the definition of chaotic motion. Although similarities between the PPG and Rössler's single band chaos were found, results in Chapter 2 demonstrated that only a comparative understanding of PPG dynamics could be achieved while its true dynamics remains unclear. Therefore to obtain insight into the characteristics of short-term prediction we will follow the constructive approach in which DNP is used as method for comparing properties between the PPG and well-known systems generating chaos. Since, as seen from results of Chapter 2, chaotic Lorenz and Rössler's models do not possess short-term prediction properties that resemble those of the PPG, following the constructive approach, different types of chaotic models should be chosen for comparative study of the PPG's short-term prediction characteristics. As both Lorenz and Rössler's models belong to autonomous systems [Thompson and Stewart, 1991], in this chapter the PPG predictability is compared with a non-autonomous chaotic system. Even though finding similar DNP performance would not mean that the dynamics are identical between the PPG and a system possessing similar properties, as in the previous chapter, a comparative understanding of the PPG dynamics is expected to be achieved. Therefore, one of the goals in this chapter is investigation of the PPG dynamics' short-term predictability characteristics in comparison with a well-known chaotic non-autonomous system.

Another question that inevitably arises from the DNP results of the previous chapter is related to the wide fluctuation of prediction performance that can be observed in DNP's CC and RRMSE curves for many time series, as seen in Fig. A.9-12. Variations in these fluctuations not only from subject to subject, but also those between measurement repeats for the same subject might be meaningful. Therefore, what causes this phenomenon is another question under investigation in this chapter.

In Chapter 2, the results of DNP's CC and RRMSE were averaged over the PPG reconstructed trajectory and therefore correspond to the reconstructed trajectory overall, except for the portion that was chosen as the library if the calculation method involves library creation.

Results representing the properties of PPG dynamics obtained from whole reconstructed trajectory will be referred to herein as global scale results or properties; thus conventional prediction results obtained in Chapter 2 will be called global prediction. As seen from the reconstructed attractor (Fig. 2.4) and Poincaré sections (Fig. 2.9), trajectories expansion and density depend on the local region along the reconstructed attractor and therefore it can be assumed that prediction performance might differ locally on each part of the reconstructed trajectory. From one point of view this possible variation of dynamical properties among different parts or regions along the reconstructed trajectory might be able to explain the considerable fluctuations observed in global prediction performance. On the other hand, by itself, investigation of local dynamics properties might provide one with a deeper understanding of the PPG dynamics and as a result promote further development of PPG applications, since every region along the reconstructed attractor can be associated with the cardiac cycle's phases: atrial contraction, isovolumetric contraction, rapid ejection, reduced ejection, isovolumetric relaxation, rapid filling and reduced filling.

In contrast with global prediction, prediction calculated on a fixed region of the reconstructed trajectory will be called local prediction. Therefore, for a better understanding of PPG dynamics, in addition to the comparative study of global short-term prediction, this chapter also aims to investigate local short-term prediction.

3.2. Methodology

3.2.1. Comparative study of global short-term DNP

As mentioned above, in this chapter a non-autonomous chaotic system is used for comparative investigation of the PPG's short-term predictability. One of the well-known examples of non-autonomous systems is the chaotic Duffing's forced oscillator, which is utilized in this chapter. Duffing's forced oscillator is described by the following equation:

$$\ddot{x} + k\dot{x} + x^3 = Bcos(\omega t), \tag{3.1}$$

where the system coefficients were chosen as k=0.05, B=7.5, ω=1, which corresponds to a chaotic regime [Thompson and Stewart, 1991]. Numerical simulation was done by the 4th order Runge-Kutta method with time step 0.01, and the calculated time series size was 60 000 data points.

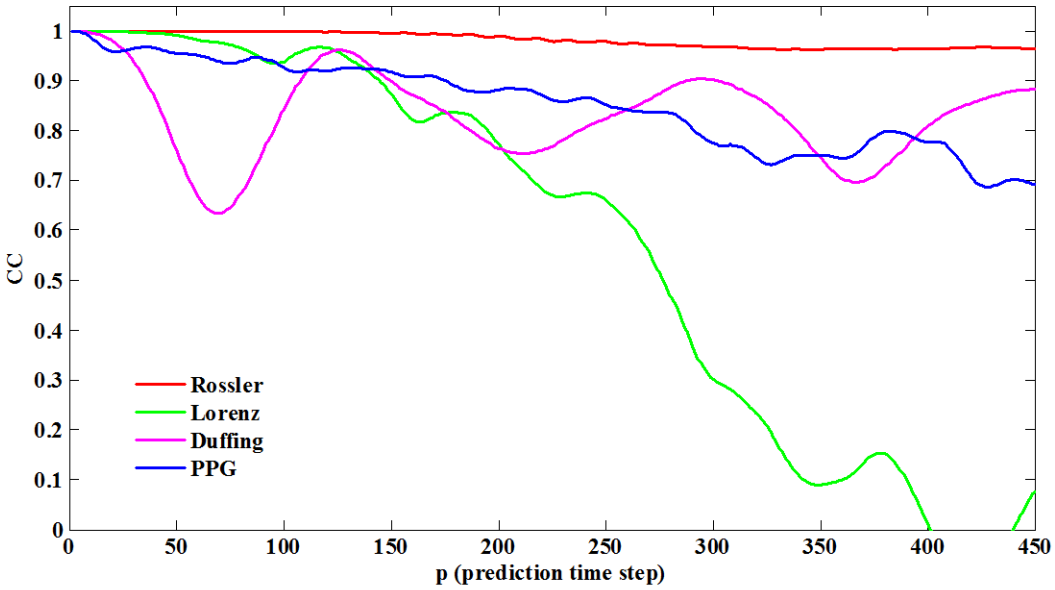

Fig. 3.1 *Correlation coefficient (CC) curves for nonlinear deterministic prediction of Rössler's single band chaos, chaotic Lorenz, chaotic Duffing's forced oscillator and the PPG.*

DNP CC for Duffing's forced oscillator in comparison with Rössler, Lorenz and PPG DNPs are shown in Fig. 3.1, where it is seen that the short-term CC curve corresponding to Duffing's data has a significantly faster drop, compared with Rössler's and Lorenz's curves. Therefore, Duffing's chaotic forced oscillator was used for comparative study of PPG predictability.

3.2.2. Local DNP

DNP short-term performance shown in Fig. 3.1 is referred to as the prediction performance averaged over the PPG reconstructed trajectory, i.e. the global DNP. However as seen from the reconstructed trajectory (Fig. 2.4) and Poincaré section (Fig. 2.9), the trajectories density and

evolving process differs along the reconstructed attractor. Therefore, it is expected that prediction performance might differ locally depending on the region of the trajectory where the DNP is conducted. In order to investigate local short-term predictability of the PPG in a fixed region on the reconstructed trajectory, CC and REMSE need to be calculated over this local region. Let t_1^i and t_2^i be starting and ending points of the i^{th} region on the reconstructed trajectory, then formulas (2.1) – (2.2) can be rewritten as

$$CC_i(p) = \frac{\sum_{t=t_1^i}^{t_2^i}(Z(t+p) - \bar{Z}(t+p))\left(Z^*(t+p) - \overline{Z^*}(t+p)\right)}{\sqrt{\sum_{t=t_1^i}^{t_2^i}(Z(t+p) - \bar{Z}(t+p))^2}\sqrt{\sum_{t=t_1^i}^{t_2^i}\left(Z^*(t+p) - \overline{Z^*}(t+p)\right)^2}},$$

$$RRMSE_i(p) = \sqrt{\frac{\sum_{t=t_1^i}^{t_2^i}\left(Z(t+p) - Z^*(t+p)\right)^2}{\sum_{t=t_1^i}^{t_2^i}(Z(t+p) - \bar{Z}(t+p))^2}}.$$

CC_i and $RRMSE_i$ defined by these formulas are the local correlation coefficient and relative root mean square error corresponding to the i^{th} region.

3.3. Results

3.3.1. Global short-term prediction

Similar to section 2.3.5, DNP was applied to the data sets described in section 2.2. However, Duffing's chaotic forced oscillator (3.1) was chosen as the model for comparison instead of Rössler and Lorenz models.

Fig. 3.2 (a) and (b) demonstrate short-term prediction's CC and RRMSE, respectively, for the PPG, chaotic Duffing's time series and Duffing's time series with 7% noise induction. Results for Rössler's single band chaos prediction (same as in the section 2.3.5) were added to illustrate differences in prediction performance. Fig. A. 27-30 show results of global short-term prediction CC and RRMSE for all PPG datasets and Fig. 3.3-3.6 demonstrate 450 steps forward DNP performance for Rössler and Duffing, Duffing with 7% noise and PPG data. As seen from

Fig. 3.2, even a short-term prediction performance for both Rössler and Duffing's time series shows considerable differences, and while the CC curve for Rössler's time series does not demonstrate any noticeable decline for short-term (30 time steps forward) prediction, the CC curve corresponding to Duffing's time series has a distinguishable decline. Noise induction on the Duffing's data preserves the CC's curve declining trend and results in a decrease in the prediction performance. As is clearly seen in Fig. 3.2 (a), PPG short-term prediction's CC has significant similarity with 7% noise induced Duffing's forced oscillator over a range from 1 to 16 steps forward prediction. Although, as can be seen from Fig. A.27-30, CC and RRMSE values for the PPG and noise induced Duffing have differences for many other time series starting from 10 steps forward prediction, what is significant is that for both, the PPG and noise induced Duffing's data show a similar trend of a relatively rapid CC curve decline, compared with Rössler's data. Differences between prediction performance for the PPG and Duffing with Rössler are even more enhanced in RRMSE plots. The RRMSE for Duffing and the PPG have a rapid increase unlike the RRMSE for Rössler, whose curve remains close to zero and almost flat, as seen in Fig. 3.5-6 and Fig. A.29-30. Additionally, in many cases DNP performance for Duffing's data and the PPG have similar high fluctuations of CC and RRMSE curves that were not observed in Rössler's DNP, as seen in Fig. 3.3-3.6.

Therefore, the PPG short-term predictability has some similarity with the predictability of noise induced Duffing's forced oscillator's data rather than with Rössler, although as shown in Chapter 2, on a global scale, the PGG reconstructed attractor has some topological similarity to the noise induced Rössler's single band chaos.

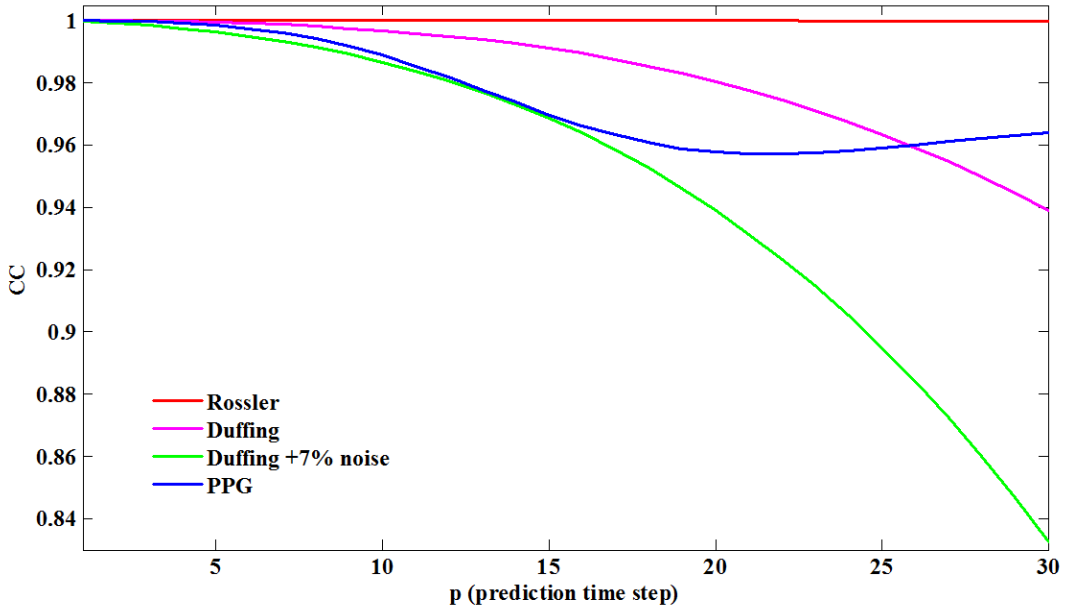

(a)

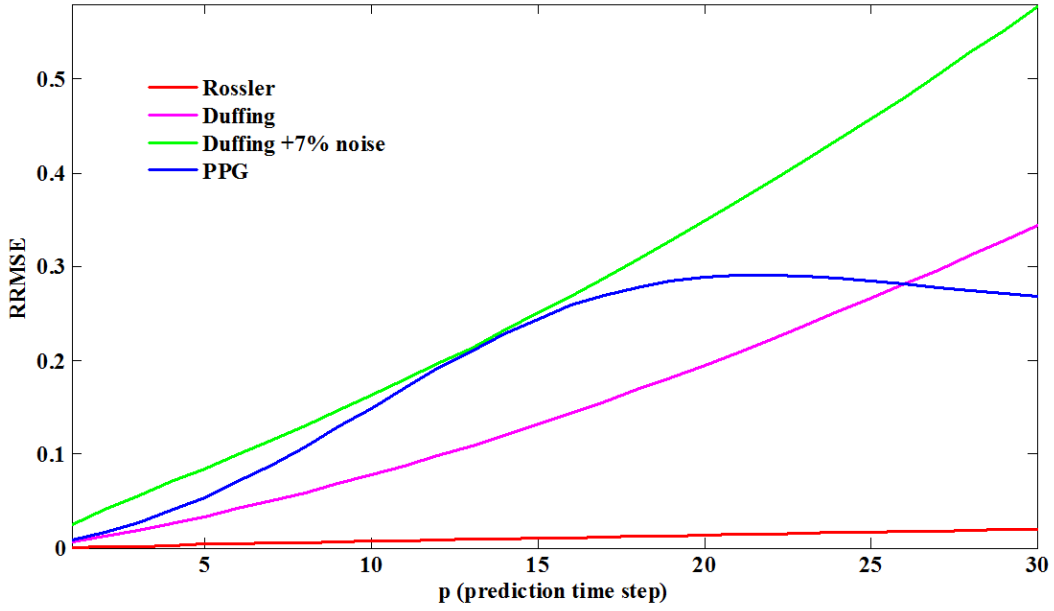

(b)

Fig. 3.2 *(a) Correlation coefficient (CC) and (b) relative root mean squared error (RRMSE) curves for deterministic nonlinear prediction of Rössler's single band chaos, chaotic Duffing's forced oscillator, chaotic Duffing's forced oscillator data with 7% additive noise and the PPG.*

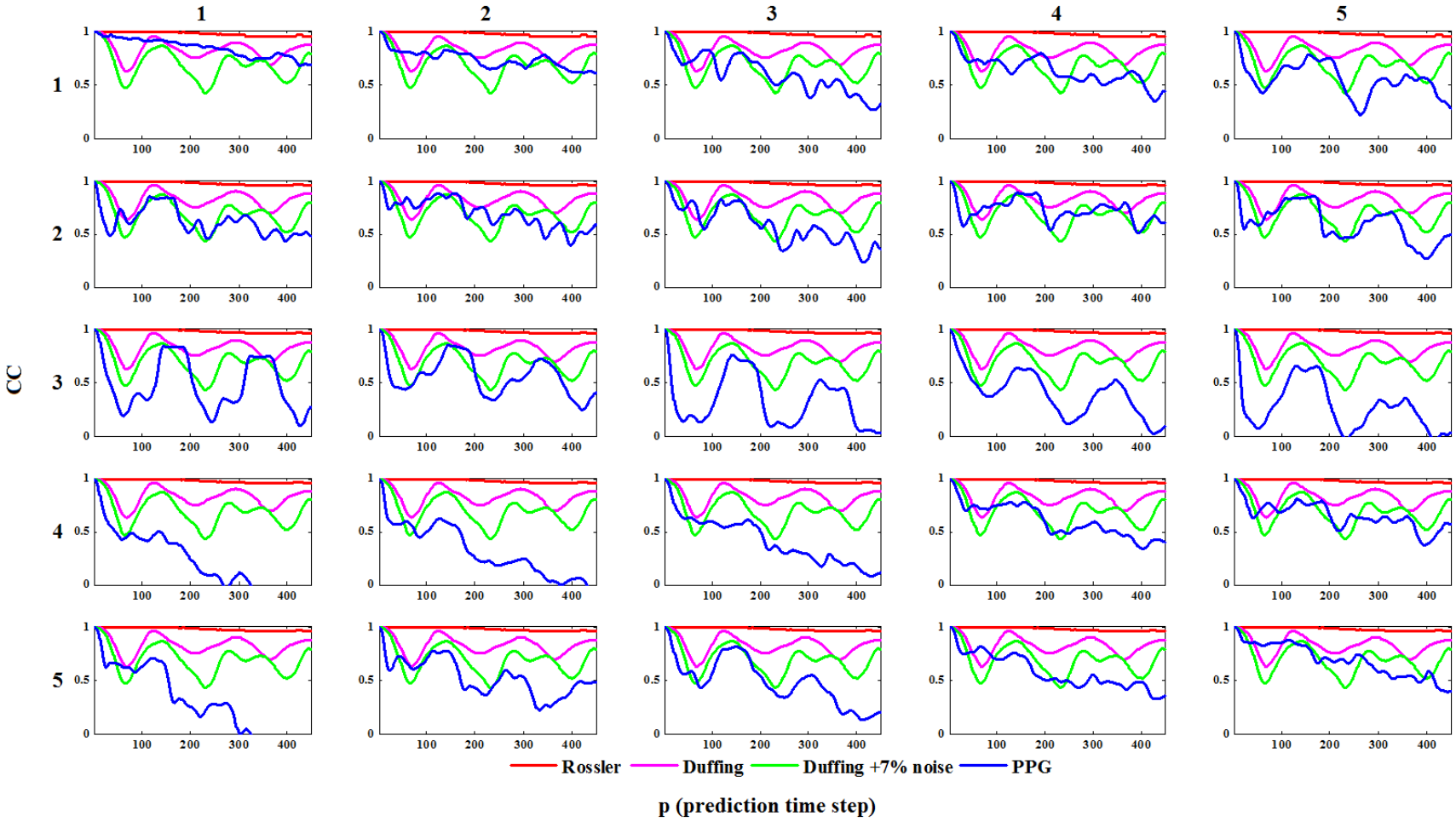

Fig. 3.3 *Correlation coefficient (CC) for deterministic nonlinear prediction of Rössler's single band chaos, chaotic Duffing's forced oscillator, chaotic Duffing's forced oscillator with 7% additive noise and the PPG for 5 measurement repeats (columns) of subjects 1-5 (rows).*

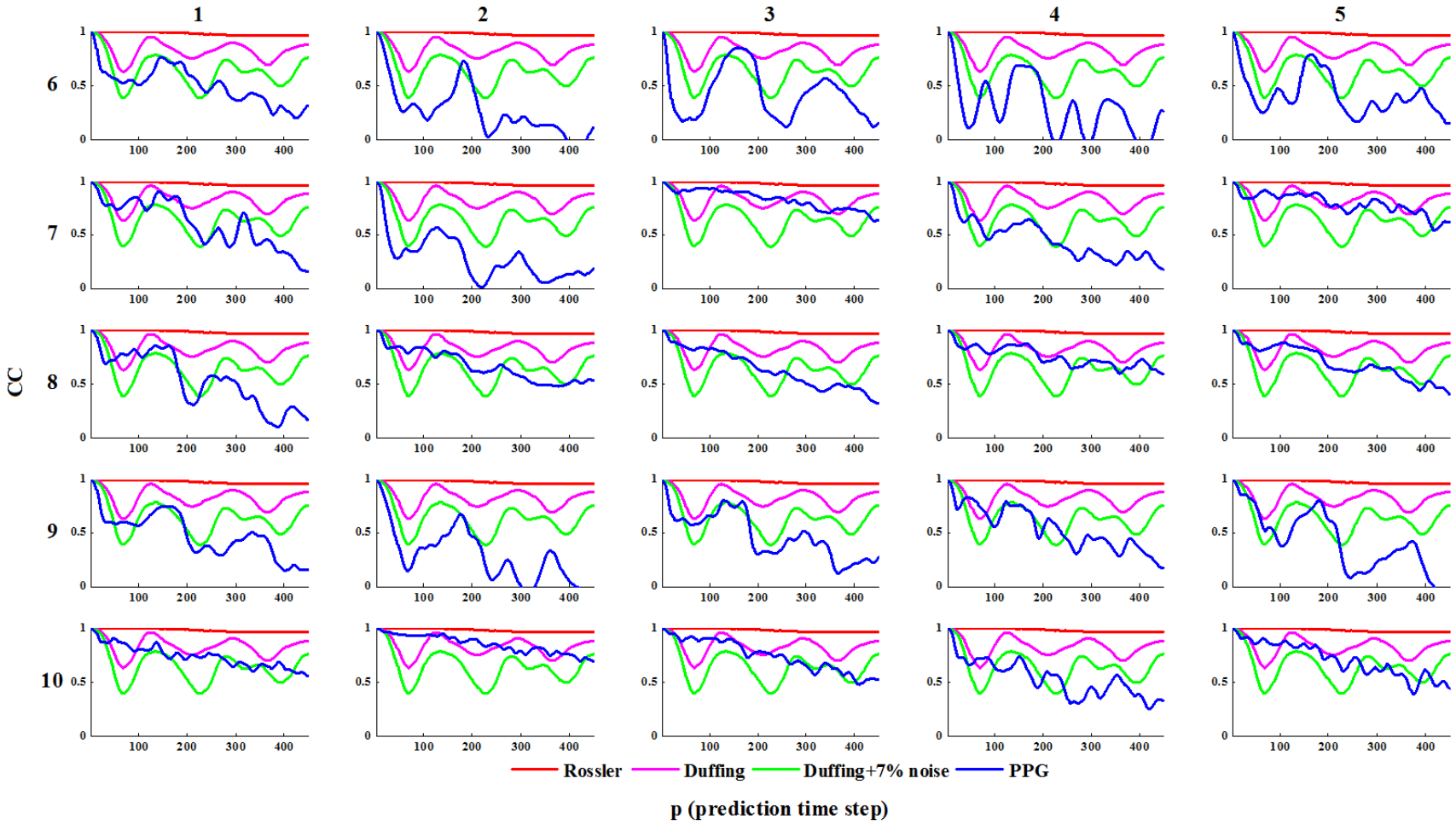

Fig. 3.4 *Correlation coefficient (CC) for deterministic nonlinear prediction of Rössler's single band chaos, chaotic Duffing's forced oscillator, chaotic Duffing's forced oscillator with 7% additive noise and the PPG for 5 measurement repeats (columns) of subjects 6-10 (rows).*

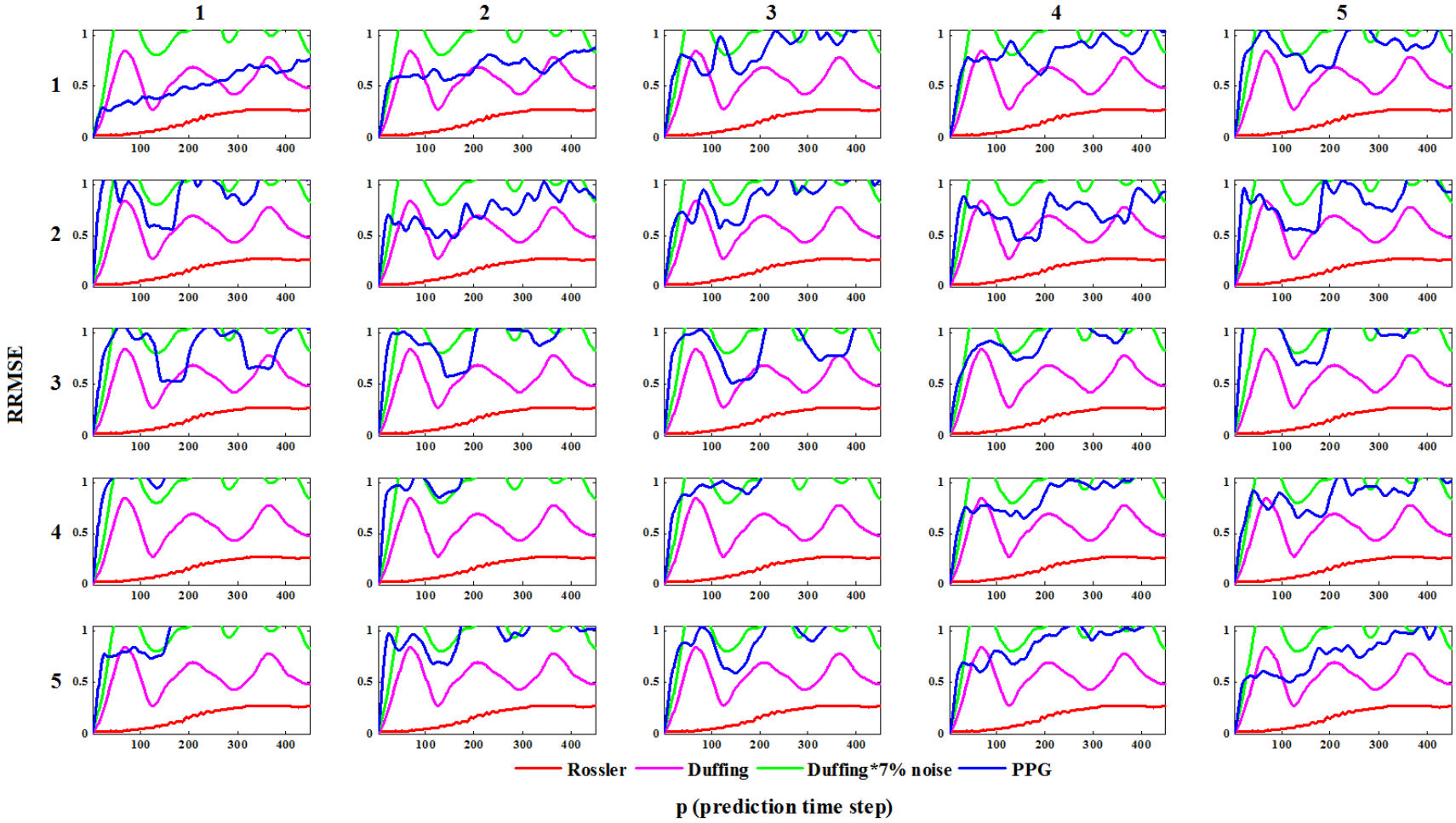

Fig. 3.5 *Relative root mean square error (RRMSE) for deterministic nonlinear prediction of Rössler's single band chaos, chaotic Duffing's forced oscillator, chaotic Duffing's forced oscillator with 7% additive noise and the PPG for 5 measurement repeats (columns) of subjects 1-5 (rows).*

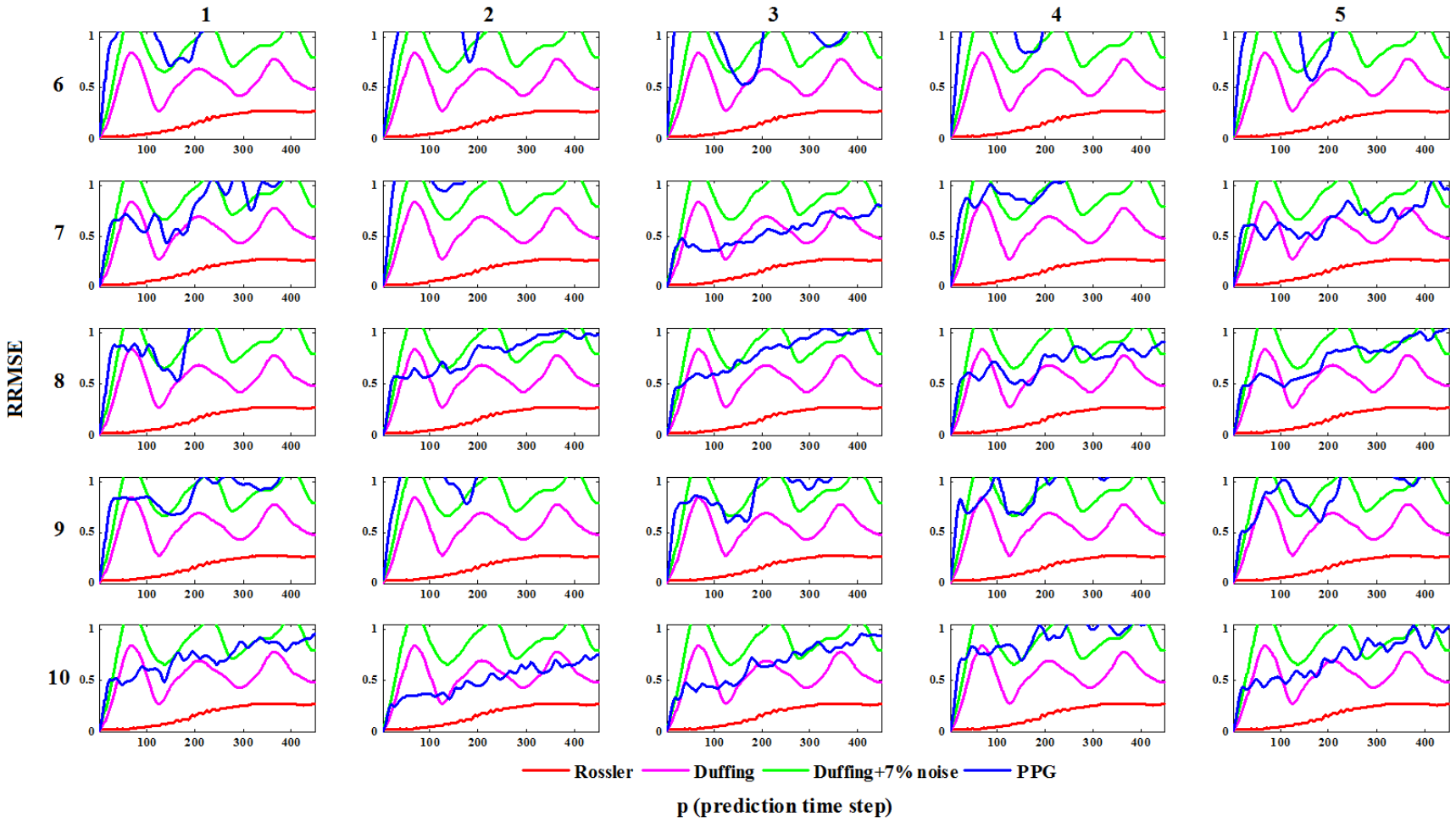

Fig. 3.6 *Relative root mean square error (RRMSE) for deterministic nonlinear prediction of Rössler's single band chaos, chaotic Duffing's forced oscillator, chaotic Duffing's forced oscillator with 7% additive noise and the PPG for 5 measurement repeats (columns) of subjects 6-10(rows).*

3.3.2. Local regional short-term prediction

In order to achieve a better understanding of local PPG dynamics by utilizing short-term prediction, 4 regions on the reconstructed trajectory (Fig. 3.7) were chosen empirically for conducting local short-term prediction. Examples of 4 similar local regions for the 1st subject's 1st measurement, 4th subject's 1st measurement, 8th subject's 1st measurement and 10th subject's 2nd measurement are shown in the first row of Fig. 3.8

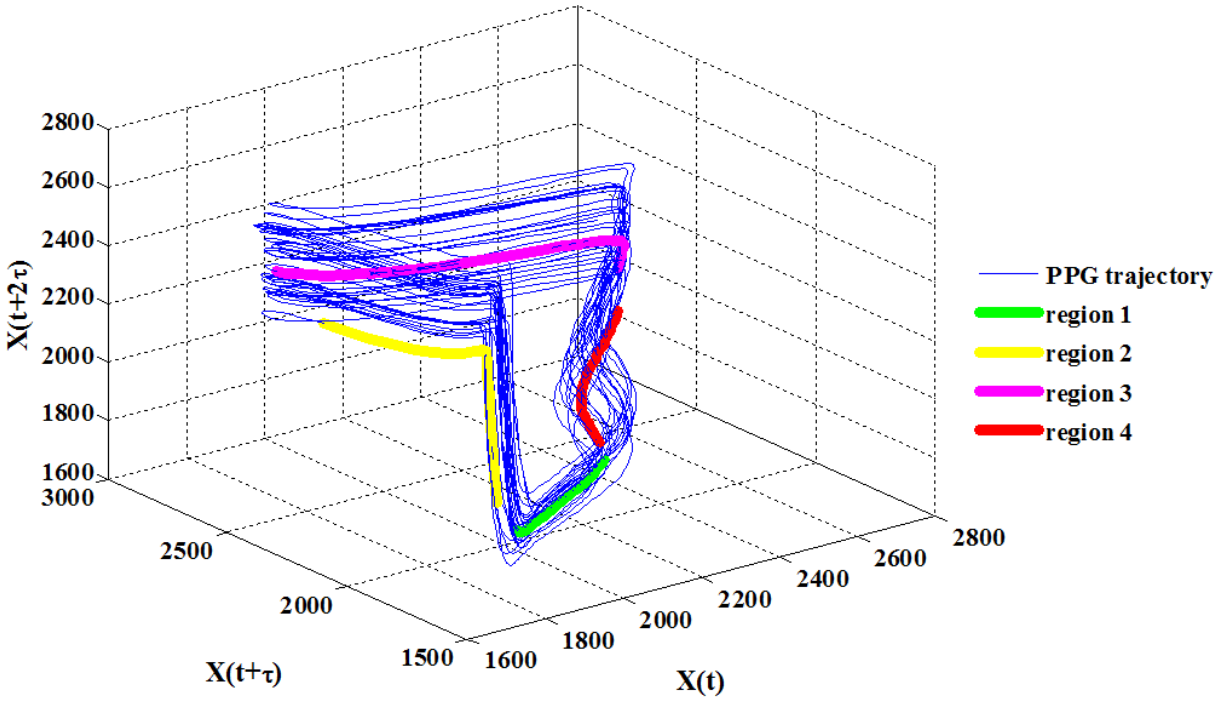

Fig. 3.7 *Four local regions on the portion of the reconstructed PPG trajectory in which local short-term prediction was conducted (for better visualization only part of the reconstructed trajectory is shown).*

The middle and bottom rows in Fig. 3.8 show the local CC and RRMSE, respectively, over the four chosen regions and global short-term DNP (blue lines). The upper row of Fig. 3.8 shows

the corresponding 4 regions on each reconstructed trajectory. As seen in Fig. 3.8 in the range of 1-5 steps forward prediction there is almost no observable difference in the prediction performance between different regions on the reconstructed trajectory for the CC, while clear differences can be seen in the RRMSE; and for predictions longer than 5 steps considerable differences in both local CC and RRMSE curve shape can be observed. Thus, DNP performance in regions 1, 3 and 4 (green, magenta and red lines) all show significantly different decreasing trends for shown subjects.

Fig. 3.8 demonstrates examples of local components that contribute to global short-term prediction performance after averaging along the reconstructed trajectory. With the same prediction step length, but different predictee, the predicted value may appear in a region with higher or lower averaged prediction performance, i.e. global CC or RRMSE values might be affected by local predictability. Therefore, predictability differences on the local level might be able contribute to understanding of significant fluctuations observed in global short-term predictions (Fig. 3.3-6).

A study of local predictability also allows the identification of regions with the lowest or highest prediction performance, thus for example for the 8^{th} subject's 1^{st} measurement (3^{rd} column in Fig. 3.8), among the 4 different regions shown on the trajectory, the lowest prediction performance is observed in region 2 (yellow line), which corresponds to the bending part of the reconstructed attractor. The highest prediction performance among 4 regions is observed in region 3 (magenta line) that according to Poincaré section corresponds to the folded part of the reconstructed trajectory.

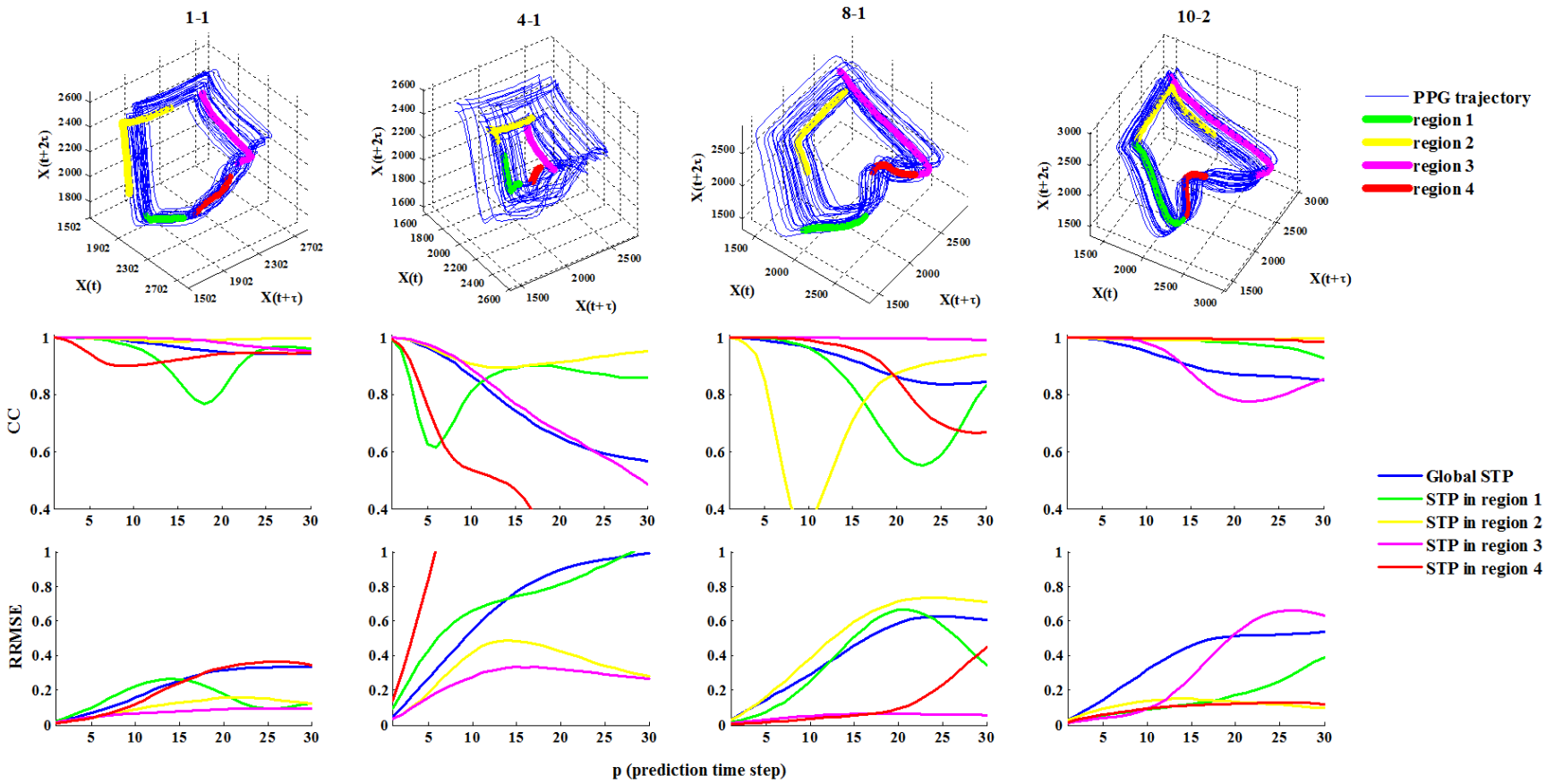

Fig. 3.8 *Four local regions on part of reconstructed PPG trajectory in which local short-term prediction was conducted (upper row); Correlation coefficient (CC) (middle row) and relative root mean squared error (RRMSE)(bottom row) curves for local short-term deterministic nonlinear prediction in 4 regions of reconstructed PPG trajectory for subjects 1, 4, 8 and 10.*

3.4. Discussion

The objective of this chapter was to provide additional insight into the short-term predictability of the PPG as it may uncover new characteristics of PPG dynamics and help to find answers to the questions that arose from the DNP results in Chapter 2. With regard to detecting chaotic motion in the PPG (Chapter 2), only the existence of short-term prediction needed to be proven, while its characteristics were of no interest. Besides that, none of the numerous studies dealing with conventional or nonlinear time series analysis of the PPG have investigated the behavior of short-term predictability. However as seen in Fig. 3.2-6, short-term prediction itself can provide useful and valuable information about the features of PPG dynamics. Thus, the performance of global (overall trajectory) short-term prediction showing rapid decline, which was not observed when the Rössler and Lorenz models were utilized, was found to be similar to short-term prediction properties of 7% noise induced Duffing's forced oscillator, even though the trajectory evolving process and PPG attractor topology were found to be similar to noise induced Rössler's single band chaos. Besides that, similarities in CC and RRMSE fluctuations could be observed in most of the PPG time series and noise induced chaotic Duffing's forced oscillator prediction performance, which were not observed for Rössler's CC and RRMSE. As Duffing's chaotic forced oscillator is classified as a non-autonomous system, these results reveal the possibility that PPG dynamics is a non-autonomous system, although further detailed investigation of the similarities between non-autonomous systems and the PPG is required.

An additional investigation of local predictability (Fig. 3.8) showed that depending on the region along the reconstructed trajectory, DNP performance can significantly differ from forming a slowly growing RRMSE curve (region 3 in Fig. 3.8 for subject 4) to its quick rise (region 4 in Fig. 3.8 for subject 4). These differences do not question the existence of short-term prediction, but emphasize the importance of studying local dynamics behavior. Predictability differences between local regions might be one of the reasons leading to significant fluctuations in the global CC and RRMSE curves.

3.5. Conclusion

In this chapter careful attention was paid to the performance of short-term prediction over the reconstructed trajectory, i.e. global DNP, as well as the local DNP. Global short-term prediction was investigated by comparisons with Duffing's forced oscillator in the chaotic regime. Results of a comparative study of the PPG signal, from one point of view, allowed a detailed study of the PPG short-term predictability properties and at the same time demonstrated certain similarities between global prediction performance of the PPG and 7% noise induced Duffing's forced oscillator. Additionally, results of the global short-term prediction emphasized that despite certain similarities in the dynamics properties with Duffing's data or trajectory topology with Rössler's single band chaos, the actual PPG underlying dynamics were not revealed and its aspects can only be investigated by comparative studies, as in the constructive approach. Based on these results it is expected that further comparative investigation of the PPG and non-autonomous systems might be beneficial for revealing the PPG dynamics properties.

Additional analysis of local predictability demonstrated that local regions along the reconstructed attractor have considerably different predictability. Since different areas on the PPG attractor refers to different phases of blood pulsation information of local, differences between regions on the reconstructed PPG trajectory might provide useful data for new application studies and a deeper understanding of the PPG dynamics. However, further investigation of the local characteristics of the reconstructed dynamics is required.

Chapter 4. Application of Photoplethysmogram for Detecting Physiological Effects of Tractor Noise

4.1. Introduction

Agriculture work-related operations can significantly affect farmers' health by exposure to various natural and artificial effects, such as heat, humidity, noise, vibration etc. Many studies have paid close attention to the physiological effect of whole-body vibration [Kittusami et al., 2004; Muzammil et al., 2004] and the problem of power machinery operator's hearing loss due to noise exposure [McBride et al., 2003; Murphy, 1992; World health organization]. However, the effects of agriculture machinery on the CVS, which consists of heart and vessels' network and transports blood through the body, results in even more hazardous consequences for the operator's health. These farm work related effects might be especially severe for aging farmers' health. Recently it has been reported by the Japanese Ministry of Agriculture, Forestry and Fisheries (MAFF) that a substantial number of farm workers in Japan are over 60 years old. Annually about 400 farmers die while performing agriculture work and 70% of these die while operating agriculture machinery [Takai et al., 1992; Takai, 2000]. According to MAFF data, the number of fatalities in the agricultural industry has remained stable over the last 40 years, while significantly decreasing in other sectors; for example, fatal cases in the construction sector have decreased 5-fold since 1971.

The need to protect farmer's health during farm work has made monitoring of CVS performance during exposure to agricultural machinery noise, vibration etc. an extremely important issue.

Nowadays the advantages of wireless and wearable sensor technology, such as installation flexibility, mobility, increased robustness and decreased maintenance complexity and cost have made it extremely useful and promising for various applications in the agriculture and food industries [Kawakura and Shibasaki, 2014; Wang et al., 2005]. However, there is still a shortage of techniques to deal with farm workers' health monitoring in the agricultural industry.

Exposure to heat, vibration, high level noise etc. has significant impact on cutaneous blood flow as shown in Table A.1. And PPG is one of commonly used nowadays techniques that allows registration of changes in cutaneous blood circulation.

Though tractor operator exposed to combination of various effects, physiological impact of each of them need to be studied carefully before assessment of factors combination can be done. Therefore this study sought to investigate the effect of tractor noise on the operator's CVS performance by utilizing a PPG finger sensor. In an attempt to develop a simple and reliable method to estimate changes in an operator's state of health during farming under noise exposure tools of nonlinear time series analysis, such as time-delay embedding and Wayland test along with Fourier analysis have been applied to the PPG signal measured on young subjects exposed to tractor sound (noise level exceeding 80 dBA) and in a controlled environment with background noise (noise level less than 43dBA) to obtain indexes reflecting changes in CVS output.

4.2. Materials and Methods

Data were collected from seven healthy 20- to 25-year old volunteers among students of Tokyo University of Agriculture and Technology (TUAT). Experimental data collection was approved by TUAT authorities. Written informed consent was obtained from participants prior the experiment. At the time of the study all subjects were healthy, physically active to similar levels, were not taking any medication, and none declared a history of heart disease. The PPG signal first was recorded with the subject in a relaxed sitting position in a controlled environment with background noise level and then with tractor sound corresponding to engine speeds at 900 rpm (low), 1900 rpm (medium) and 2750 rpm (high). A T125F ISEKI tractor was used for generating sound. During data collection with tractor noise exposure subjects were facing the right side of the tractor at a distance of 1.5 m from the tractor engine (Fig. 4.1).

For each condition two measurement repeats were conducted. The measurement period was 5 min with 5 msec sampling steps. For all data collection sessions, a BACS (Computer convenience, Inc.) transmission-mode pulse oximeter (Fig. 2.1) was located on the right

forefinger same as in the experiment described in section 2.2. The first measurement was preceded by a blood pressure check.

Fig. 4.1 *Data collection experiment under exposure of tractor noise.*

Examples of data collected from the same subject with background noise level and under exposure to high noise are shown in Fig. 4.2(a) and Fig. 4.3 (a) respectively. Fig. A.31-32 show all collected PPG time series. The noise level was measured at the head of the subject using a CUSTOM SL-1370 sound level meter. The measured averaged noise levels for reference (background noise) and three engine speeds (low, medium and high) were 42dBA, 72dBA, 82dBA and 87dBA, respectively.

4.3. Results and Discussion

The PPG as a physiological signal derived from the cardiovascular system shows an extreme intricacy arising from the interaction of many processes, structure units and feedback loops in humans. As it was demonstrated in the Chapter 2 among various methods applicable for analyzing and extracting information from such a complex signals like the PPG, methods of nonlinear time series analysis appear to be useful for studying the underlying properties of the signal. In this study Fourier analysis, time-delay reconstruction technique and the Wayland test were applied to collected PPG data.

4.3.1. Fourier Analysis

Spectral analysis is one of the widely used tools for time series, including PPG signal [Akar et al., 2013], analysis. In this study spectral analysis was applied to the PPG data. Examples of typical plots of the spectrum in the studied time series corresponding to background noise level and the PPG recorded under high noise exposure are shown in Fig. 4.2 (b) and Fig. 4.3 (b), where the predominant component's period (HF) is approximately equal to the heart beat cycle period. Lower frequency components (LF) correspond to respiration and other effects, such as thermoregulation and nervous system activity. Results of Fourier analysis for all PPG time series are show in Fig. A.33-34.

One of indexes typically applied for heart rate variability studies is the ratio of lower frequency to high frequency, which is equal in this study to fundamental component frequency, correspondingly LF and HF in Fig. 4.2 (b) and Fig 4.3 (b). This ratio is recognized as a useful index for assessing cardiac sympatho-vagal balance for healthy subjects [Pagani et al., 1986; Reyers et al., 2013]. The ratio of these two significant frequency components (LF/HF) is shown in Table 4.1.

TABLE 4.1 Value of LF/HF under exposure to noise.

Noise level	Repeat	Subject						
		1	2	3	4	5	6	7
Ref.,	1	0.195	0.464	0.808	0.387	0.504	0.183	0.736
42 dBA	2	0.227	0.472	0.878	0.54	0.34	0.335	1.36
Low,	1	0.411	0.608	1.184	0.382	0.253	0.277	0.57
72 dBA	2	0.527	0.918	1.278	336	0.322	0.262	0.621
Med.,	1	0.681	0.855	1.421	0.377	0.482	0.155	1.516
82 dBA	2	0.46	1.366	1.467	0.711	0.679	0.456	2.244
High,	1	0.579	0.979	0.868	0.815	0.406	0.332	1.616
87 dBA	2	0.657	1.361	1.344	0.887	1.01	0.264	1.452

4.3.2. Time-Delay Embedding

Following time-delay embedding method performed in Chapter 2, the time lag for the embedding have been defined as a quarter of the period of the spectrum predominant component

and have been reconstructed PPG trajectory in 4-dimensional phase-space. An example of typical data for a time-delay reconstructed attractor for cases of background and high tractor noise is shown in Fig. 4.2 (c) and Fig. 4.3 (c), respectively. Time-delay reconstructed trajectories for all PPG time series are show in Fig. A.35-36.

The Fig. 4.2 (c) represents typical reconstructed attractor's structure for PPG data obtained from healthy young subject in resting condition. This result is similar with reconstructed trajectory obtained for healthy subjects in the Chapter 2. Trajectories in shown attractor are continuously bending due to that folding is realized. As it can be seen from Fig. 4.2 (c) and Fig. 4.3 (c) attractor's geometry may change depend on subject's physical condition; under noise exposure attractor shrinks and PPG variability decreases, at the same time structure of attractor in Fig. 4.3-c became unclear, comparing with one corresponding to resting condition in Fig. 4.2 (c).

4.3.3. Wayland Test

Analogically to Chapter 2 the Wayland test was applied to all collected time series. Table 4.2 shows the results of WTE calculations. As it can be seen all WTE values are enough small to conclude corresponding time series are deterministic.

TABLE 4.2 Translation Error values under exposure to noise.

Noise level	Repeat	Subject						
		1	2	3	4	5	6	7
Ref.,	1	0.02	0.007	0.025	0.007	0.014	0.006	0.021
42 dBA	2	0.025	0.007	0.044	0.007	0.013	0.01	0.031
Low,	1	0.048	0.011	0.037	0.007	0.01	0.012	0.02
72 dBA	2	0.031	0.016	0.035	0.007	0.013	0.011	0.019
Med.,	1	0.064	0.017	0.027	0.01	0.016	0.012	0.039
82 dBA	2	0.06	0.024	0.028	0.01	0.03	0.017	0.076
High,	1	0.047	0.016	0.013	0.025	0.016	0.02	0.07
87 dBA	2	0.073	0.024	0.025	0.02	0.042	0.017	0.057

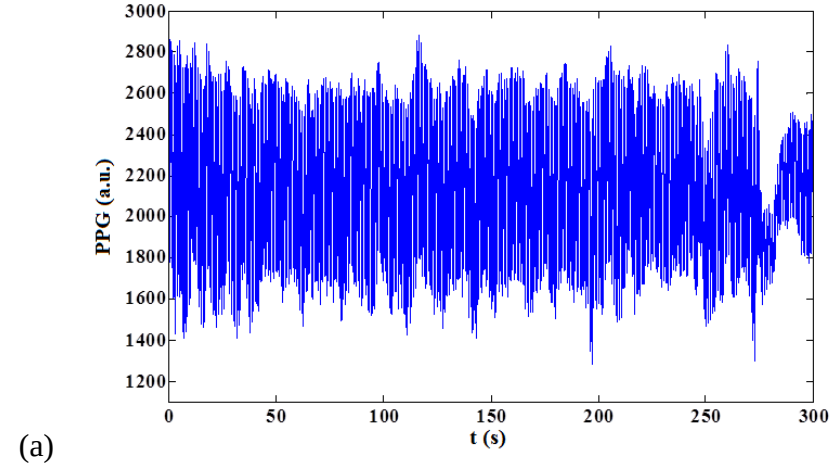

(a)

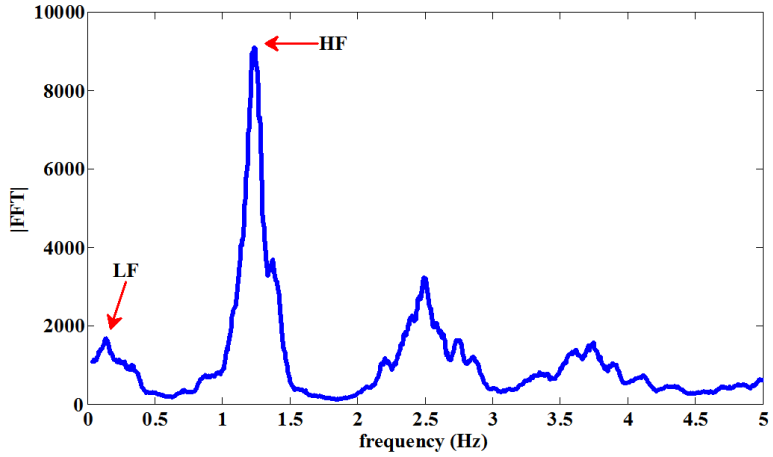

(b)

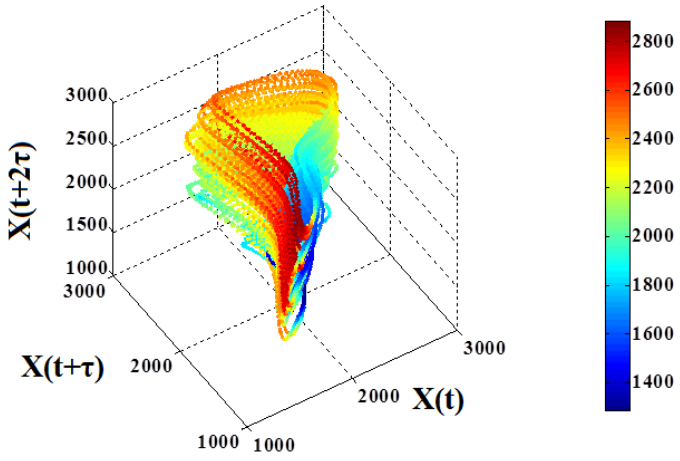

(c)

Fig. 4.2 *Case of background noise level: (a) PPG time series; (b) Fourier spectrum; (c) time-delay reconstructed trajectory.*

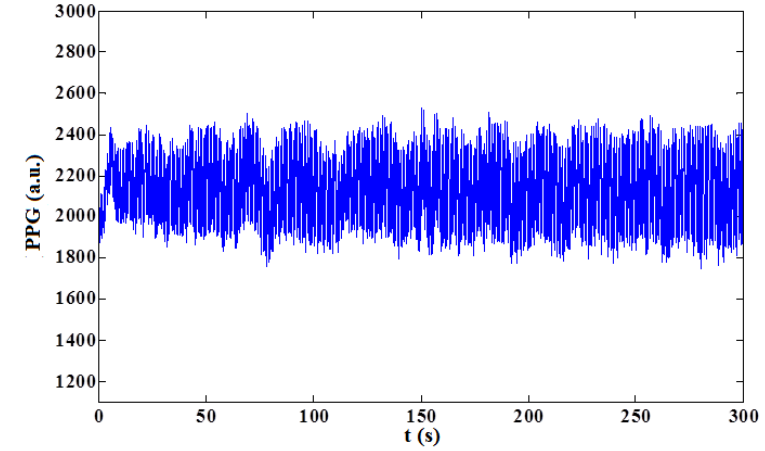

(a)

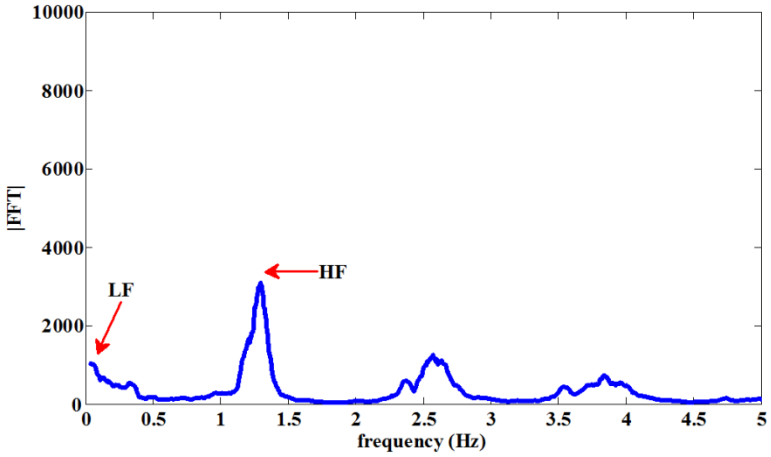

(b)

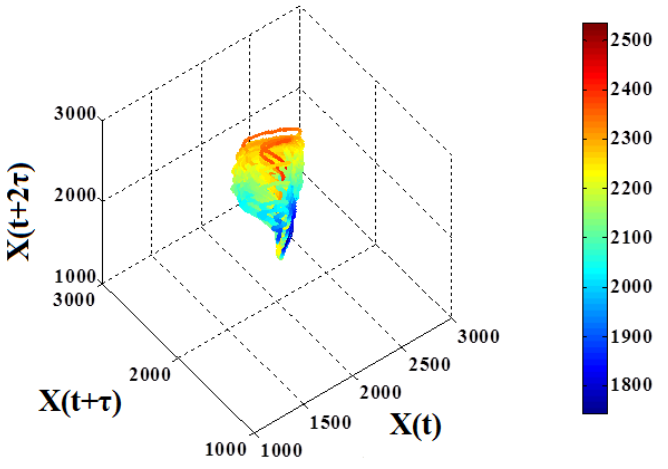

(c)

Fig. 4.3 *Case of tractor high level noise: (a) PPG time series; (b) Fourier spectrum; (c) time-delay reconstructed trajectory.*

4.3.4. Statistical Analysis

Two significant frequency components: LF and HF, the ratio LF/HF and WTE were tested with Welch's t-test, one- and two-factor ANOVA tests, where noise level was factor for one-factor ANOVA, noise and subjects were factors for two-factor ANOVA. Results are summarized in Table 4.3, which reflects the significance level α with which the null hypothesis of equal sample means is rejected. Only noise levels higher than 80 dBA are considered to be potentially harmful for human health. Table 4.4 presents permissible maximum times for noise exposure. Highlighted values indicate noise levels to which subjects were exposed during data collection. Results shown in Table 4.3 take into account noise only for medium (1900 rpm) and high engine speeds (2750 rpm), since the noise level for both of them was higher than 80 dBA.

Results demonstrated that HF and the LF/HF ratio corresponding to the reference data and data taken during tractor noise exposure differ significantly. According to Table 4.3, results obtained from Fourier analysis and the WTE could clearly distinguish between background and noisy conditions and in most of the tests α corresponding to the WTE was not larger than that for HF, LF/HF. Additionally, prevailing small values of calculated WTE indicated the deterministic nature of the PPG signal despite the presence or absence of noise. Two factor ANOVA tests showed that along with the noise level, personal features of subjects can also affect the HF, LF/HF values, while WTE is less dependent on each individual subject. This advantage of WTE makes it useful for application in health monitoring in various fields including agriculture.

TABLE 4.3 Results of t-test and ANOVA tests for the equal sample means null hypothesis check for HF, LF, LF/HF and WTE indexes.

		HF	LF	LF/HF	WTE
T-test	Ref vs. Med&High	--	0.1	0.1	0.005
ANOVA 1F	Ref vs. Med	0.05	--	0.05	0.05
	Ref vs. High	0.05	--	0.05	0.025
	Ref vs. Med&High	0.05	--	0.1	0.025
ANOVA 2F	Noise level	0.001	0.025	0.025	0.001
	Subject	0.001	0.001	0.001	--

TABLE 4.4 Noise levels and maximum noise exposure time [WHO].

Exposure level, dBA	80	82	85	88	91	94	97
Max exposure time, h	24	16	8	4	2	1	0.5

4.4. Conclusion

The results demonstrate that the WTE, as well as widely used HF and LF/HF indexes obtained by Fourier analysis, can be useful tools for assessing CVS performance under different noise conditions and are able to distinguish between data taken during exposure to tractor engine noise and background noise levels. Moreover, according to Table 4.3, the WTE appeared to be a statistically more reliable index than HF and LF/HF since it can differentiate data obtained under different levels of noise with lower significance level α. In addition, WTE is likely to be more generally applicable than HF and LF/HF due to its independence from individual subjects. Additionally, WTE revealed the presence of determinism in all measured data, which is an important characteristic of CVS processes.

This study revealed that the WTE is a valuable tool for assessing physiological burden in resting condition under exposure to different levels of noise while noise level does not have significant changes during each measurement. However, during real farm operations involving power machinery noise level would not be stable as well as operator would experience significant physiological load from vibration, temperature changes, etc. besides noise. Therefore it can be suggested that the ability of the WTE to indicate changes in the PPG arising due to noise exposure expected to be useful for upcoming studies on detecting physiological effects in environment with continuously changing noise and in conditions when operator exposed to combination of noise and other effects produced by agriculture machinery. Thus the WTE can be a useful index used for effective real-time monitoring of the CVS condition of farmers during their operation of agriculture machinery. Real time CVS monitoring is expected to decrease hazards to farmers' health.

Chapter 5. Perspective and conclusions

5.1 Perspective

The main motivation for this study was fact even though photoplethysmography technology has been used for decades and has become routinely used in health monitoring, the dynamics of the PPG signal is still not well studied and it remains unclear what type of process underlies the PPG. Despite several reports claiming the chaotic nature of the PPG in the early 1990s, it is still unclear whether PPG dynamics involves chaotic motion or not. Inspired by the idea that a better understanding of PPG dynamics and its properties may allow one to discover new possibilities for medical applications and stimulate improvement of existing health care technologies, this study have been undertaken to achieve the ultimate goal to prove that PPG dynamics is consistent with chaotic motion and to provide a comprehensive toolkit that can reveal PPG's chaotic dynamics characteristics. In addition, this study aimed to demonstrate the usefulness of methods of nonlinear time series analysis for application studies. Considering the increasing proportion of aging farmers in the agricultural industry, an additional aim of this thesis was to provide an example of the application and usefulness of nonlinear time series methods to CVS health monitoring of agriculture workers.

To fulfill these objectives, in this study two sets of data were collected. The first experiment was designed to obtain reference PPG time series from young healthy subjects that were not affected by external disturbances, such as noise, temperature fluctuations, vibration, and high light intensity, in the absence of any effects of mental activity, stress, sickness, etc. In the second experiment, data were collected from subjects that were affected by different levels of external noise produced by agriculture machinery, while other conditions were similar to the first experiment. Both experiments were conducted in a controlled environment taking into account factors that may considerably affect the PPG signal.

To meet the ultimate goal of this study, comprehensive nonlinear time series analyses were applied to the collected PPG time series. Methods of nonlinear time series analysis were

carefully chosen in order to test all defining properties of chaotic dynamics. Methods of nonlinear time series analysis were conducted using a set of programs developed in MATLAB.

Selected methods were applied to the data collected in circumstances of noise produced by agriculture machinery to demonstrate the applicability of the PPG signal for detection of physiological effects of noise, which act as an external irritant, and to illustrate the usefulness of nonlinear time series methods in distinguishing the effects of different levels of noise on the PPG.

5.2 Conclusions

1. Comprehensive nonlinear time series analysis. Results of the PPG signal investigation based on comprehensive nonlinear time series analysis described in Chapter 2 allowed to conclude that PPG data from young human subjects is consistent with motion on a strange attractor. Due to comparative investigation in accordance with the constructive approach of the PPG and Rössler's single band chaos, a topological similarity between the PPG reconstructed trajectory and Rössler's single band chaos was found. As a result, PPG's reconstructed attractor was classified as a folded band type. Additionally, the obtained results demonstrated the effectiveness of the designed comprehensive nonlinear time series analysis methodology as a chaotic dynamics investigation toolkit, which covers most essential properties of a chaotic signal.

2. Short-term predictability properties of the PPG. It was also found that deterministic nonlinear prediction, which has not previously been applied either to a theoretical investigation or to an applied study of PPG dynamics, is quite useful for chaotic dynamics investigation and is also a promising tool for future application studies. Additional investigation was devoted to the short-term predictability properties of the PPG signal in Chapter 3. These results demonstrated that the PPG signal's global (corresponding to overall reconstructed trajectory) and local (in a fixed region on the reconstructed trajectory) dynamics may differ considerably. This finding clearly demonstrates that detailed PPG dynamics investigations cannot concentrate only on global or local dynamics. In addition, it creates an opportunity for further improvement of photoplethysmographic technology applications in health monitoring, as PPG trajectory local

regions can be associated with different phases of blood circulation, which is correlated with heart cycles. Additionally results of global short-term prediction were found to be similar to the DNP performance of the chaotic Duffing's forced oscillator. It implies that different aspects of complex PPG dynamics can be reproduced by various chaotic models and depend on study objectives well-known chaotic models, such as Rössler's single band chaos or chaotic Duffing's forced oscillator, can be utilized for comparative study of the PPG signal's chaotic properties. However none of the discussed models' dynamics is identical to the PPG dynamics, and only a comparative understanding of the PPG properties was achieved.

3. Application for Agricultural Ergonomics. An application study related to occupational health monitoring was conducted in Chapter 4 and its results allow to conclude that the PPG signal itself and in particular, the nonlinear time series analysis of the PPG is highly valuable for health monitoring applications in the agricultural field, as PPG can potentially be used for detecting physiological changes in agriculture workers' blood circulation during the operation of farm machinery or while performing other agricultural work. The results obtained also emphasized the usefulness of nonlinear time series analysis methods for detecting blood circulation changes via the PPG signal compared with conventional analysis.

In summary, it can be concluded that comprehensive nonlinear time series analysis has high potential for effective and reliable PPG dynamics investigation. Its application to the PPG will not only improve one's understanding of PPG dynamics, but also stimulate the development of new PPG signal-based applications for health monitoring in general and particularly in the agricultural industry.

References

Abarbanel, H. D. I. The analysis of observed chaotic data in physical systems. Rev. of modern physics 1993;65:1331-1392.

Agache, P. G., Dupond, A.-S. Assesment of scin blood flow in vascular diseases. Bioengineering of the skin: Cutaneous Blood Flow and Erythema. CRC Press, USA. 1995, pp. 155-170.

Akar, S. A., Kara, S., Latifoglu, F., Bilgic, V. Spectral analysis of photoplethysmographic signals: The importance of processing. Biomedical signals processing and control 2013;8:16-22.

Allen, J. Photoplethysmography and its application in clinical physiological measurement. Physiological measurement 2007;28:1-39.

Bernardi, L., Leuzzi, S. Laser Doppler flowmetry and photoplethysmography: basic principles and hardware. Bioengineering of the skin: Cutaneous Blood Flow and Erythema. CRC Press, USA. 1995, pp. 31-56.

Bezruchko, B.B., Smirnov, D.A., Extracting Knowledge From Time Series. Springer, Berlin, 2010.

Bortolotto, L. A., Blacher, J., Kondo, T., Takazawa, K., Safar, M. E. Assesment of vascular aging and atherosclerosis in hypertensive subjects: second derivative of photoplethysmogram versus pulse wave velocity. American journal of hypertension 2000;13:165-171.

Cao, L. Practical method for determining the minimum embedding dimension of a scalar time series. Physica D 1997;110:43-50.

Elgendi, M. Detection of c, d and e waves in the acceleration photoplethysmogram. Computer methods and programs in biomedicine 2014;117:125-126.

Elgendi, M. On the analysis of fingertip photoplethysmogram signals. Current cardiology reviews 2012;8:14-25.

Elgendi, M., Jonkman, M., DeBoer, F. Heart rate variability and the acceleration plethysmogram signals measured at rest. Biomedical engineering systems and technologies. Springer-Verlag Berlin Heidelberg 2011, pp. 266-277.

Elgendi, M., Norton, I., Brearley, M., Abbot, D., Schuurmans, D. Detection of a nd b waves in the acceleration photoplethysmogram. Biomedical engineering online 2014;13:1-18.

Ende, M., Louis, A. K., Maass, P., Mayer-Kress, G. EEG signal analysis by continuous wavelet transform techniques. Nonlinear analysis of Physiological data. Springer, Berlin, 1998, pp. 213-220.

Fedotov, A. A., Akulov, S. A. Matematicheskoe modelirovanie i analiz pogreshnostei izmeritel'nykh preobrazovatelei biomeditsinskikh signalov (Mathematical modeling and error analysis of biomedical signal transducers). FIZMATLIT, Moscow; 2013. (in Russian).

Fujimoto, Y., Yamaguchi, T. valuation of mental stress by analyzing accelerated plethysmogram applied chaos theory and examination of welfare space installed user's vital sign. Proceedings of the 17th world congress the international federation of automatic control 2008:8232-8235.

Gil, E., Vergara, J. M., Laguna, P. Detection of decreases in the amplitude fluctuation of pulse photoplethysmography signal as indication of obstructive sleep apnea syndrome in children. Biomedical signal processing and control 2008;3:267-277.

Glass, L. Introduction to controversial topics in nonlinear science: is the normal heart rate chaotic? Chaos 2009;19:1-4.

Goldenberg, A. L., Rigney, D. R., West, B. j. Chaos and fractals in human physiology. Scientific American 1990: 43-49.

Han, H., Kim, J. Artifacts in wearable photoplethysmographs during daily life motions and their reduction with least mean square based active noise cancellation method. Computers in biology and medicine 2012;42:387-393.

Hashimoto, J., Chonan, K., Aoki, Y., Nishimura, T., Ohkubo, T., Hozawa, A., Suzuki, M., Matsubara, M., Araki, T., Imai, Y. Pulse wave velocity and the second derivative of the finger photoplethysmogram in treated hypertensive patients: their relationship and associating factors. Journal of hypertension 2002;20:2415-2422.

Higgins, J. L., Froner, A. Photoplethysmographic evaluation of the relationship between skin reflectance and skin blood volume. J. Biomed. Eng. 1986;8:1130-136.

Hiroyasu, I. Changes in coronary heart disease risk among Japanese. Circulation 2008;118:2725-2729.

Iokibe, T., Kurihara, M., Maniwa, Y., Ohta, S., Uchida, I., Amata, M., Yamamoto, M. Chaos-based quantitative health evaluation and disease state estimation by acceleration plethysmogram. Japan society for fuzzy theory and intelligent informatics 2003;15(5): 565-576.

Ivanov, P. Ch., Nunes Amaral, L. A., Goldberger, A.L. and et. al. Multifractality in human heartbeat dynamics. Nature 1999;399:461-465.

Japanese Ministry of Health, Labour and Welfare statistical reports: http://www.mhlw.go.jp/toukei/list/81-1a.html

Kamal, A. A. R., Harness, J. B., Irving, G., Mearns, A. J. Skin photoplethysmography – a review. Computer methods and programs in Biomedicine1989;28:257-269.

Kawakura, S., Shibasaki, R. Wearable sensors to measure and analyse outdoor agricultural workers' motion. Agricultural Information research 2014; 23:82-102. (In Japanese).

Kennel, M., B., Brown, R., Abarbanel, H., D., I. Determining embedding dimension for phase-space reconstruction using a geometrical construction. Physical review A 1992;45(6):3403-3411.

Kittusamy, N. K., Buchholz, B. Whole-body vibration and postural stress among operators of construction equipment: A literature review. Journal of safety research 2004;35:255-261.

Kohjitani, A., Miyata, M., Iwase., Y., Ohno, S., Tohya, A., Manabe, Y., Hashiguchi, T., Sugiyama, K. Association between autonomic nervous system and the second derivative of the finger photoplethysmogram indices. Journal of atherosclerosis and thrombosis 2015;21:1-8.

Komatsu, K.-I., Fukutake, T., Hattory, T. Fingertip photoplethysmography and migraine. J. of the neurological sciences 2003;216:17-21.

Letellier, C. Chaos in nature. World scientific series on nonlinear science, series A, vol. 81. Singapore, 2013.

Lorenz, E., N. Deterministic nonperiodic flow. Journal of the atmospheric science 1963;20:130-141.

Maniwa, Y., Tokutaka, H., Fujimira, K., Ohkita, M., Iokibe, M., Tada, K. Use of chaos and self-organizing maps for acceleration plethysmogram information. Japan society for fuzzy theory and intelligent informatics 2004;16(3):253-261.

Mascro, S.A., Asada, H.H. Photoplethysmograph Fingernail Sensors for measuring Finger Forces Without Haptic Obstruction. IEEE transaction on robotics and automation 2001;17:698-708.

McBride, D. I., Firth, H. M., Herbison, G. P. Noise exposure and hearing loss in agriculture: a survey of farmers and farm workers in the southland region of New Zeland. JOEM 2003;45(12):1281-1288.

McClintock, P. V. E., Stefanovska, A. Noise and determinism in cardiovascular dynamics. Physica A 2002;314: 69-76.

Miao, T., Oyama-Higa, M., Sato, S., Kojima, J., Reika, S. Chaos of Photoplethysmogram in relation to scalp-EEG: a model and experiments. Int. J. Computer aided Engineering and technology 2012;4(6):557-566.

Miao, T., Shimizu, Shimiyama, O., Oyama-Higa, M. Modelling plethysmogram dynamics based on baroreflex under higher cerebral influences. IEEE international conference on systems, man and cybernetics 2006: 2868-2873.

Miao, T., Shimizu, T., Makabe, H., Oyama-Higa, M., Sakamoto, K. Chaos in ear plethysmograms: tracking experiment and a model. IEEE international conference on systems, man and cybernetics 2008: 2982-2987.

Millasseaua S. C., Ritter J. M., Takazawa K., Chowienczyk P. J. Contour analysis of the photoplethysmographic pulse measured at the finger. Journal of Hypertension 2006, 24:1449–1456.

Ministry of Agriculture, Forestry and Fisheries (MAFF). Annual reports and statistics: http://www.maff.go.jp/e/

Murphy, D. J. Safety and health for production agriculture. USA: The American society of agriculture engineers; 1992.

Muzammil, M., Siddiqui, S. S., Hasan, F. Physiological effect of vibration on tractor drivers under variable ploughing conditions. Journal of occupational health 2004;46:403-409.

Nakajima, K., Tamura, T., Miike, H. Monitoring of heart and respiratory rates by photoplethysmography using a digital filtering technique. Med Eng. Phys. 1996;18(5):365-372.

National heart foundation of Australia. Data and statistics. Web page online access: *http://www.heartfoundation.org.au/information-for-professionals/data-and-statistics/Pages/default.aspx*

Packard, N. H., Crutchfield, J. P. , Farmer, J. D., Shaw, R. S. Geometry from a Time Series. Phys. Rev. Lett. 1980;45:712-716.

Pagani, M., Lombardi, F., Guzzetti, S., Rimoldi, O., Furlan, R., Pizzinelli, P., Sandrone, G., Malfatto, G., Dell'Oro, S., Piccaluga, E. Power spectra analysis of heart rate and arterial pressure variabilities as a marker of sympatho-vagal interaction in man and conscious dog. Circulation research 1986;59:178-193.

Paluš, M. Chaotic measures and real-world systems: does the Lyapunov exponent always measure chaos? Nonlinear analysis of Physiological data. Springer, Berlin, 1998, pp. 49-67.

Perc, M. Nonlinear time series analysis of the human electrocardiogram. European Journal of physics 2005;26:757-768.

Perez-Martin, A., Meyer, G., Demattei, C., Böge, G., Laroche, J.-P., Quere, I., Dauzat, M. Validation of a fully automatic photoplethysmographic device for toe blood pressure measurement. Eur. J. Vasc. Endovasc. Surg. 2010:1-6.

Pham, T.D., Thang, T.C., Oyama-Higa, M., Sugiyama, M. Mental-disorder detection using chaos and nonlinear dynamical analysis of photoplethysmographic signal. Chaos, Solitons & Fractals 2013;51:64-74.

Pilt, K., Ferenets, R., Meigas, K., Lindberg, L.-G., Temitski, K., Viigimaa, M. New photoplethysmographic signal analysis algorithm for arterial stiffness estimation. The scientific world journal 2013: 1-9.

Poon, C.-S., Merrill, C.K. Decrease of cardiac chaos in congestive heart failure. Nature 197;389:492 – 495.

Reyers Del Paso, G. A., Langewitz, W., Mulder, L. J. M., Roon, A. V. The utility of low frequency heart rate variability as an index of sympathetic cardiac tone: A review with emphasis on a reanalysis of previous studies. Physiology 2013; 50:477-487.

Sakai, K. Nonlinear Dynamics and Chaos in Agricultural Systems, Elsevier, Netherlands, 2001.

Sakai, K., Noguchi, Y., Asada, S. Detecting chaos in a citrus orchard: Reconstruction of nonlinear dynamics from very short ecological time series. Chaos, Solitons & Fractals 2008;38(5):1274-1282.

Sato, S., Miao, T.,Oyama-Higa, M. Studies on five senses treatment. Knowledge-based systems in biomedicine. Springer-Verlag Berlin Heidelberg, 2013, pp. 155-175.

Schäfer, A., Vagedes, J. How accurate is pulse rate variability as an estimate of heart rate variability? A review on studies comparing photoplethysmographic technology with an electrocardiogram. International journal of cardiology 2013;166:15-29.

Serup, J. Cutaneous blood flow and erythema: standardization of measurements. Bioengineering of the skin: Cutaneous Blood Flow and Erythema. CRC Press, USA. 1995, pp. 57-64.

Shelhamer, M. Nonlinear Dynamics in Physiology. A state-Space Approach, World Scientific, Singapore, 2007.

Shelley, K. H. Photoplethysmography: beyond the calculation of arterial oxygen saturation and heart rate. Anesthesia and analgesia 2007;105(6):31-36.

Shi, P., Zhu, Y., Allen, J., Hu, S. Analysis of pulse rate variability derived from photoplethysmography with the combination of lagged Poincaré plots and spectral characteristics. Medical engineering and physics 2009;81:866-871.

Skinner, J. E., Zebrowski, J. J., Kowalic, Z. J. New nonlinear algorithms for analysis of heart rate variability: low-dimensional chaos predicts lethal arrhythmias. Nonlinear analysis of Physiological data. Springer, Berlin, 1998, pp. 129-167.

Small, M., Tse, C. K., Ikeguchi, T. Chaotic Dynamics and Simulation of Japanese Vowel Sounds. Proceedings of the 2005 European Conference on Circuit Theory and Design 2005:2:169-172.

Small, M., Yu, D., Harrison, R. G. Surrogate Test for Pseudoperiodic Time Series Data. Physical review letters 2001;87(18):1-4.

Sumida, T., Arimitu, Y. Mental conditions reflected by the chaos of pulsation in the capillary vessels. International journal of bifurcation and chaos 2000;10(9):2245-2255.

Sviridova, N., Sakai, K. Distinguishing Deterministic Chaos and Periodicity in Human Photoplethysmogram. Proceedings of International Symposium on Nonlinear Theory and its Applications 2014;537-540.

Takai, M. Overview of regional 36516-farm accidents in 13-years and the safety engineering for farm equipment. Journal of the Japanese society of agricultural machinery 2000;62:4-7. (In Japanese)

Takai, M., Hata, S.-I., Sakai, K. Studies on the farm fatal accidents in Hokkaido. Part 2. General aspects and accidents on the road. Japanese journal of farm work research 1992;27(2):139-145.

Tamura, T., Maeda, Y., Sekine, M., Yoshida, M. Wearable photoplethysmographic sensors – Past and present. Electronics 2014;3:282-302.

The Heart foundation of U.S. Heart disease: scope and impact. Web page online access: *http://www.theheartfoundation.org/heart-disease-facts/heart-disease-statistics/*

The national heart foundation of New Zealand. Statistics. Web page online access: *http://www.heartfoundation.org.nz/know-the-facts/statistics*

Theiler, J. On the evidence of low-dimensional chaos in an epileptic electroencephalogram. Physics letters A 1995;196:335-341.

Theiler, J., Eubank, S., Longtin, A., Galdrikian, B., Farmer, D. Testing for nonlinearity in time series: the method of surrogate data. Physica D 1992;58:77-94.

Thiyagarajan, R., Kathirvel, K., Jayashree, G. C. Ergonomic intervention in sugarcane harvesting knives. African journal of agricultural research 2013;8(6):574-581.

Thompson, J. M. T., Stewart, H. B. Nonlinear dynamics and chaos. John Wiley and sons, U.K., 1991.

Tsuda, I. Chaotic pulsation in human capillary vessels and its dependence on mental and physical conditions. International journal of Bifurcation and chaos 1992;2(2):313-324.

Usman, S., Rozi, R. M., Reaz, M. B. I., Ali, M. A. M., Analysis of area under curve of PPG and its relation with HbA1c. IEEE EMBS international conference on biomedical engineering and sciences 2012: 260-263.

Wahlberg, J. E., Lindberg, M. Assessment of skin blood flow – an overview. Bioengineering of the skin: Cutaneous Blood Flow and Erythema. CRC Press, USA. 1995, pp.23-30.

Wang, N., Zhang, N., Wang, M. Wireless sensors in agriculture and food industry – Recent development and future perspective. Computers and electronics in agriculture 2005;50:1-14.

Wayland, R., Bromley, D., Pickett, D., Passamante, A. Recognizing Determinism in a Time Series. Physical review letters 1993;70:580-582.

West, B. J. Fractal physiology and chaos in medicine. Studies of nonlinear phenomena in life science, vol. 16. World scientific. Singapore, 2013.

WHO Occupational exposure to noise: evaluation, prevention and control. World health organization. Online access: http://www.who.int/occupational_health/publications/occupnoise/en/

Wolf, A., Swift, J. B., Swinney, H. L., Vastano, J. Detemining Lyapunov Exponents from a Time Series. Physica D 1985;285-317.

Yamada, K., Yamashita, J., Miao, T. Determination of the effect of break times and caffeinated coffee based on earlobe pulse rate analysis. Japanese journal of farm work research 2009;44(1):11-19. (In Japanese).

List of tables

List of figures

Nomenclature

The most commonly used symbols and abbreviations are listed below. The specific symbols that were used in a particular system or equation are described at their place of appearance in the text.

AC	alternative current
APG	acceleration photoplethysmogram
BP	blood pressure
BS	biological signal
CC	correlation coefficient
CBF	cutaneous blood flow
CD	correlation dimension
CVD	cardiovascular disease
CVS	cardiovascular system
DC	direct current
DNP	deterministic nonlinear prediction
ECG or EKG	electrocardiogram
FNN	false nearest neighbors
FR	frequency
|FT|	Fourier transform amplitude
HF	high frequency
HRV	heart rate variability
LE	Lyapunov exponent
LF	low frequency
LLE	largest Lyapunov exponent
NIR	near infrared

PPG	photoplethysmogram
RRMSE	relative route mean square error
STP	short-term prediction
WTE	Wayland test translation error
A	angle at which reconstructed trajectory was sliced by rotating plane in order to obtain Poincaré section
$CC(p)$	correlation coefficient between actual signal and p-steps forward predicted signal
$CC_i(p)$	local correlation coefficient between actual signal and p-steps forward predicted signal in ith region
e_{trans}	local translation error
m_0	starting dimension in modified FFN method
M	embedding dimension
N	number of nearest neighbors
N	Number of points in the PPG time series
P	prediction time step
$RRMSE(p)$	relative root mean square error between actual signal and p-steps forward predicted signal
$RRMSE_i(p)$	local relative root mean square error between actual signal and p-steps forward predicted signal in ith region
t	time
t_1^i	starting time point of the ith region
t_2^i	ending time point of the i^{th} region
v_j	j^{th} translation vector
$X(t)$	data points of the PPG time series at the time t
$Z(t)$	points of time-delay reconstructed trajectory corresponding to the time t
$Z^*(t+p)$	is p steps forward prediction of the predictee $Z(t)$
$Z_i(m)$	i^{th} reconstructed vector in m dimensional phase-space
$Z^i(t)$	i^{th} nearest neighbor of $Z(t)$
τ	time-delay lag

Acknowledgments

This work was inspired, supported and contributed to in various ways by many wonderful people during the last three years; they made it possible for me to fulfill this study. With all my heart, I would like to thank each of them.

First of all, I would like to express my sincere gratitude to my principal supervisor Dr. Kenshi Sakai for his continuous encouragement, suggestions and patient guidance during all stages of this research and whose broad knowledge in various disciplines always inspired new ideas in this research. I also would like equally to thank my co-advisers Dr. Hirotaka Saito, Dr. Masami Matsui, as well as Dr. Sakae Shibusawa, Dr. Takashi Okayama for their support and valuable suggestions. I would like specially to acknowledge Dr. Shrinivasa K. Upadhyaya, Professor in the Biological and Agricultural Engineering Department at UC Davis, for his kind support and guidance during my intensive study at UC Davis. As well, I would like to express my appreciation to Dr. Christiana Drake, Department of Statistics, Dr. James P. Crutchfield, Physics Department, Dr. Alan Hastings, Department of Environmental Science and Policy, and Dr. Naoki Saito, Department of Mathematics at UC Davis for their time and valuable discussions on different aspects of this research.

I also would like to thank all members of TUAT FOLENS head office and especially to Dr. Hirokazu Ozaki and Dr. Sachi Ninomiya-Lim, as well as all staff and students of FOLENS program for all the interesting, inspiring and informative time together during various FOLENS activities. My special thanks also go to Japanese language teachers of TUAT international center for the great experience of Japanese language and culture.

My deep gratitude also extends to Dr. Victor D. Vlasenko, academic secretary of Computing Center of Far-Eastern Branch Russian Academy of Science, and all faculty members of the Applied Mathematics Department of Pacific National University, who have been continuously encouraging my studies since my undergraduate course and helped me to discover the beautiful world of mathematical sciences.

I also would like to thank my dear friends among TUAT students Maria Mishina, Natsuho Kaneko, Yohei Okazaki and Nehal Hasnine as well as STEP program exchange students from Russia Natalia Kolyadina, Margarita Krivorotko, Elena Kazantseva and Diana Mindaleva for their support with my experiments and our precious time together.

I would like to address special thanks to my loving parents, whose unwavering support and faith in me, good wishes and consideration always encouraged me to pursue my dreams through the years. I also would like to pay tribute to the memory of my beloved grandmother (1938-2013), who strengthened my spirit and will and encouraged me to follow my way.

Finally, I would like to acknowledge the Japanese Ministry of Education, Culture, Sports, Science and Technology (MEXT) for providing the Japanese Government Scholarship to support my PhD studies, without which I would not have been able to pursue a PhD in Japan.

Publications based on the thesis

Journal publications

- Sviridova, N., Sakai, K. Application of photoplethysmogram for detecting physiological effects of tractor noise. Engineering in agriculture, environment and food, 2015. [In press]
- Sviridova, N., Sakai, K. Human photoplethysmogram: new insight into chaotic characteristics. Chaos, solitons and fractals, 2015; 77:53-63.

International conference presentations

- Sviridova, N., Sakai, K. Detecting nonlinear dynamics in human heart rate variability by deterministic nonlinear prediction. Dynamics Days XXXIII Dynamics Days 2013 EU, Spain, Madrid, June 2013
- Sviridova, N. V., Sakai, K. Application of nonlinear time series analysis for hemodynamic model validation on the base of photoplethysmogram signal. The 6^{th} International Young Scientists School "Systems Biology and Bioinformatics" at Bioinformatics and Systems Biology Multiconference, Russia, Novosibirsk, June 2014.
- Sviridova, N., Sakai, K. Photoplethysmograph nonlinear time series analyses application on power machinery ergonomics. XXXIV Dynamics Days Europe, Germany, Bayreuth, September 2014.
- Sviridova, N., Sakai, K. Distinguishing Deterministic Chaos and Periodicity in Human Photoplethysmogram. International Symposium on Nonlinear Theory and its Applications 2014, Luzern, Switzerland, September 2014, pp. 537-540.

Domestic conference presentations

- Sviridova, N., Sakai, K. Detecting nonlinear determinism in human heart rate variability. 72d meeting of Japanese society of agriculture machinery and food engineers, Obihiro, September 2013.
- Sviridova, N. V. Detecting Nonlinear Determinism in Human Photoplethysmograph by Surrogation for Wayland Test, The 5th International Symposium of FOLENS, November 2013.
- Sviridova, N., Sakai, K. Assessing the Effects of Farm Operations on Human Cardiovascular System by Photoplethysmogram, 73d annual meeting of Japanese society of agriculture machinery and food engineers, Okinawa, Japan, May 2014.

Appendix

A.1. Factors affecting cutaneous blood flow

Measurement of cutaneous blood flow (CBF) might be affected by various factors, such as anatomical site, physical activity, mental activity, food and drugs and temperature. Factors and the strength of their effects on CBF are listed in Table A.1 [Serup, 1995].

TABLE A.1 Factors and Variables with Effects on Cutaneous Blood Flow

Factor	Strength of effect
Age	Widely age independent
Sex	Minor or no difference
Menstrual Cycle	Minor or no difference
Race	Minor or no difference
Anatomical site	Considerable variation
Position	Ortostatic dependence
Temporal, diurnal	Minor or no effect
Temporal, day to day	May be significant
Physical activity	Considerable effect
Mental activity	Considerable effect
Food and drugs	Considerable effect
Temperature	Very significant effect

According to [Serup, 1995] in the design of CBF studies it is highly recommended to take into account the following:

1. Prior to the experiment test subjects should not take any food or drug that might influence cutaneous blood flow. Any topical treatment of the test site prior to study should be avoided unless it is part of the experiment.

2. Test subjects should not have deliberately exercised, been exposed to unusual temperatures, or been under mental stress immediately before CBF measurement.
3. Test subjects should be allowed to rest for 15 min or more under quiet conditions, preferably in the laboratory room in the position in which recordings are going to be obtained, i.e. sitting or supine, and with the test site uncovered.
4. The laboratory room and the measurement should be controlled, particularly with respect to temperature, convection of air, and noise. Measurement under direct light, including direct sunshine, which might influence skin temperature, should be avoided.
5. Measurements should be performed with the site under study at a standardized level relative to the level of the heart.

It has also been noticed in several studies utilizing a variety of methods that a decrease in skin blood flow occurs immediately following smoking. All studies indicated abnormalities in capillary blood flow and its regulation in the skin as an immediate result of smoking [Agache and Dupond, 1995]. Decreased skin blood flow in the fingers was found by photoplethysmogram measured during smoking.

A.2. Results of nonlinear time series analysis for all collected data

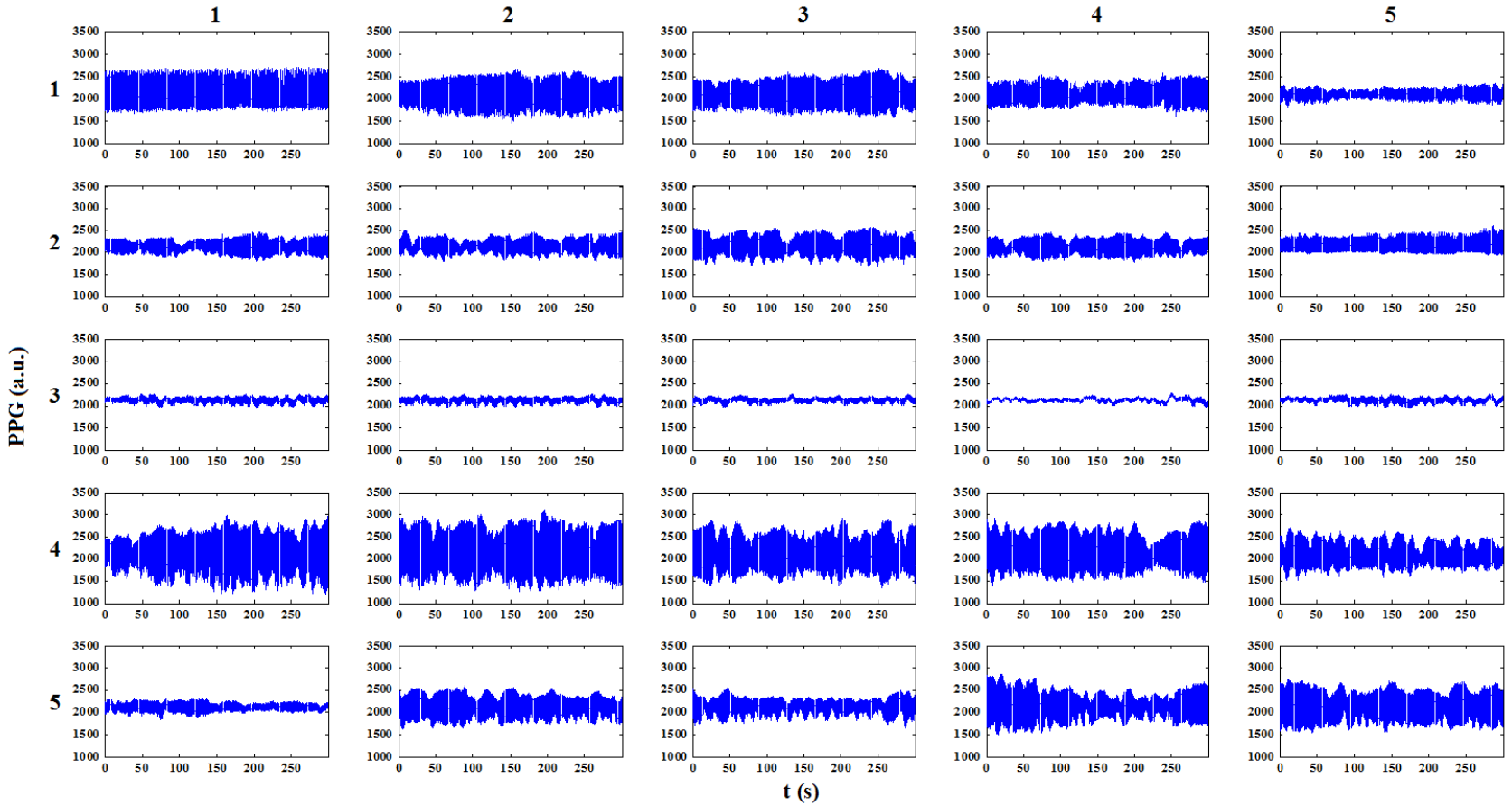

Fig. A.1 *Experimentally obtained PPG time series of subjects 1-5 (rows) with 5 measurement repeats for each (columns).*

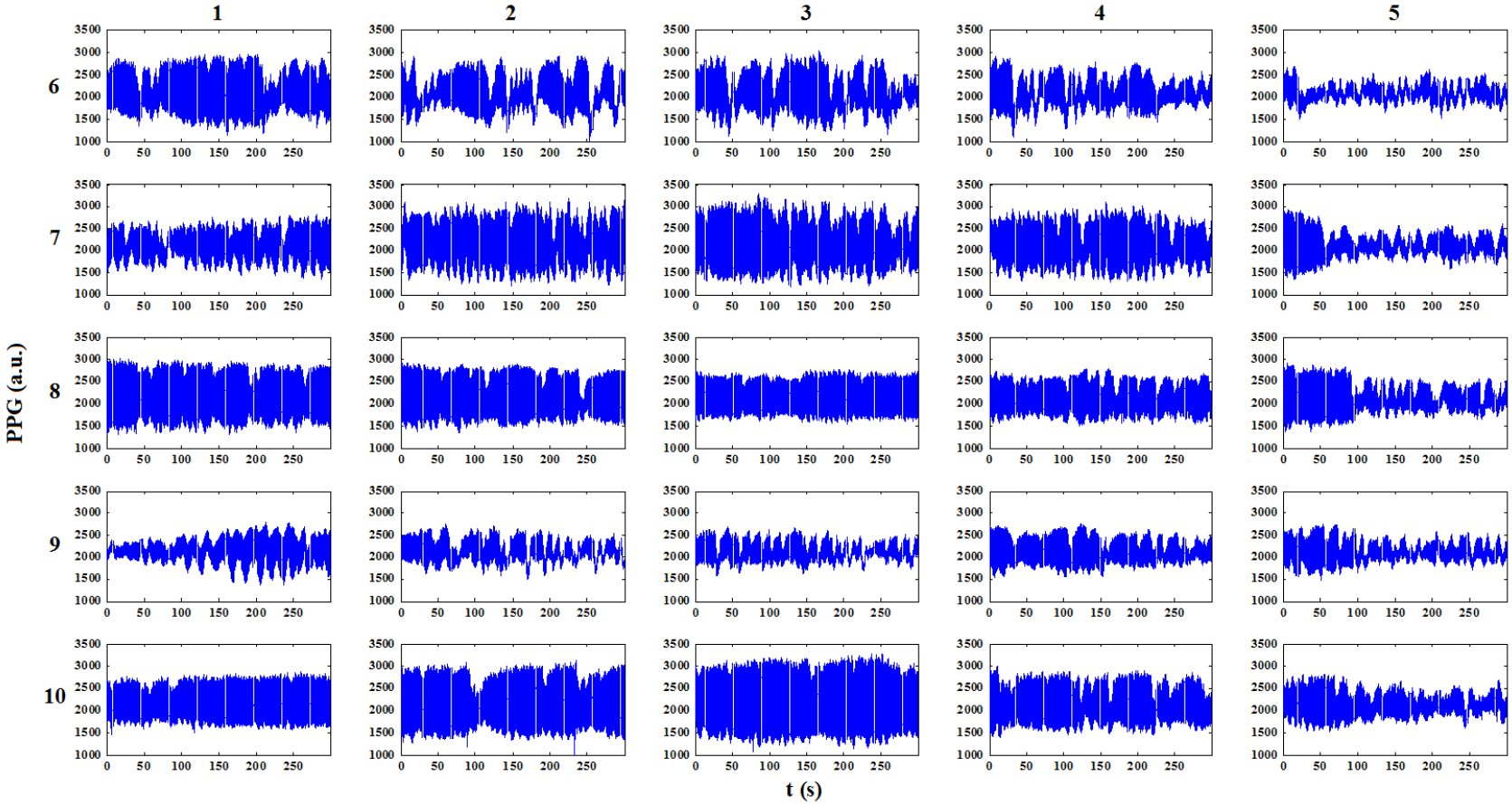

Fig. A.2 *Experimentally obtained PPG time series of subjects 6-10 (rows) with 5 measurement repeats for each (columns).*

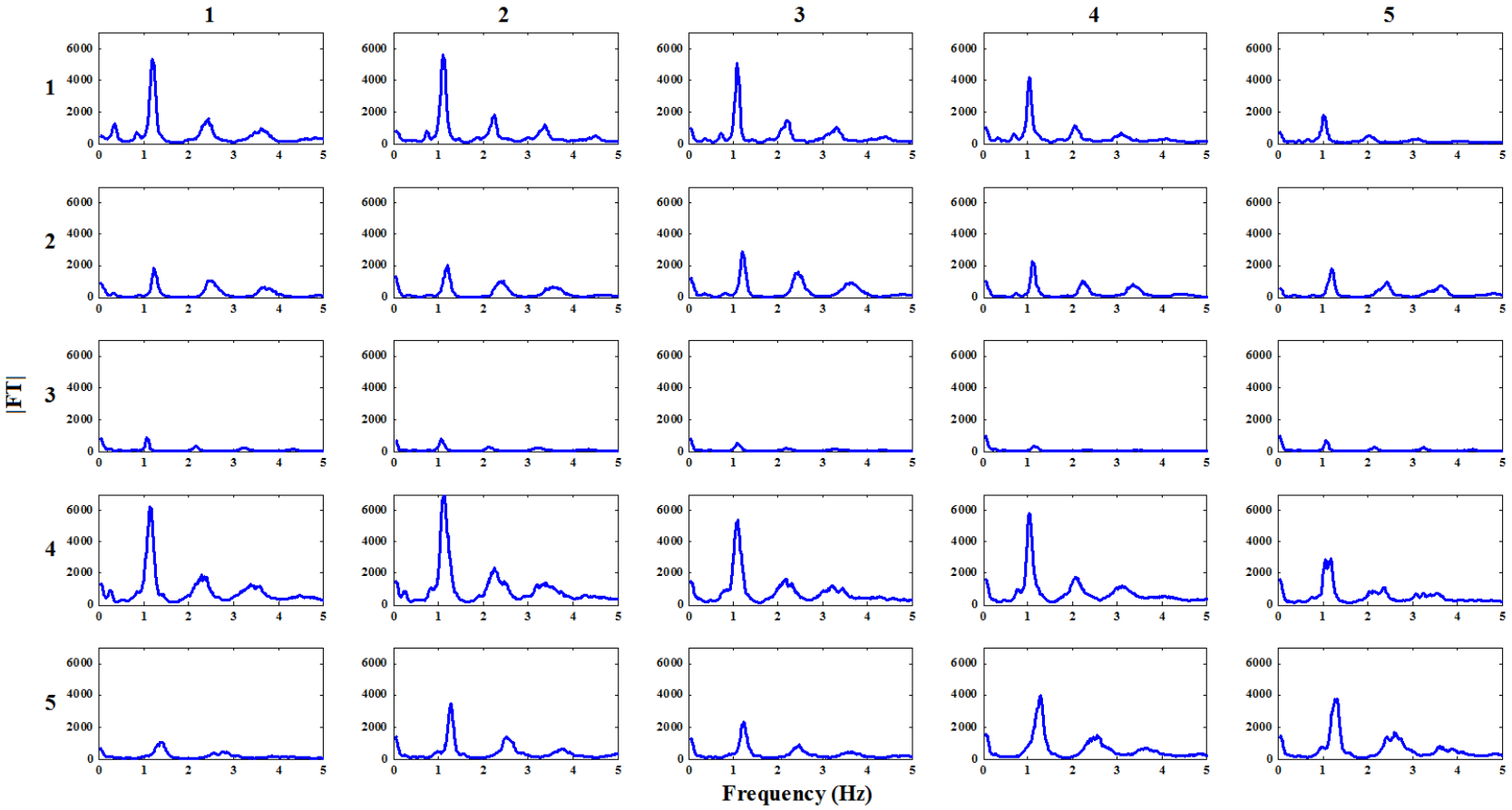

Fig. A.3 *Fourier spectrum of PPG time series for subjects 1-5 (rows) with 5 (columns) measurement repeats for each.*

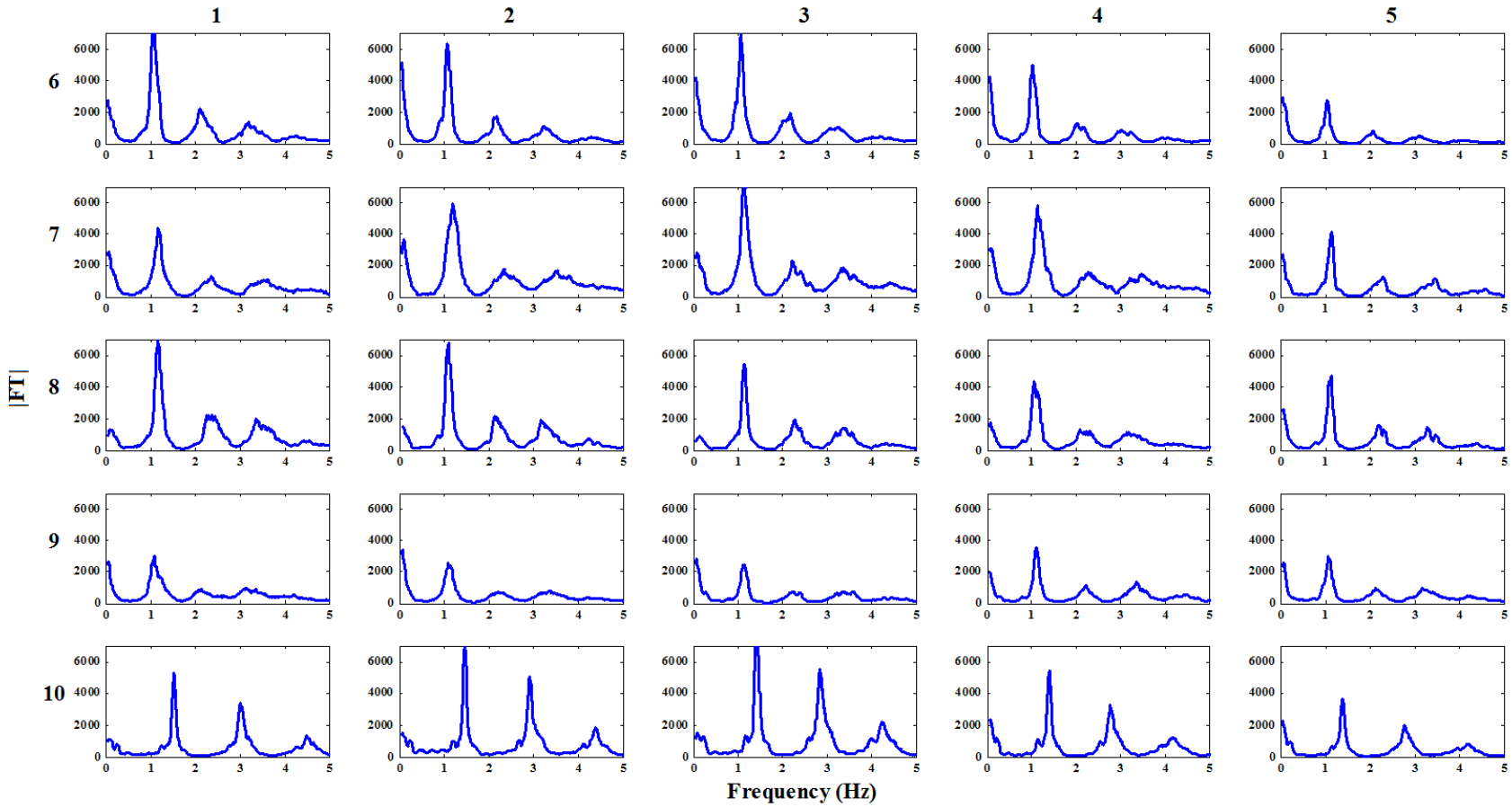

Fig. A.4 *Fourier spectrum of PPG time series for subjects 6-10 (rows) with 5 (columns) measurement repeats for each.*

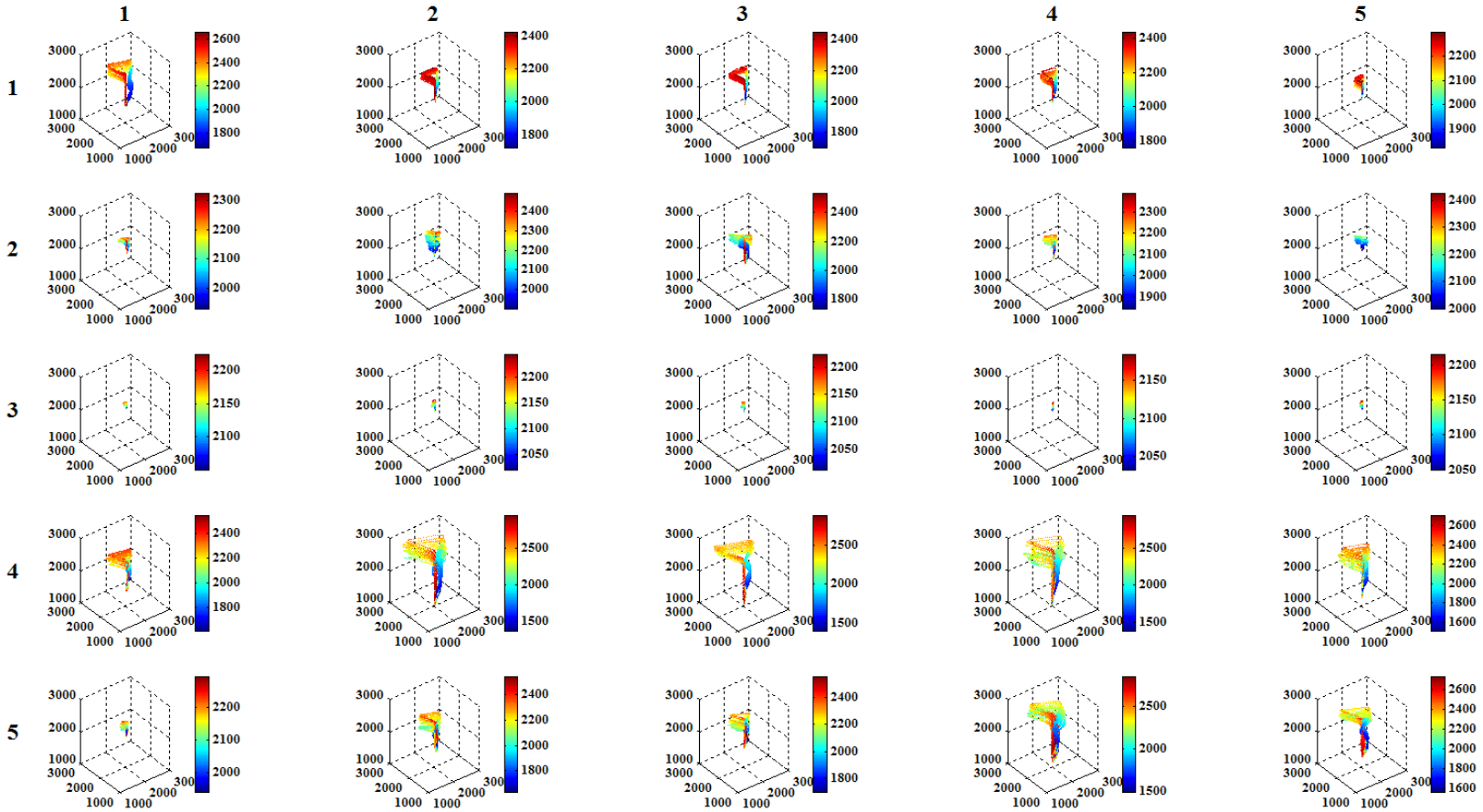

Fig. A.5 *Reconstructed trajectory of the PPG time series for subjects 1-5 (rows) with 5 measurement repeats for each (columns); x-, y-, z-axis and color bar correspond to X(t), X(t+τ), X(t+2τ) and X(t+3τ) respectively.*

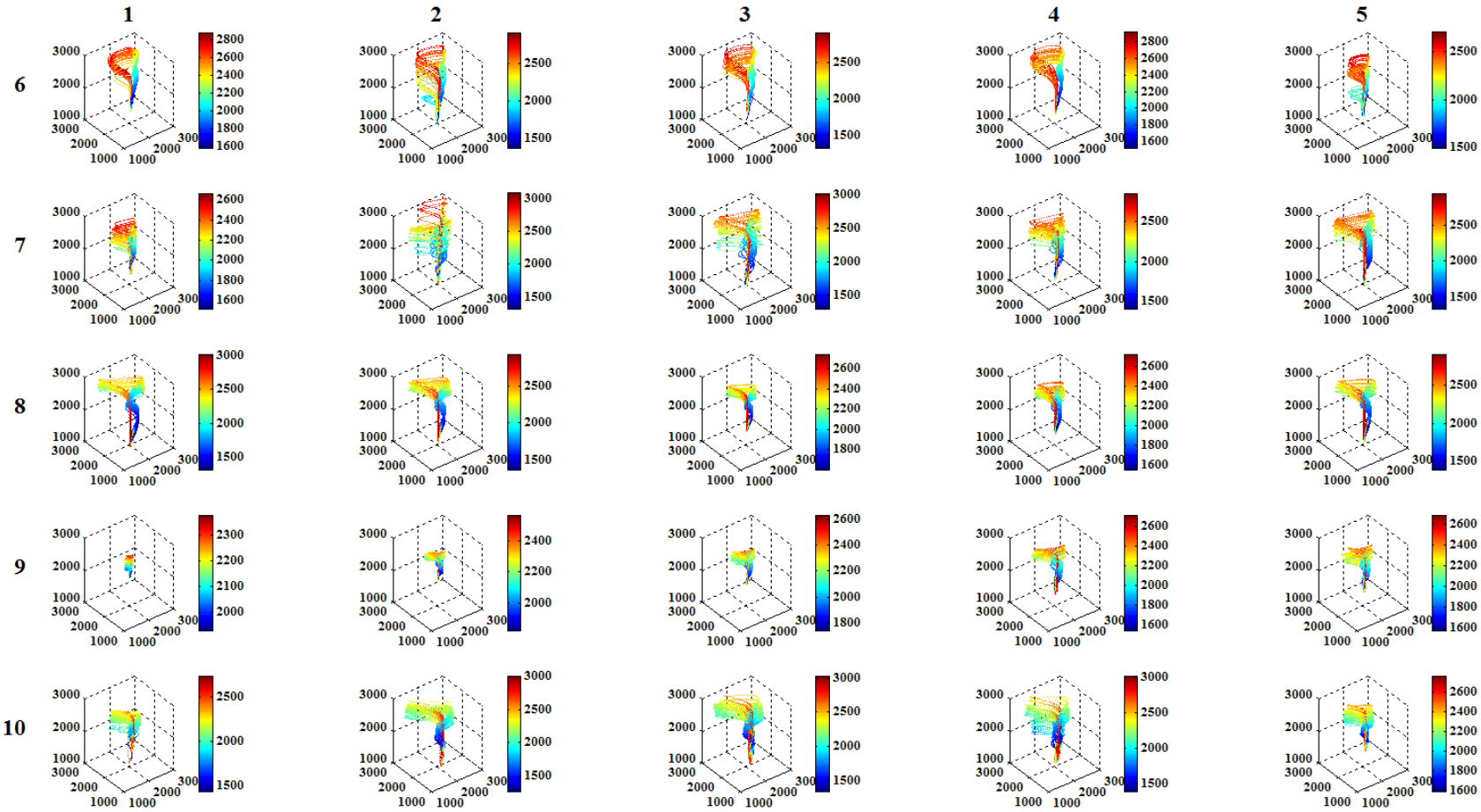

Fig. A.6 *Reconstructed trajectory of the PPG time series for subjects 6-10 (rows) with 5 measurement repeats for each (columns); x-, y-, z-axis and color bar correspond to X(t), X(t+τ), X(t+2τ) and X(t+3τ) respectively.*

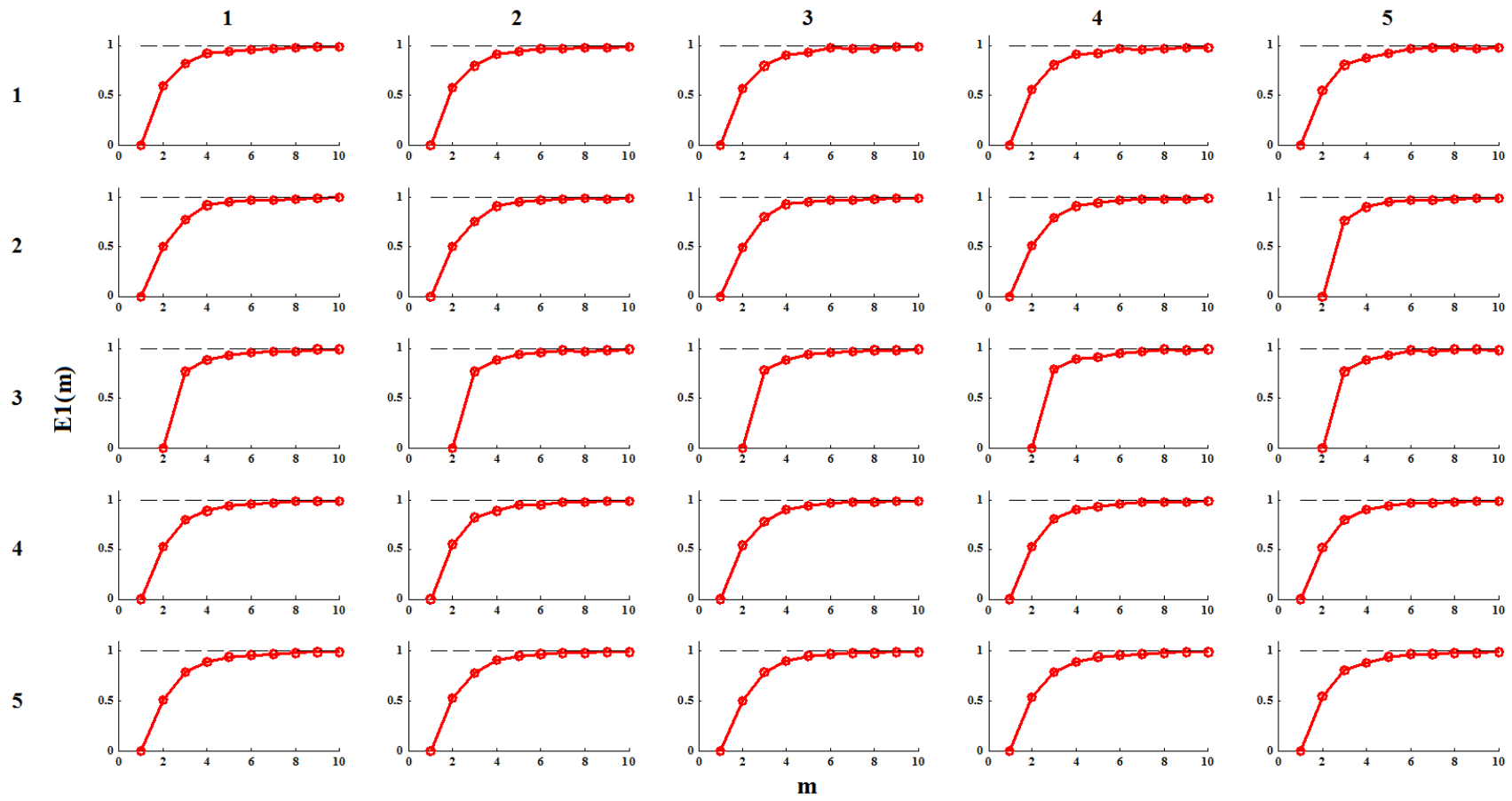

Fig. A. 7 *Determining the minimum embedding dimension by the modified method of false nearest neighbors for the PPG time series for subjects 1-5 (rows) with 5 measurement repeats for each (columns).*

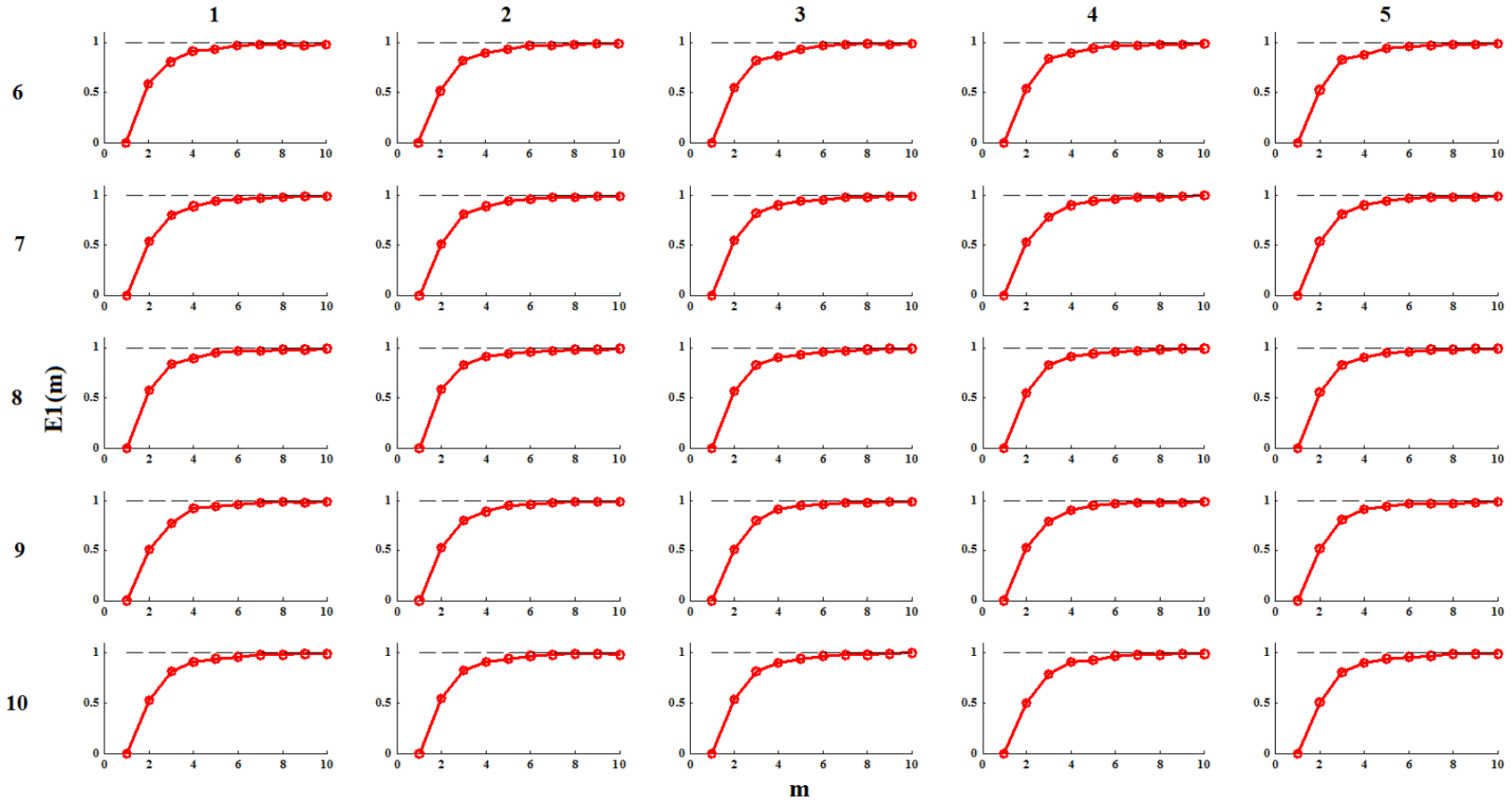

Fig. A. 8 *Determining the minimum embedding dimension by the modified method of false nearest neighbors for the PPG time series for subjects 6-10 (rows) with 5 measurement repeats for each (columns).*

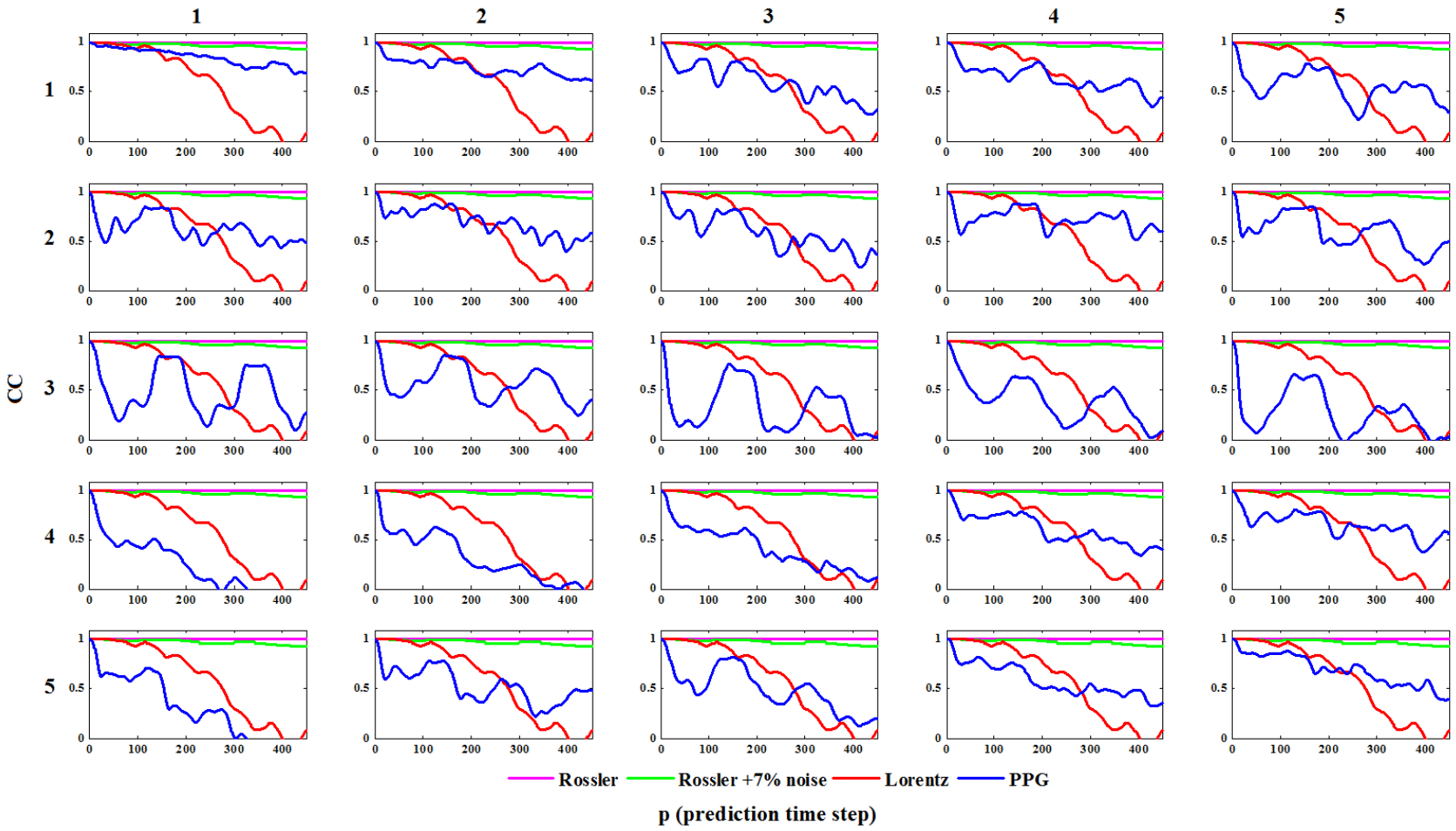

Fig. A.9 *Correlation coefficient (CC) for deterministic nonlinear prediction of Rössler's single band chaos, Rössler's single band chaos with 7% additive noise, Lorentz system in chaotic regime and the PPG for 5 measurement repeats (columns) of subjects 1-5 (rows).*

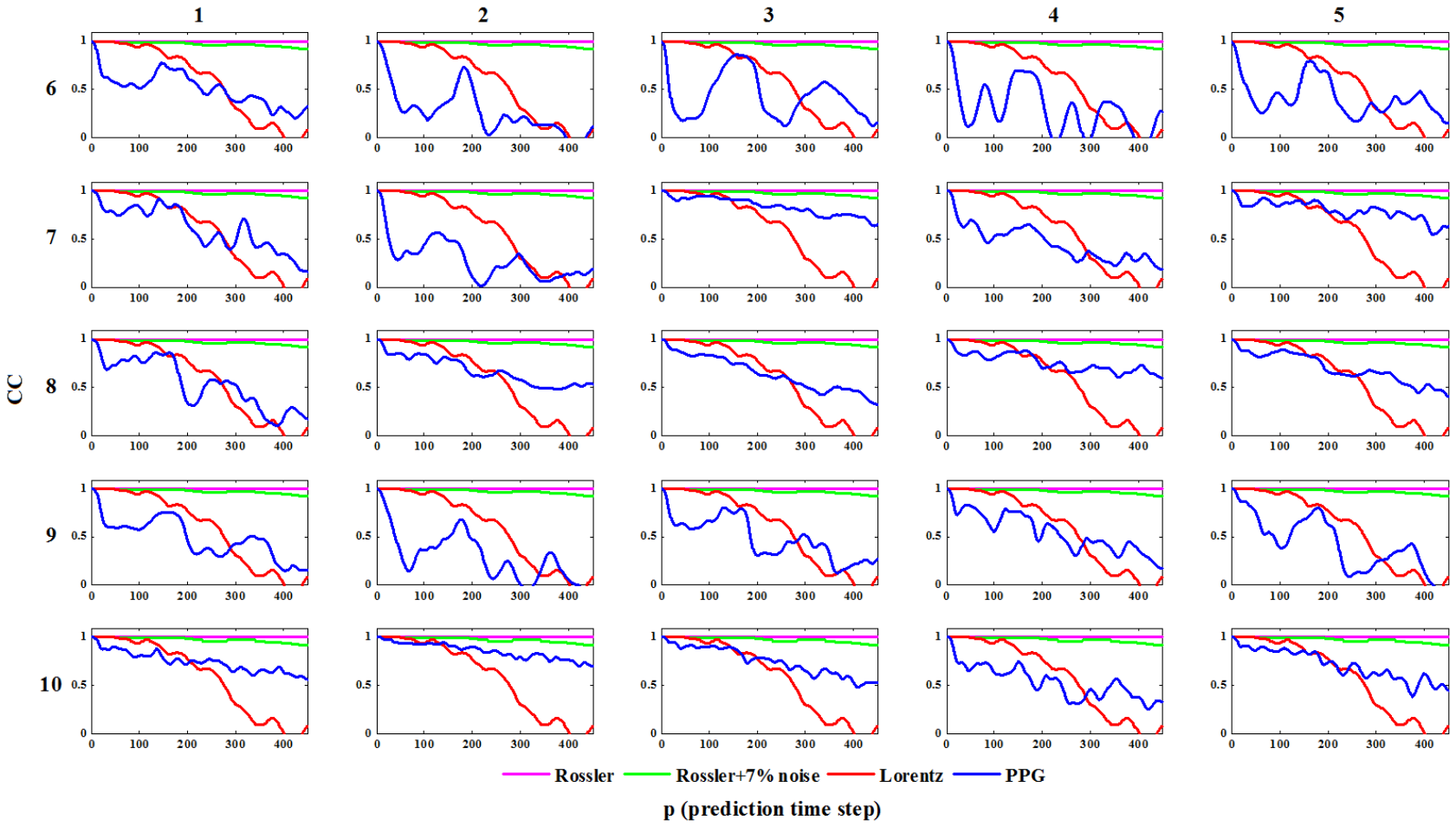

Fig. A.10 *Correlation coefficient (CC) for deterministic nonlinear prediction of Rössler's single band chaos, Rössler's single band chaos with 7% additive noise, Lorentz system in chaotic regime and the PPG for 5 measurement repeats (columns) of subjects 6-10 (rows).*

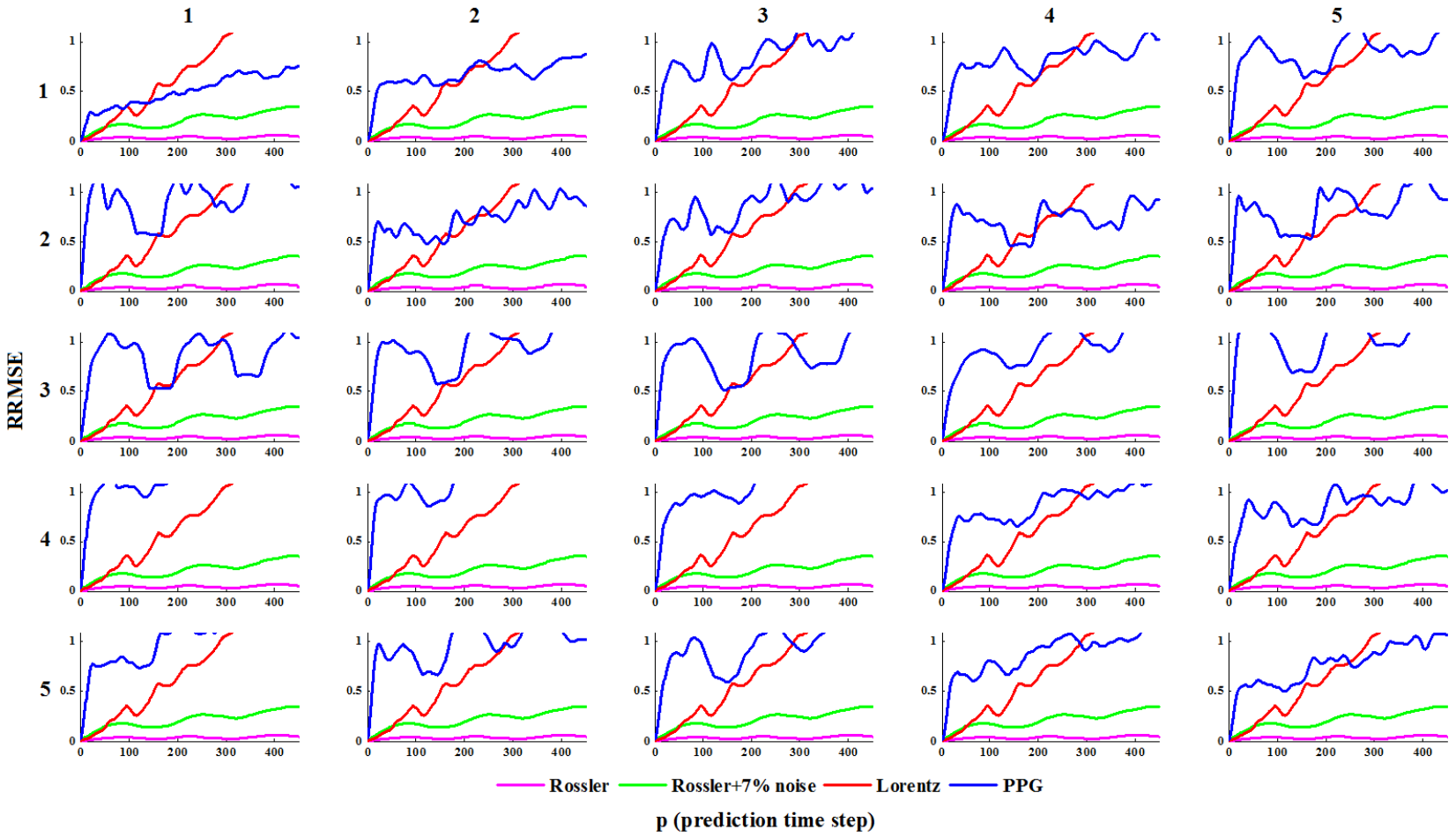

Fig. A.11 *Relative root mean square error (RRMSE) for deterministic nonlinear prediction of Rössler's single band chaos, Rössler's single band chaos with 7% additive noise, Lorentz system in chaotic regime and the PPG for 5 measurement repeats (columns) of subjects 1-5 (rows).*

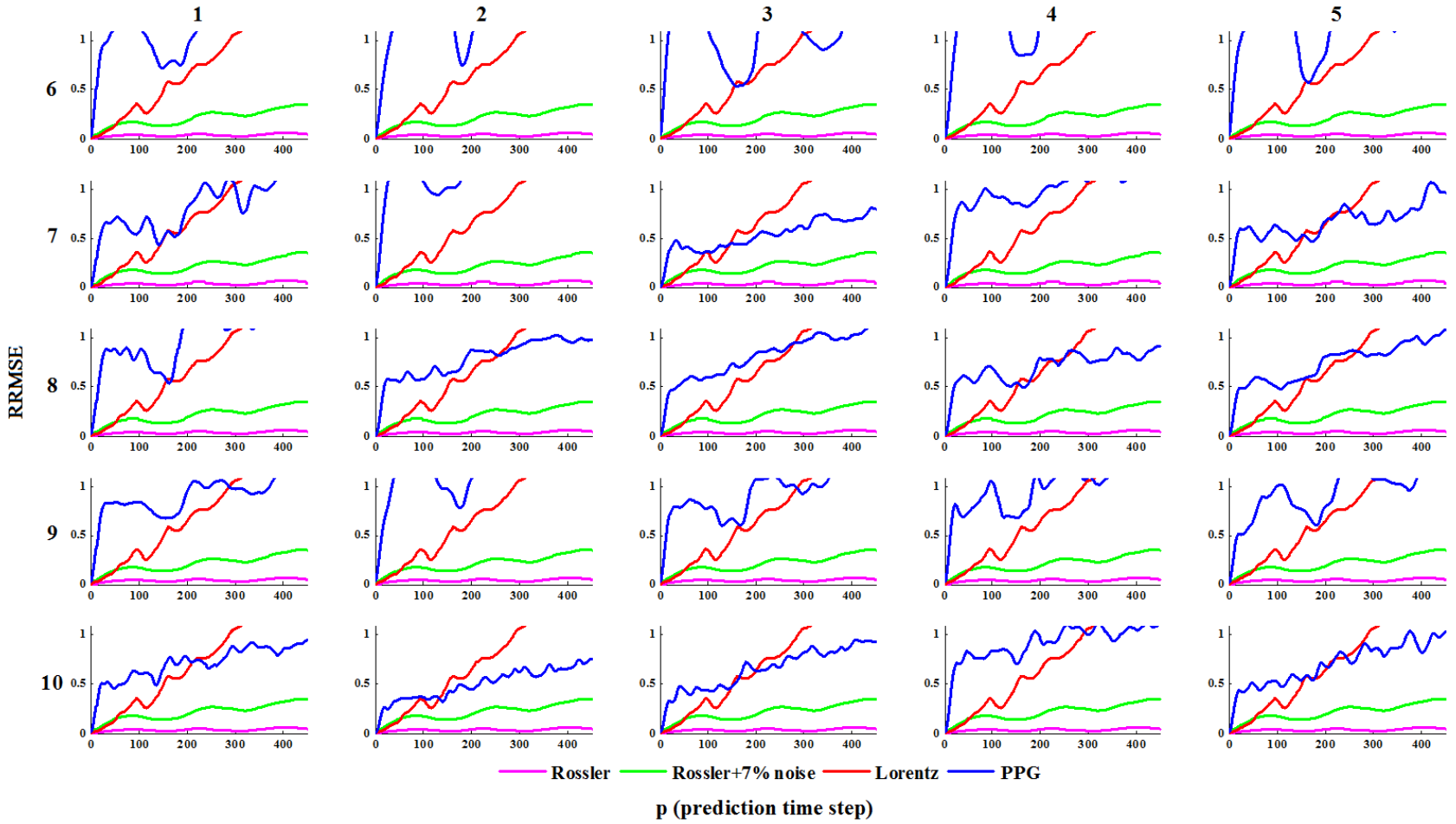

Fig. A.12 *Relative root mean square error (RRMSE) for deterministic nonlinear prediction of Rössler's single band chaos, Rössler's single band chaos with 7% additive noise, Lorentz system in chaotic regime and the PPG for 5 measurement repeats (columns) of subjects 6-10 (rows).*

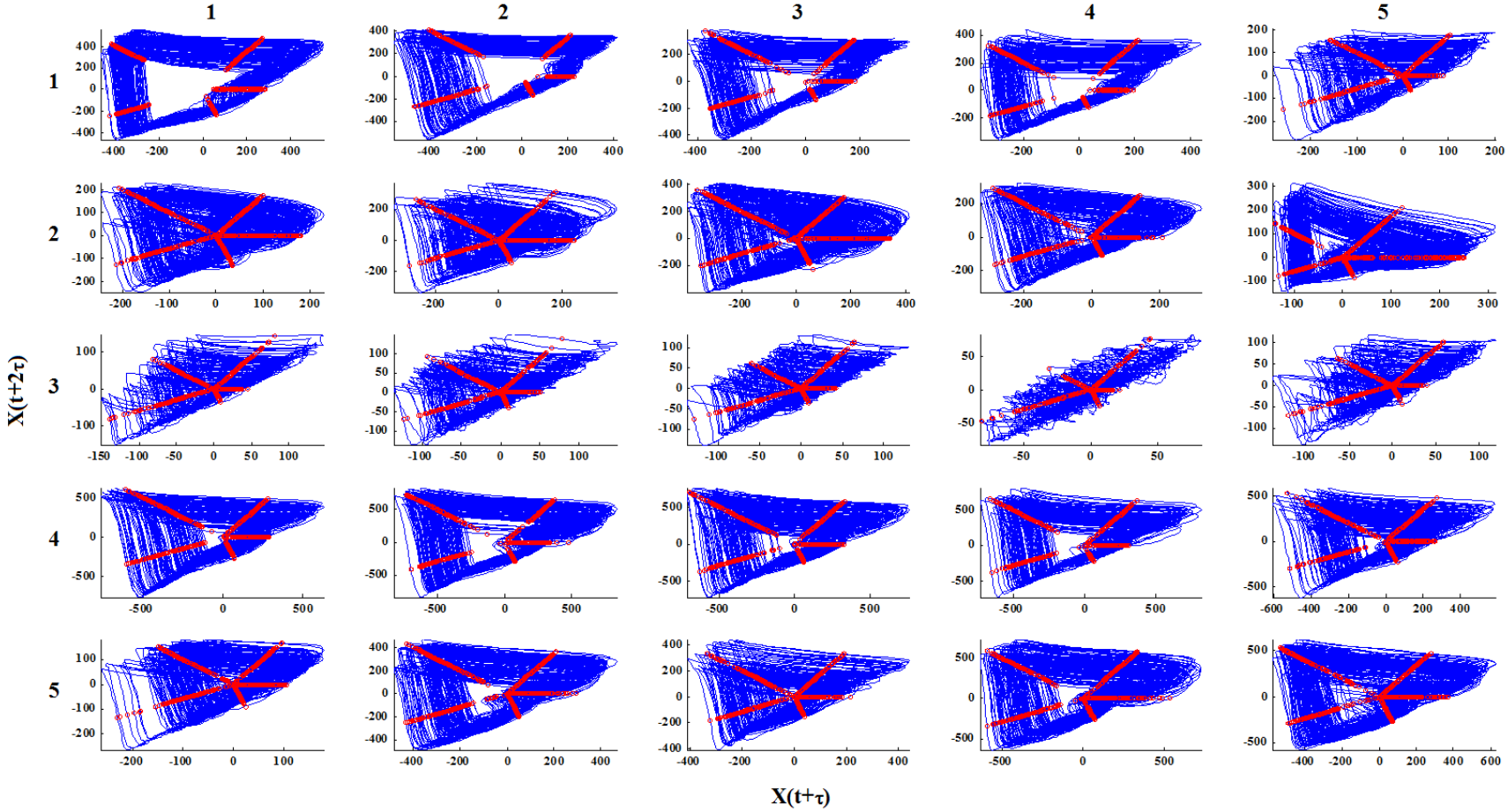

Fig. A.13 *The areas sliced by the rotating plane on the reconstructed trajectory of PPG signal of 5 measurement repeats (columns) of subjects 1-5 (rows).*

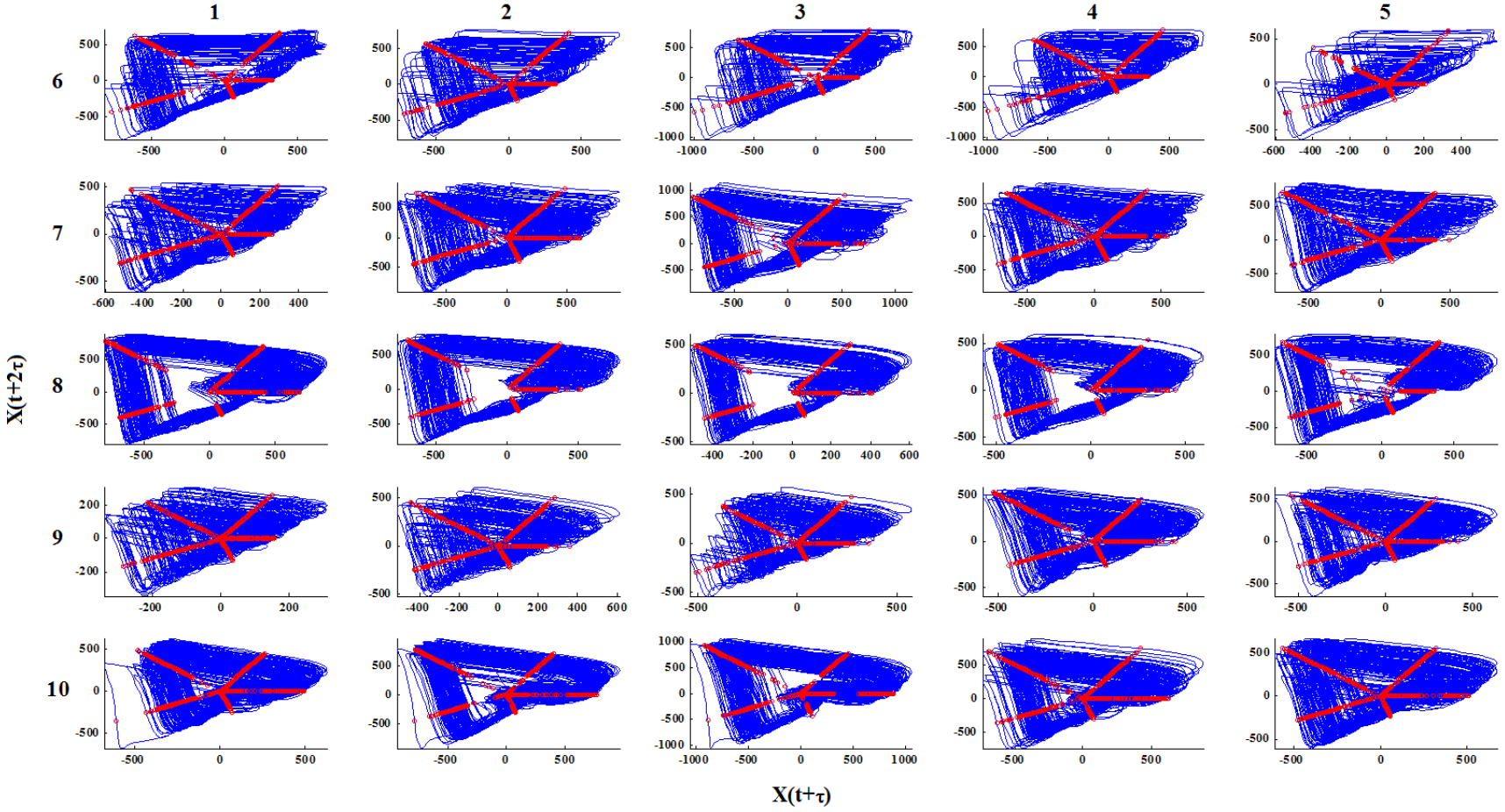

Fig. A.14 *The areas sliced by the rotating plane on the reconstructed trajectory of PPG signal of 5 measurement repeats (columns) of subjects 6-10 (rows).*

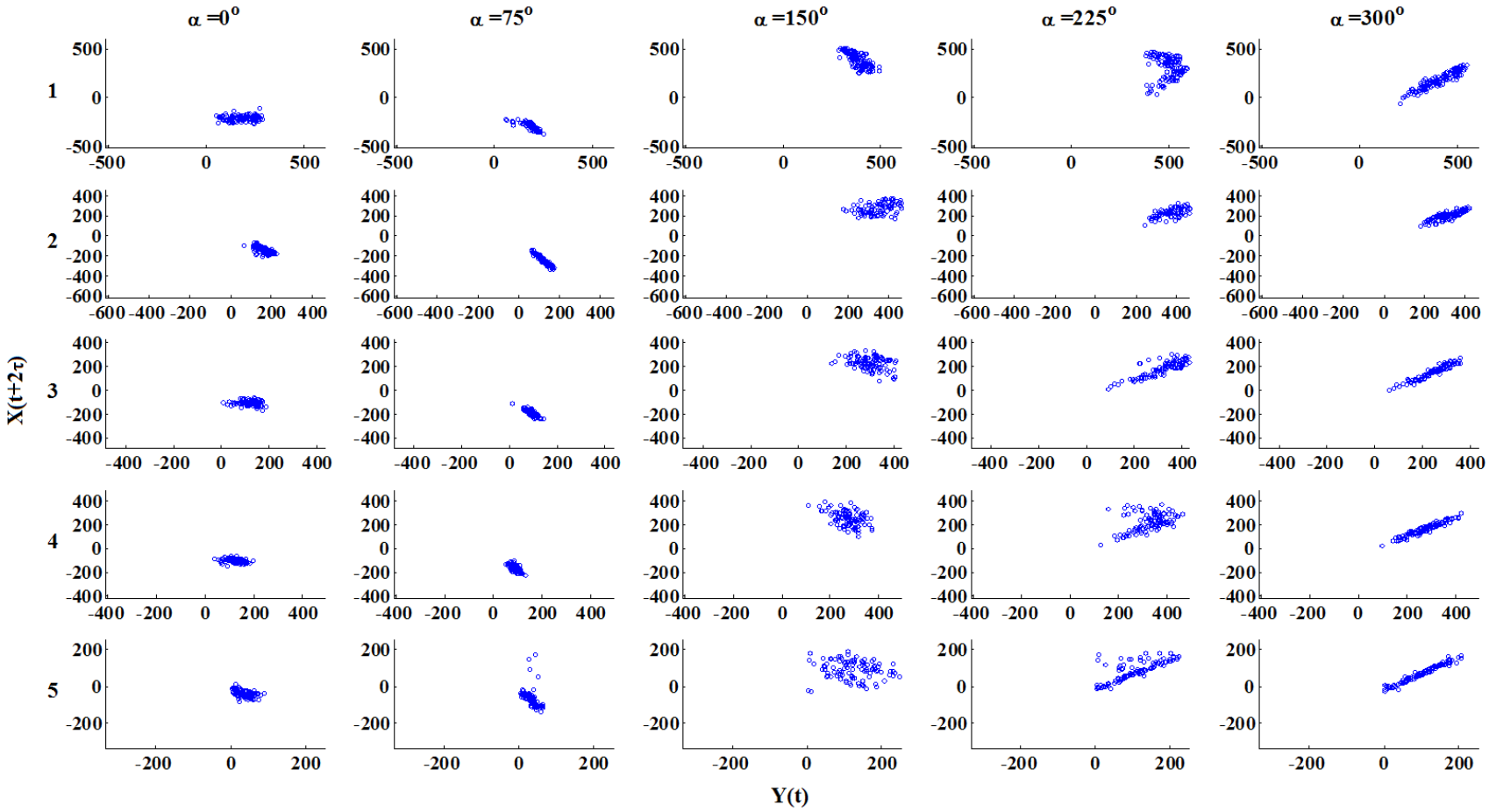

Fig. A.15 *Poincaré section obtained by slicing PPG trajectory by rotating plane at 5 angles (columns) for the 1st subject 1-5th measurement repeats (rows), where Y(t) =* $\sqrt{\boldsymbol{X(t)^2 + X(t+\tau)^2}}$.

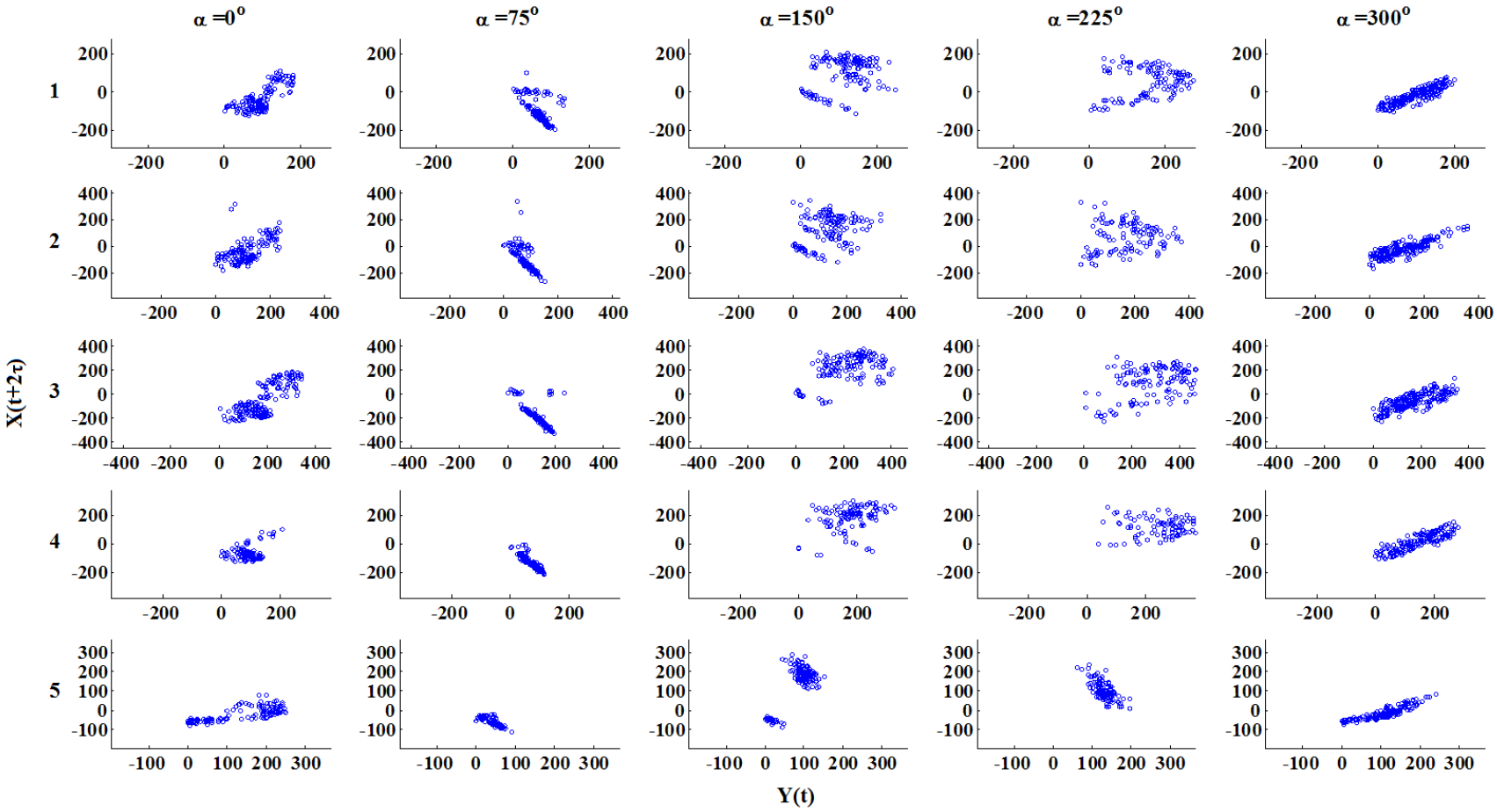

Fig. A.16 *Poincaré section obtained by slicing PPG trajectory by rotating plane at 5 angles (columns) for the 2nd subject 1-5th measurement repeats (rows), where Y(t) =* $\sqrt{\boldsymbol{X(t)^2 + X(t+\tau)^2}}$.

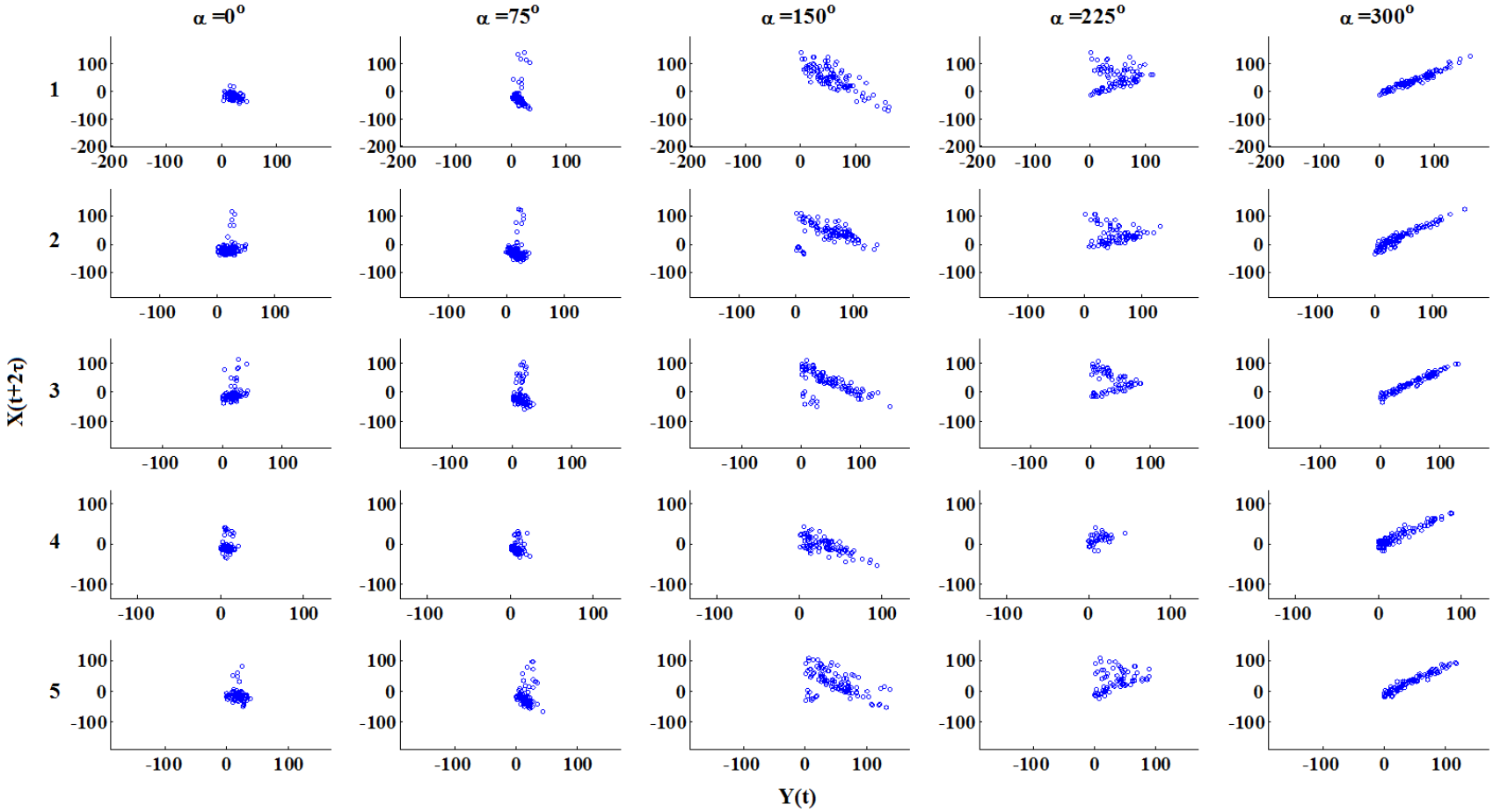

Fig. A.17 *Poincaré section obtained by slicing PPG trajectory by rotating plane at 5 angles (columns) for the 3[rd] subject 1-5th measurement repeats (rows), where Y(t) =* $\sqrt{\boldsymbol{X(t)^2 + X(t+\tau)^2}}$.

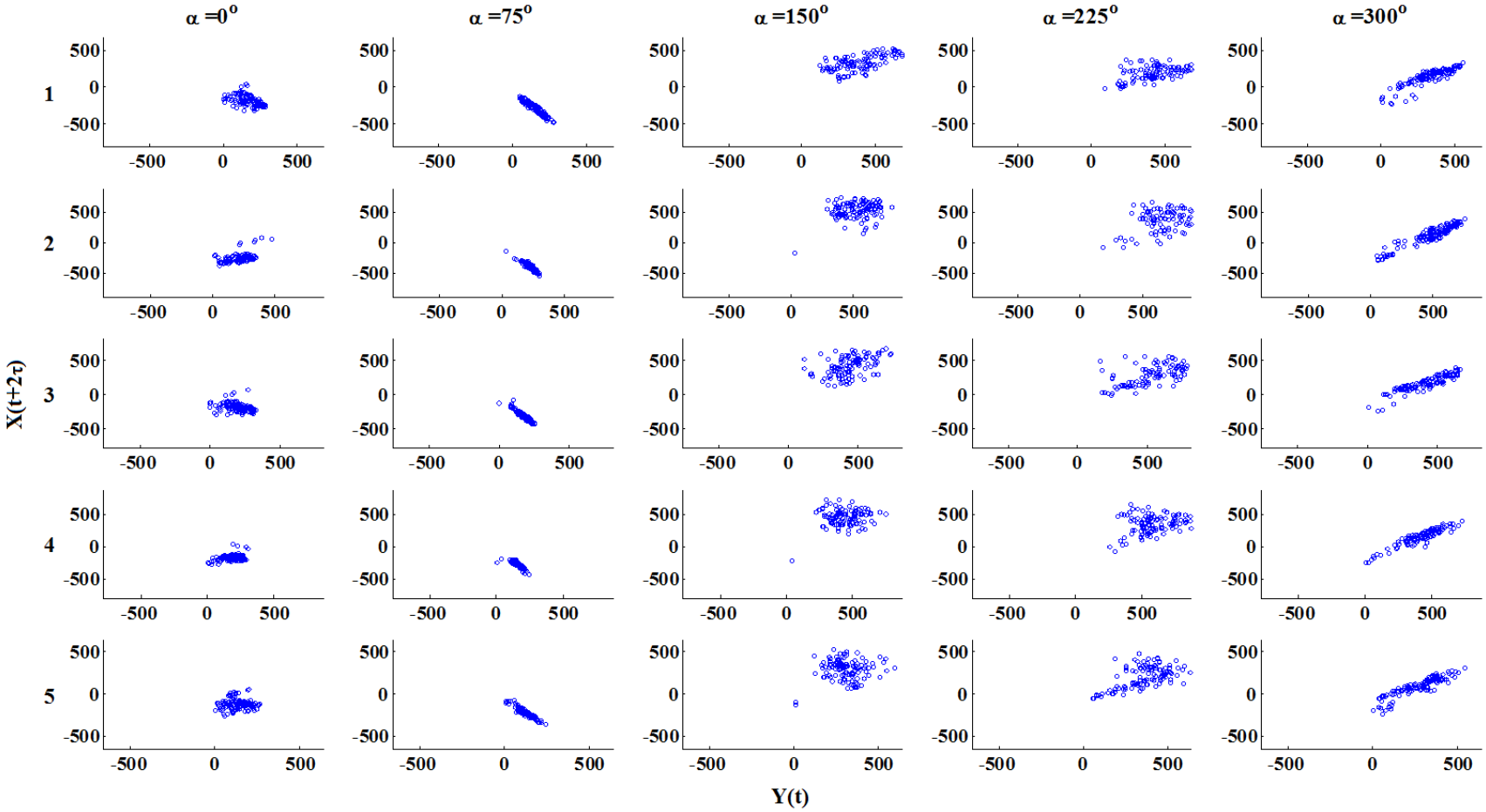

Fig. A.18 *Poincaré section obtained by slicing PPG trajectory by rotating plane at 5 angles (columns) for the 4th subject 1-5th measurement repeats (rows), where Y(t) =* $\sqrt{\boldsymbol{X(t)^2 + X(t+\tau)^2}}$.

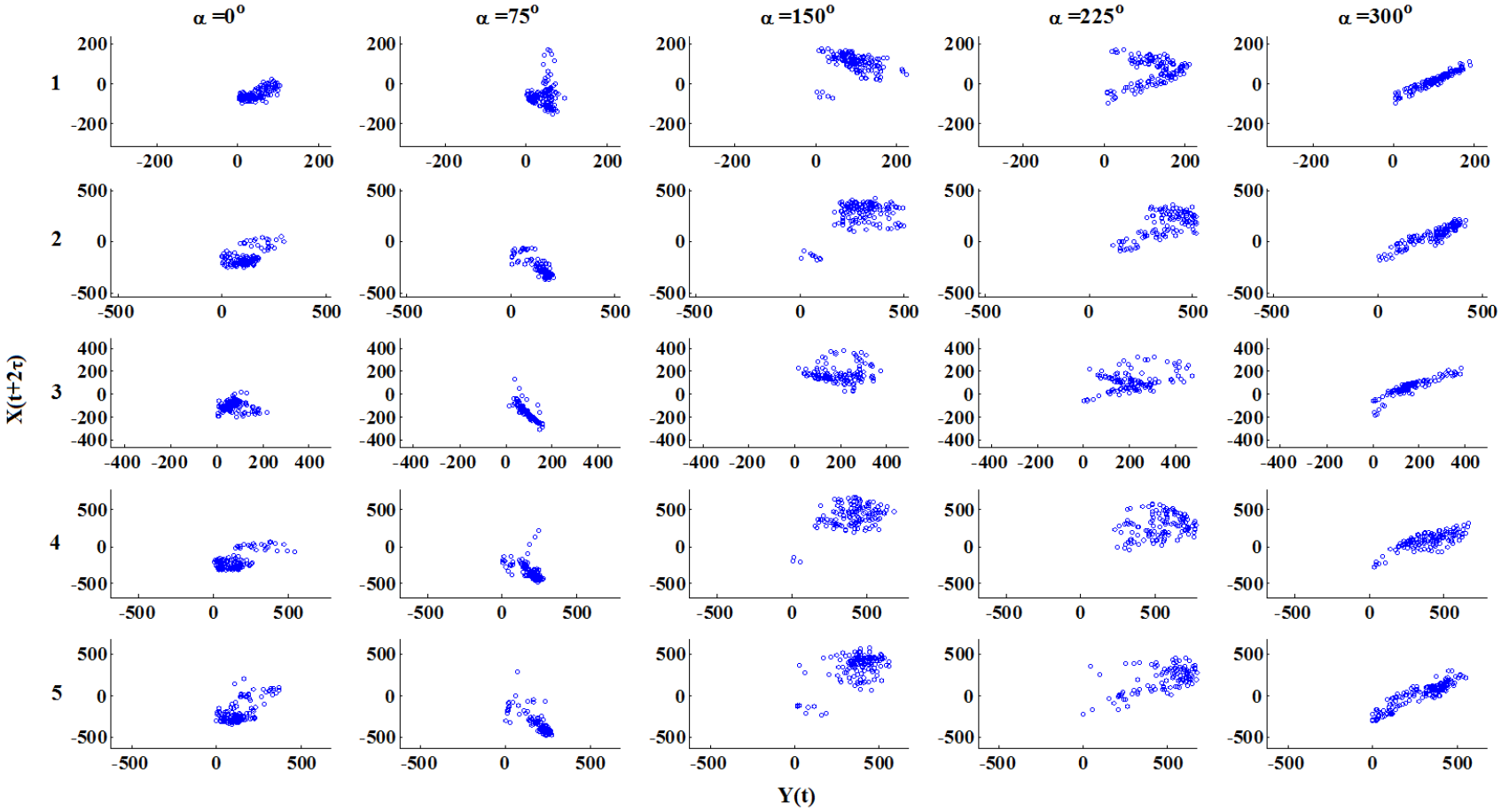

Fig. A.19 *Poincaré section obtained by slicing PPG trajectory by rotating plane at 5 angles (columns) for the 5th subject 1-5th measurement repeats (rows), where Y(t) =* $\sqrt{\boldsymbol{X(t)^2 + X(t+\tau)^2}}$.

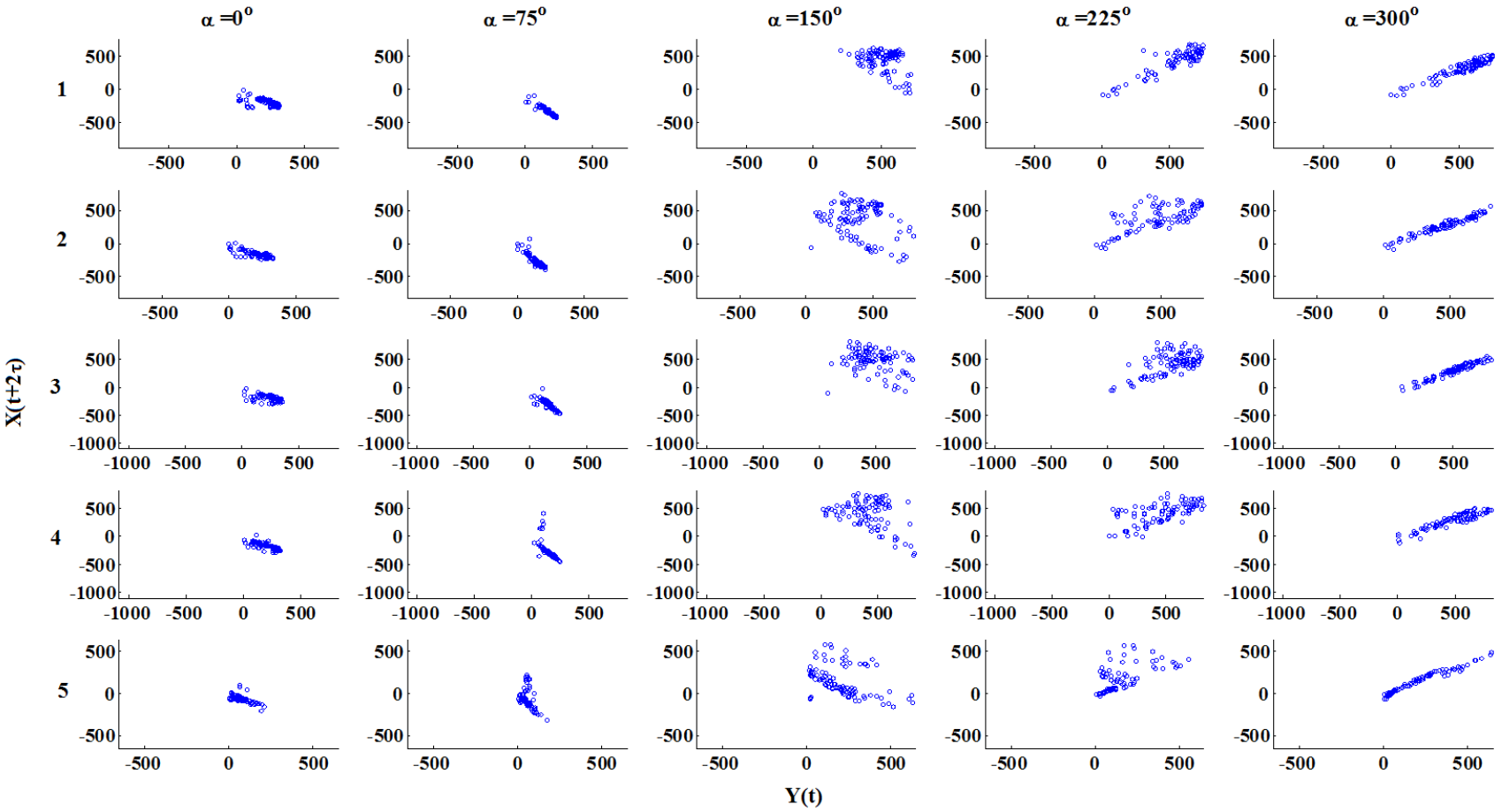

Fig. A.20 *Poincaré section obtained by slicing PPG trajectory by rotating plane at 5 angles (columns) for the 6th subject 1-5th measurement repeats (rows), where Y(t) =* $\sqrt{\boldsymbol{X(t)^2 + X(t+\tau)^2}}$.

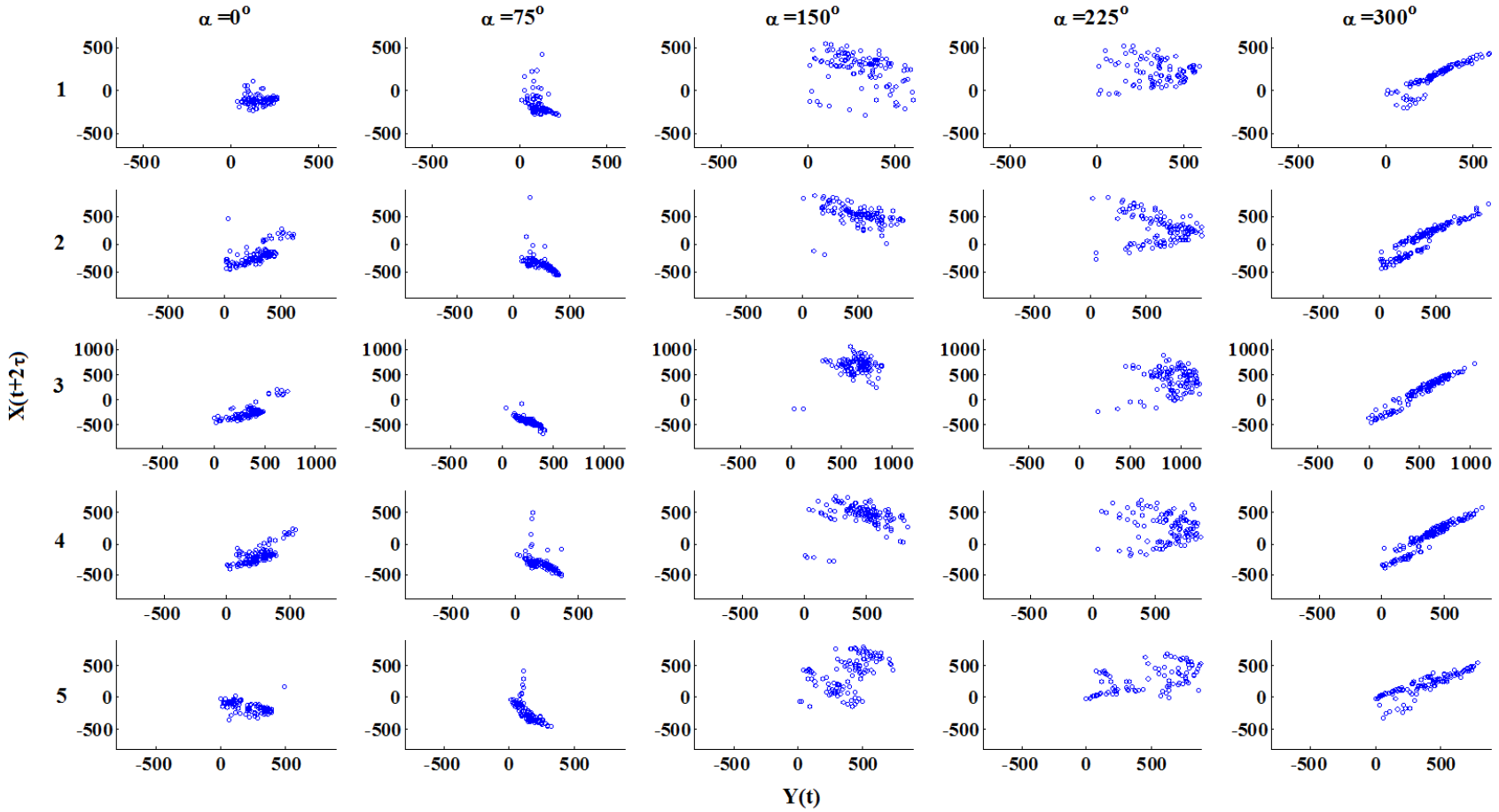

Fig. A.21 *Poincaré section obtained by slicing PPG trajectory by rotating plane at 5 angles (columns) for the 7th subject 1-5th measurement repeats (rows), where Y(t) =* $\sqrt{\boldsymbol{X(t)^2 + X(t+\tau)^2}}$.

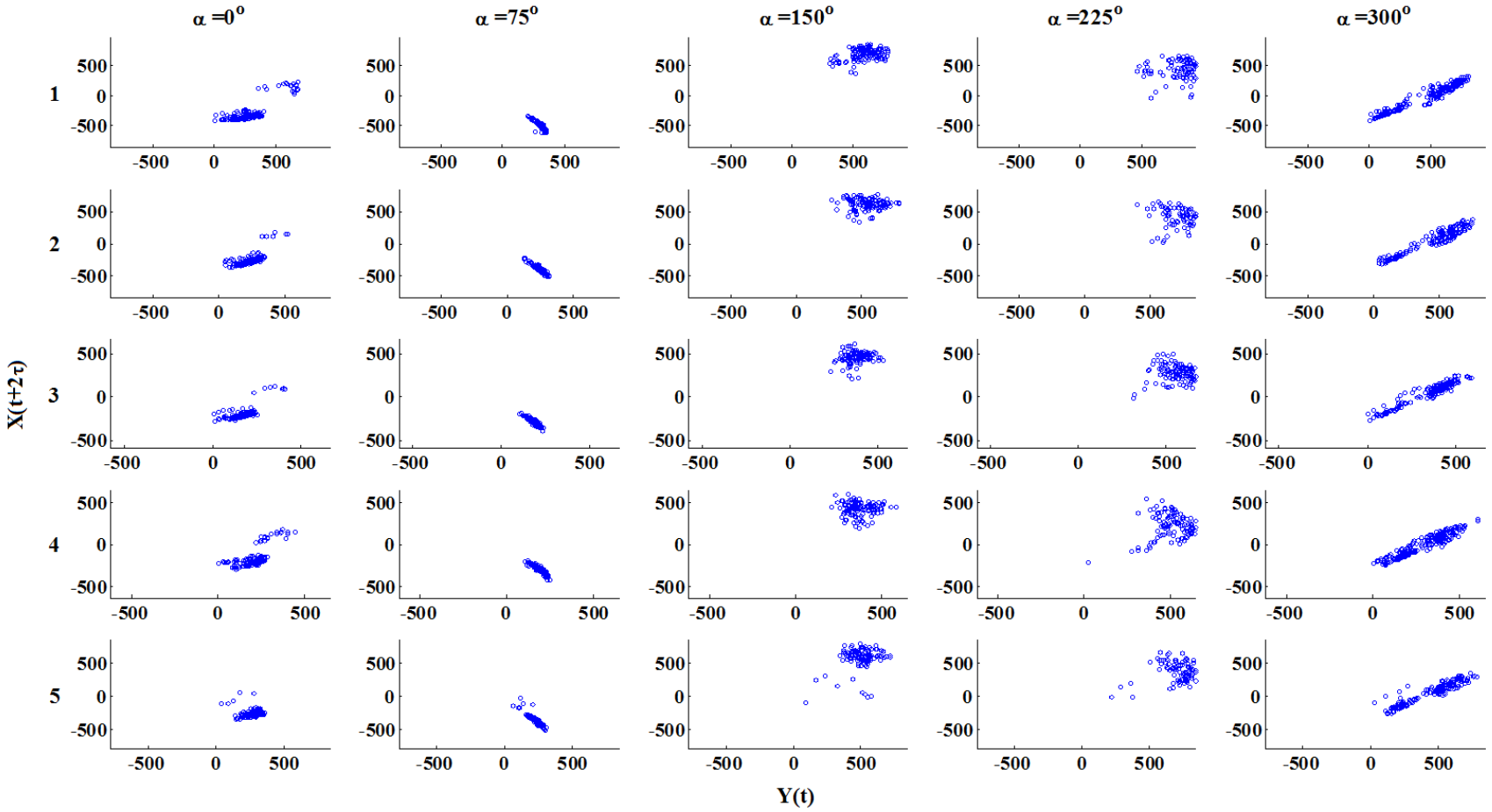

Fig. A.22 *Poincaré section obtained by slicing PPG trajectory by rotating plane at 5 angles (columns) for the 8th subject 1-5th measurement repeats (rows), where Y(t) =* $\sqrt{\boldsymbol{X(t)^2 + X(t+\tau)^2}}$.

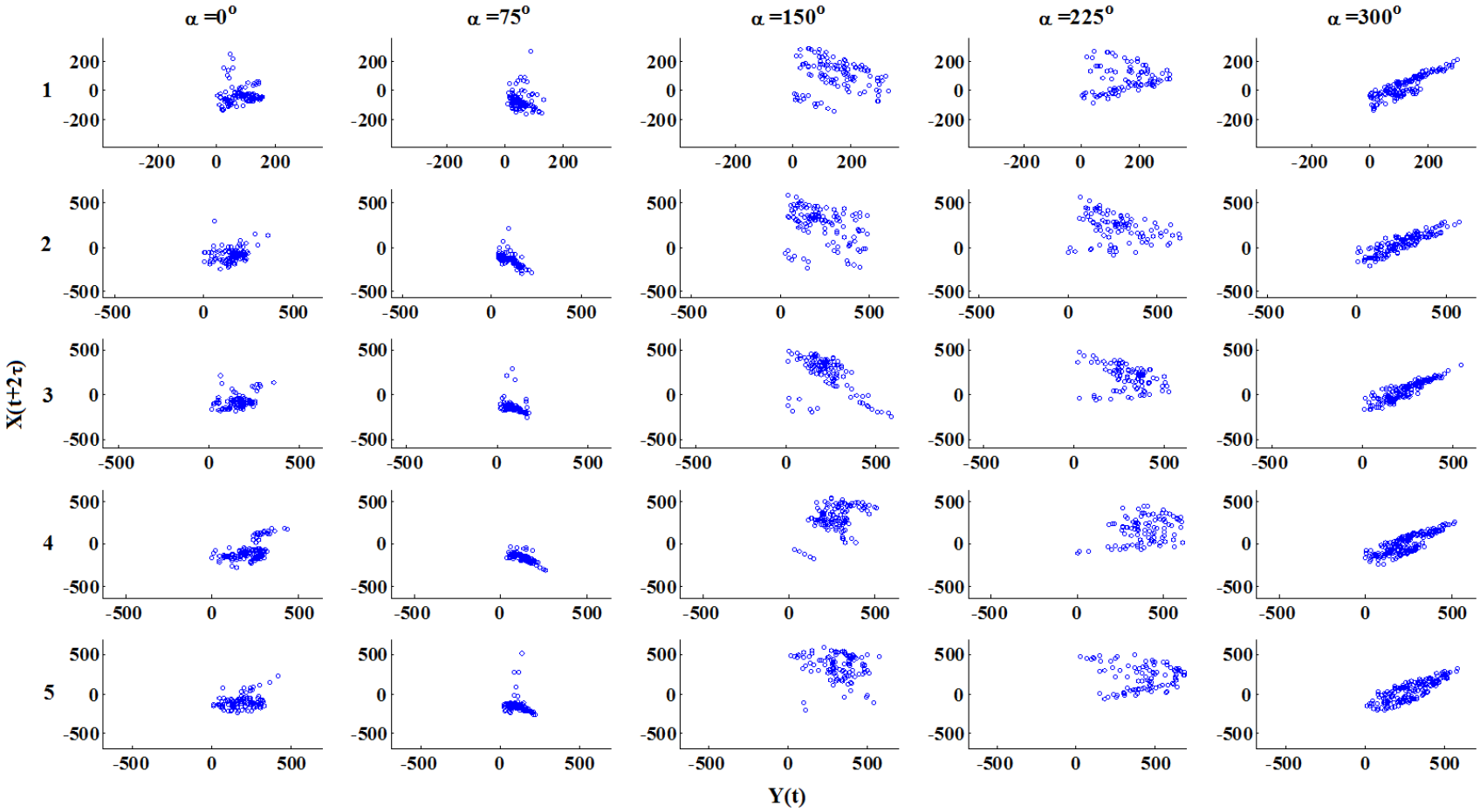

Fig. A.23 *Poincaré section obtained by slicing PPG trajectory by rotating plane at 5 angles (columns) for the 9th subject 1-5th measurement repeats (rows), where Y(t) =* $\sqrt{\boldsymbol{X(t)^2 + X(t+\tau)^2}}$.

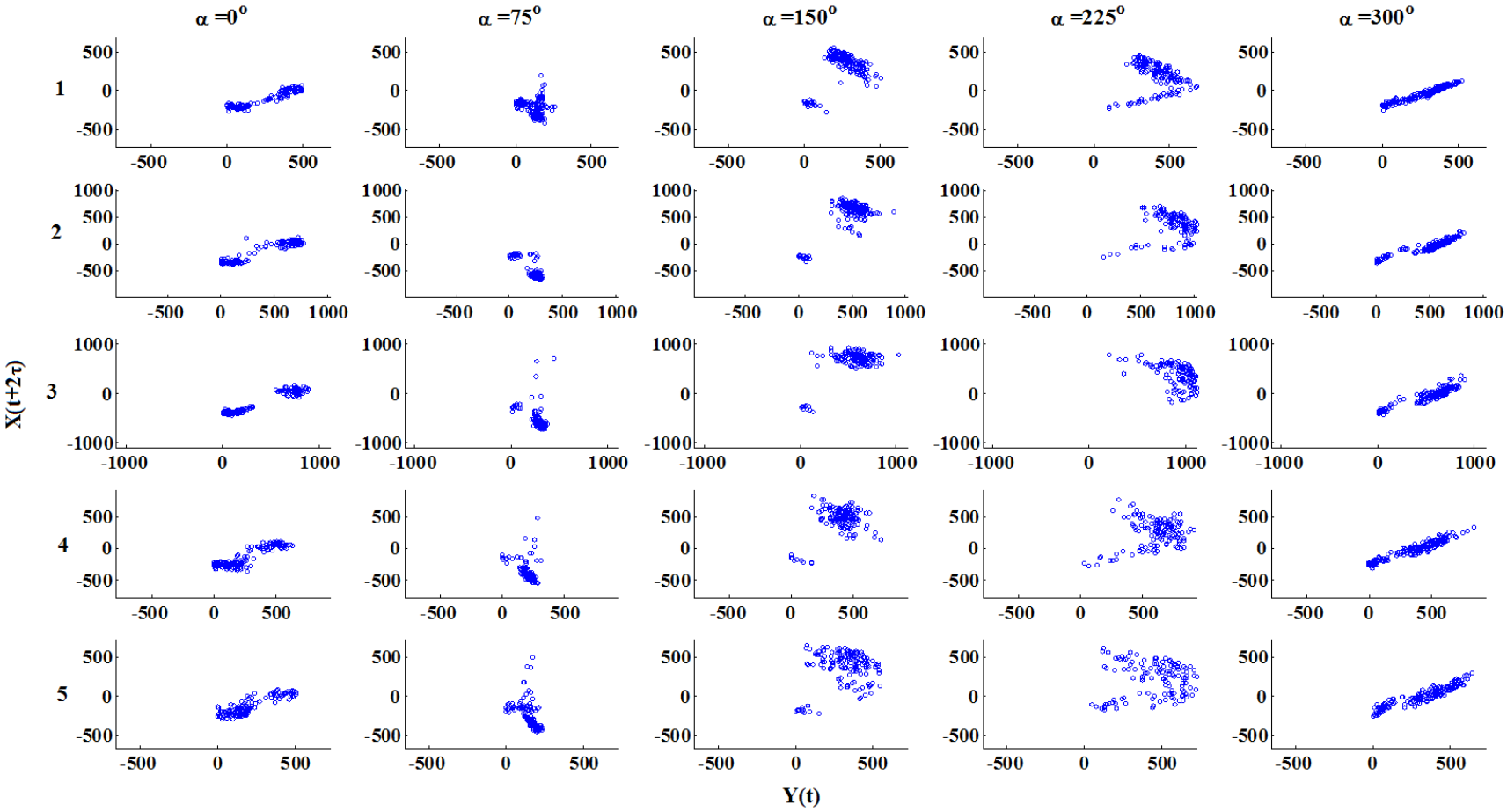

Fig. A.24 *Poincaré section obtained by slicing PPG trajectory by rotating plane at 5 angles (columns) for the 10th subject 1-5th measurement repeats (rows), where Y(t) =* $\sqrt{\boldsymbol{X(t)^2 + X(t+\tau)^2}}$.

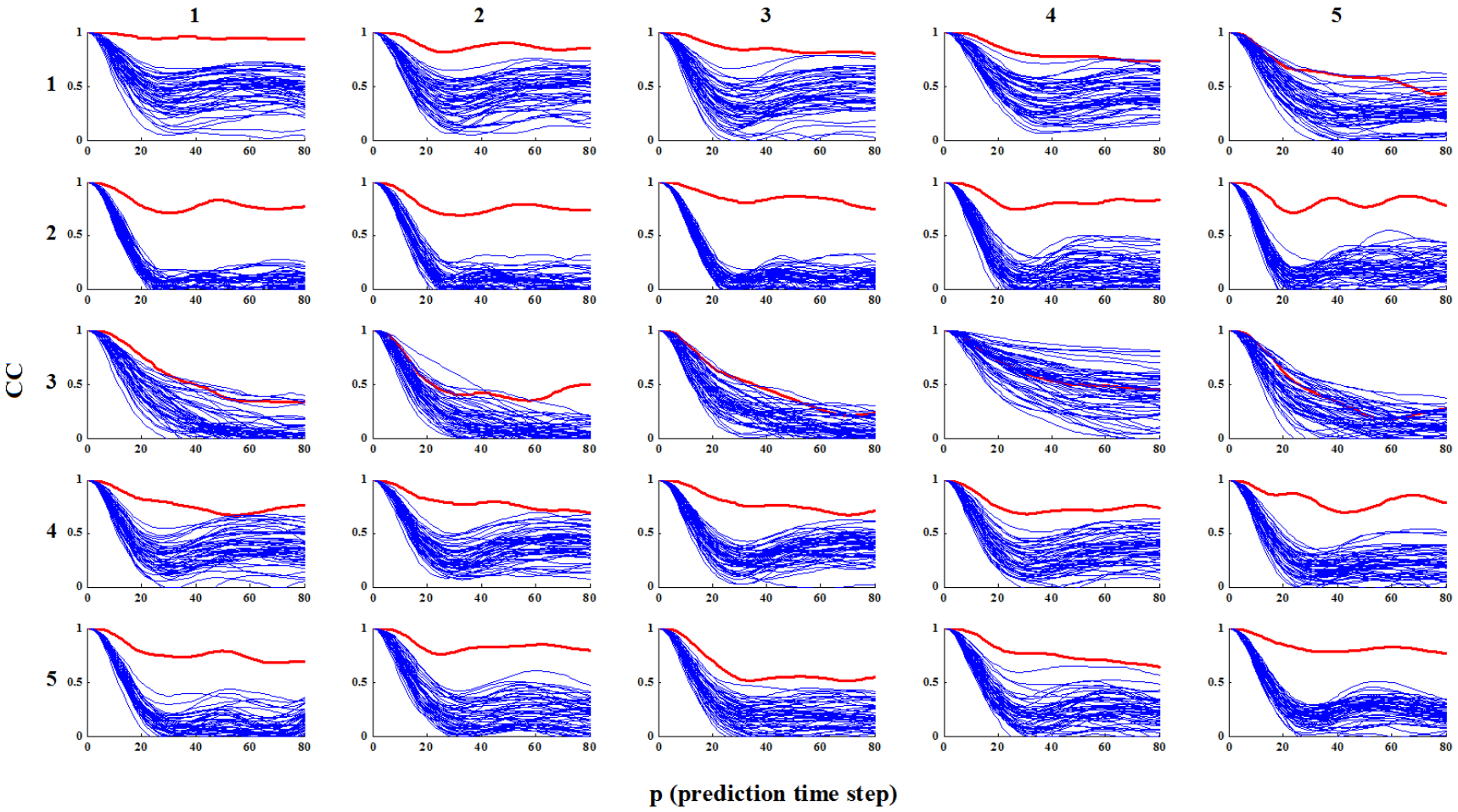

Fig. A. 25 *Correlation coefficient (CC) of deterministic nonlinear prediction for the PPG for 5 measurement repeats (columns) of subjects 1-5 (rows) (red lines) and 50 surrogate datasets (blue lines).*

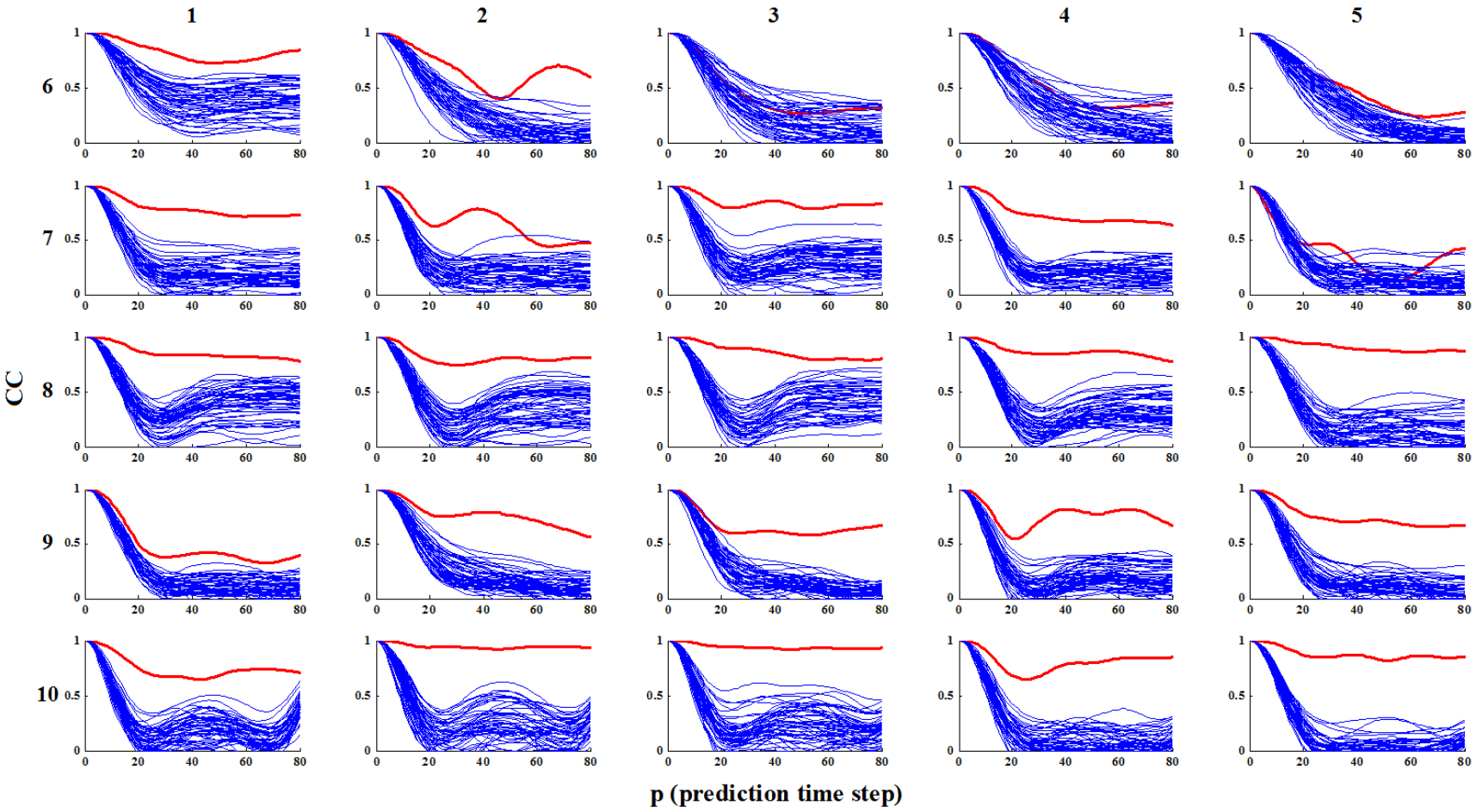

Fig. A. 26 *Correlation coefficient (CC) of deterministic nonlinear prediction for the PPG for 5 measurement repeats (columns) of subjects 6-10 (rows) (red lines) and 50 surrogate datasets (blue lines).*

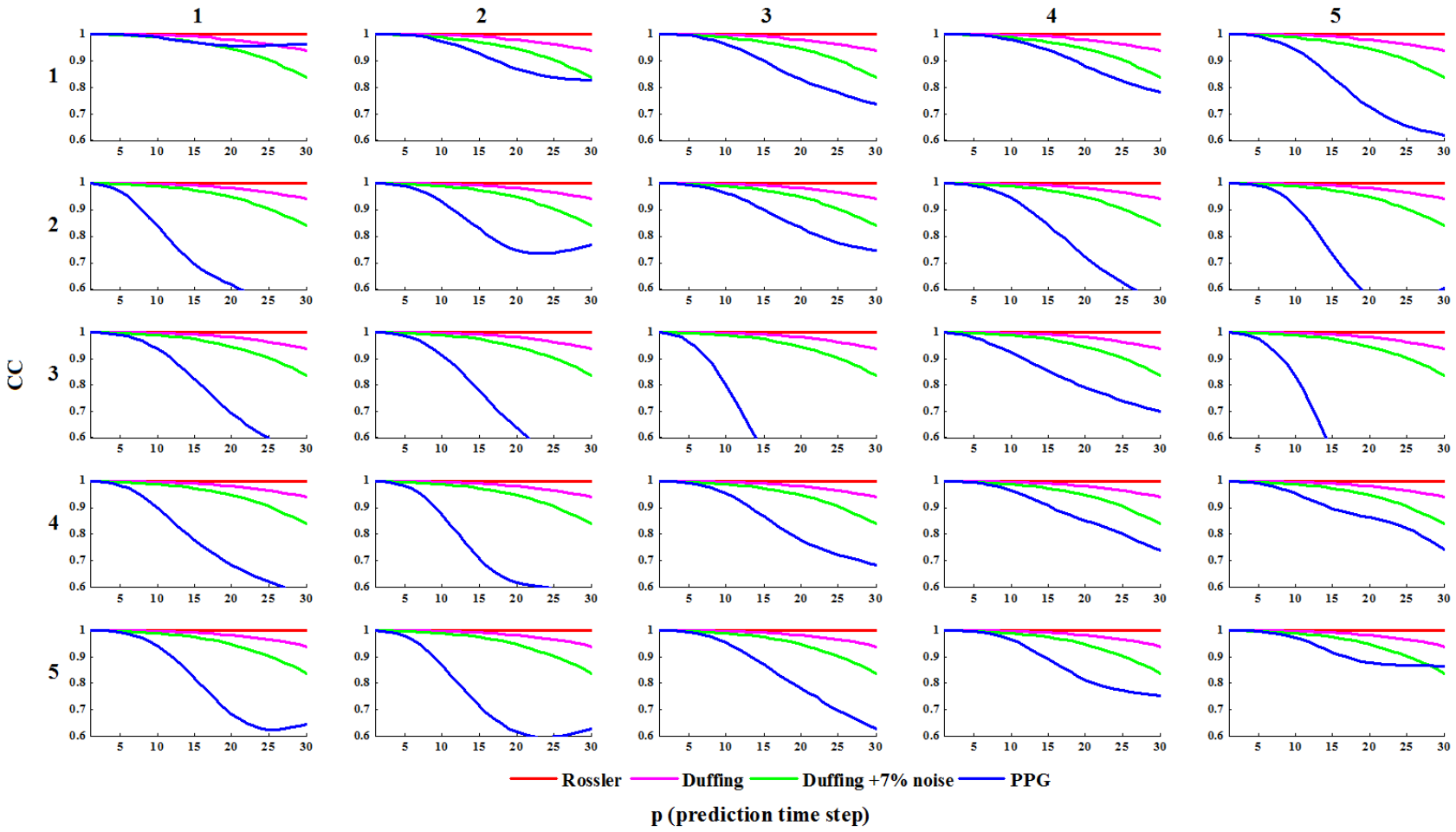

Fig. A.27 *Correlation coefficient (CC) for short-term deterministic nonlinear prediction of Rössler's single band chaos, chaotic Duffing's forced oscillator, chaotic Duffing's forced oscillator data with 7% additive noise and the PPG for 5 measurement repeats (columns) of subjects 1-5 (rows).*

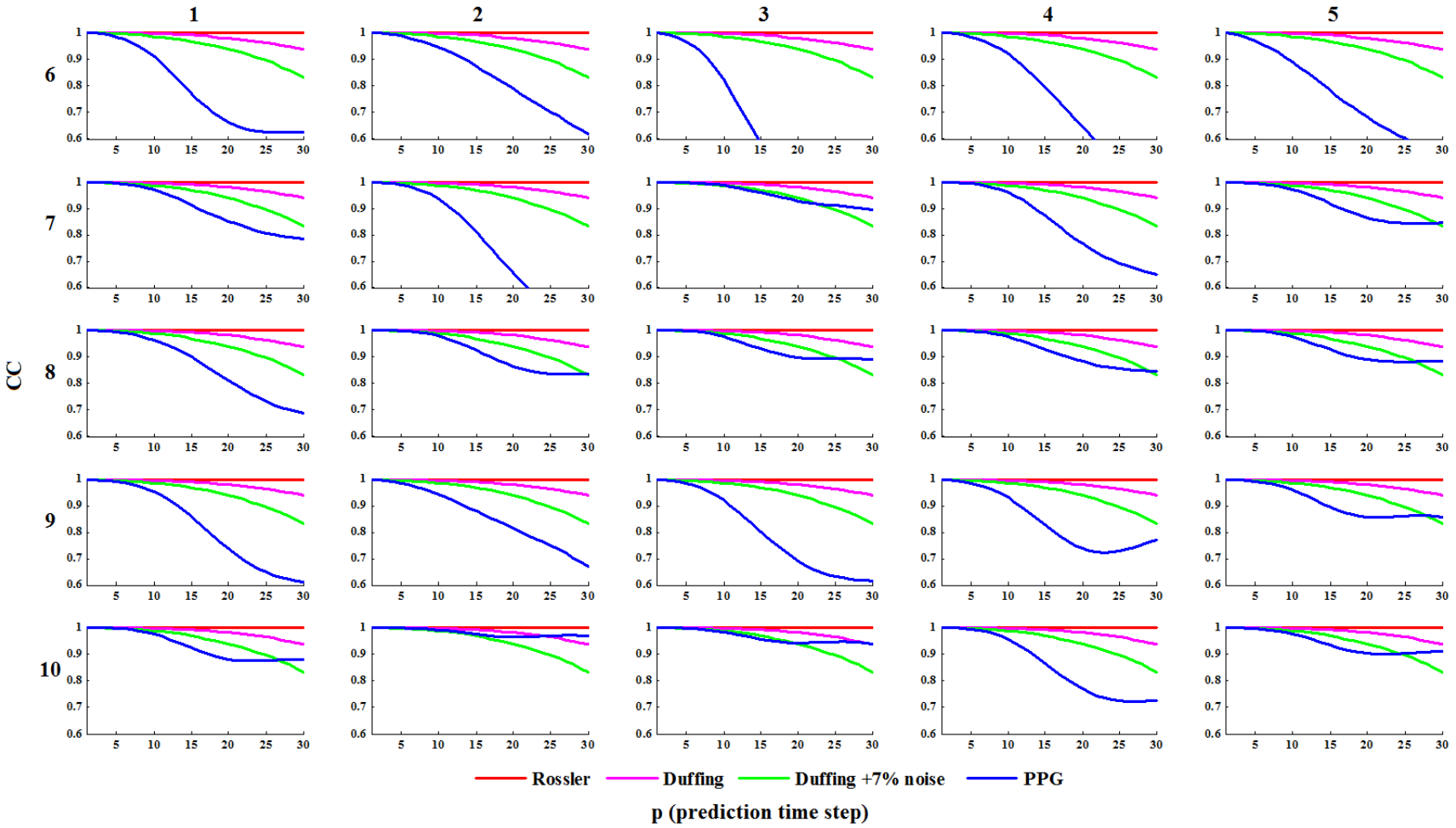

Fig. A.28 *Correlation coefficient (CC) for short-term deterministic nonlinear prediction of Rössler's single band chaos, chaotic Duffing's forced oscillator, chaotic Duffing's forced oscillator data with 7% additive noise and the PPG for 5 measurement repeats (columns) of subjects 6-10 (rows).*

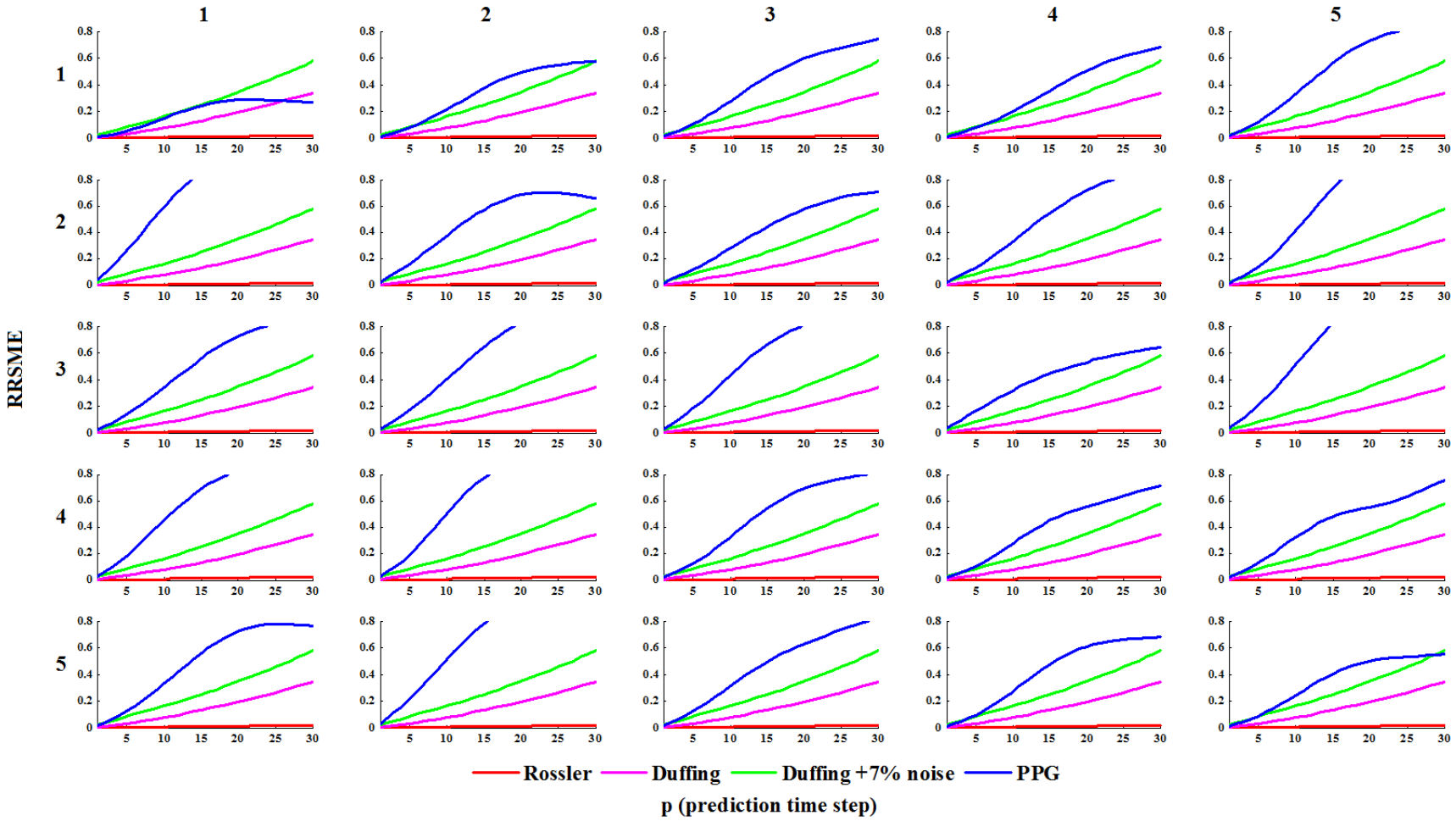

Fig. A.29 *Relative root mean square error (RRMSE) for short-term deterministic nonlinear prediction of Rössler's single band chaos, chaotic Duffing's forced oscillator, chaotic Duffing's forced oscillator data with 7% additive noise and the PPG for 5 measurement repeats (columns) of subjects 1-5 (rows).*

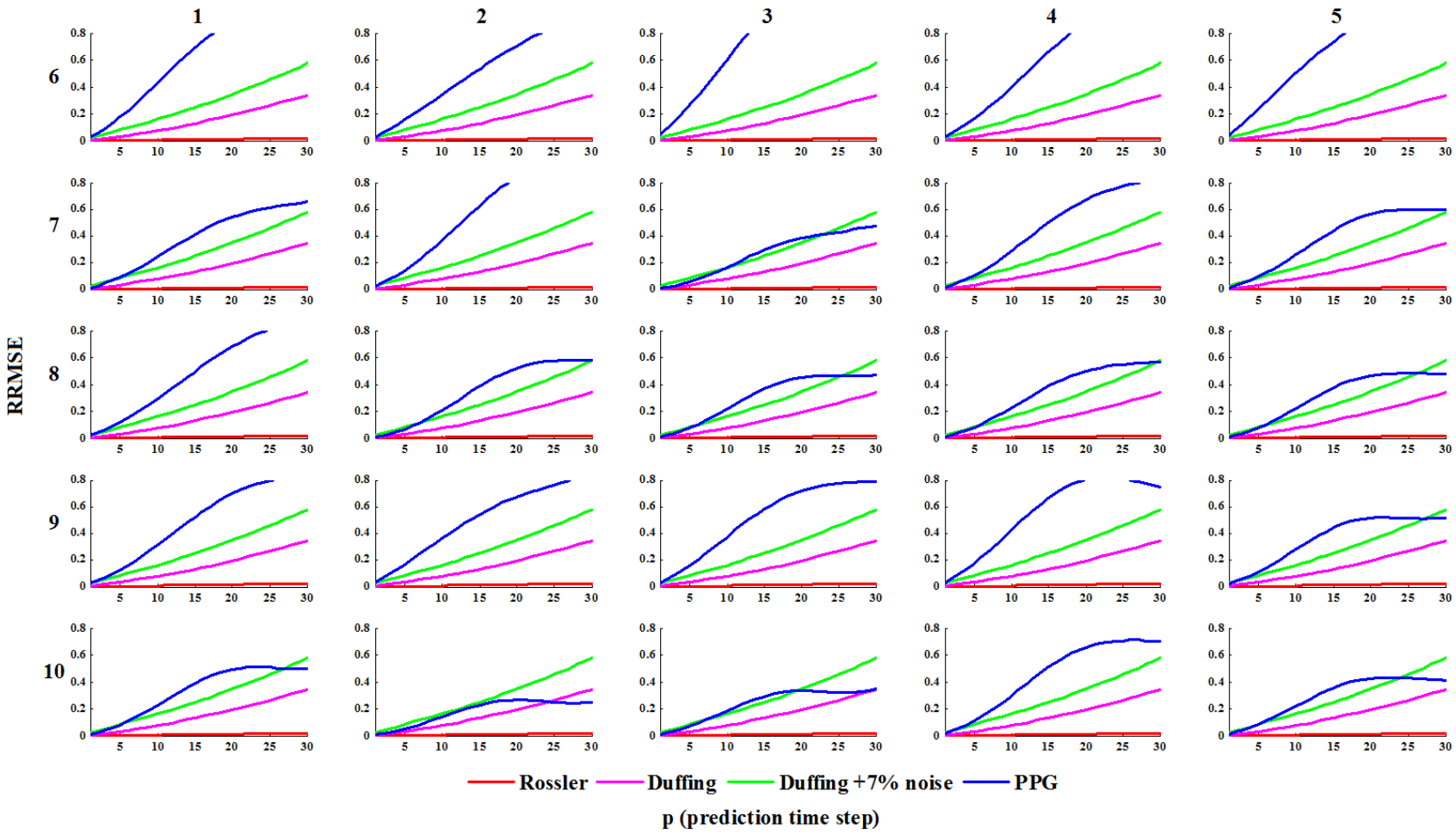

Fig. A.30 *Relative root mean square error (RRMSE) for short-term deterministic nonlinear prediction of Rössler's single band chaos, chaotic Duffing's forced oscillator, chaotic Duffing's forced oscillator data with 7% additive noise and the PPG for 5 measurement repeats (columns) of subjects 6-10 (rows).*

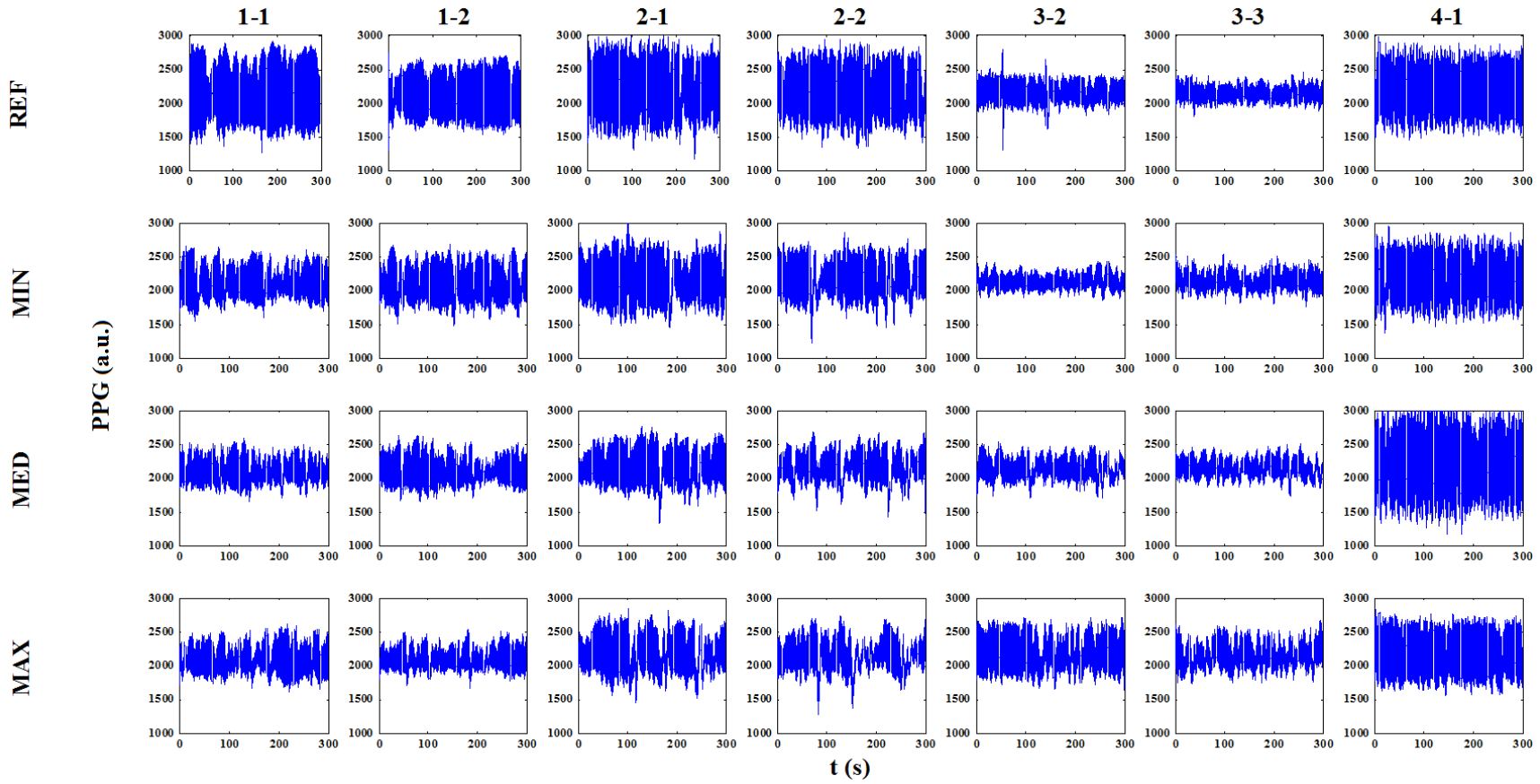

Fig. A. 31 *Experimentally obtained PPG time series of two measurement repeats of subjects 1-3 and 1st measurement repeat for subject 4 (columns) for reference, minimum, medium and maximum levels of noise (rows).*

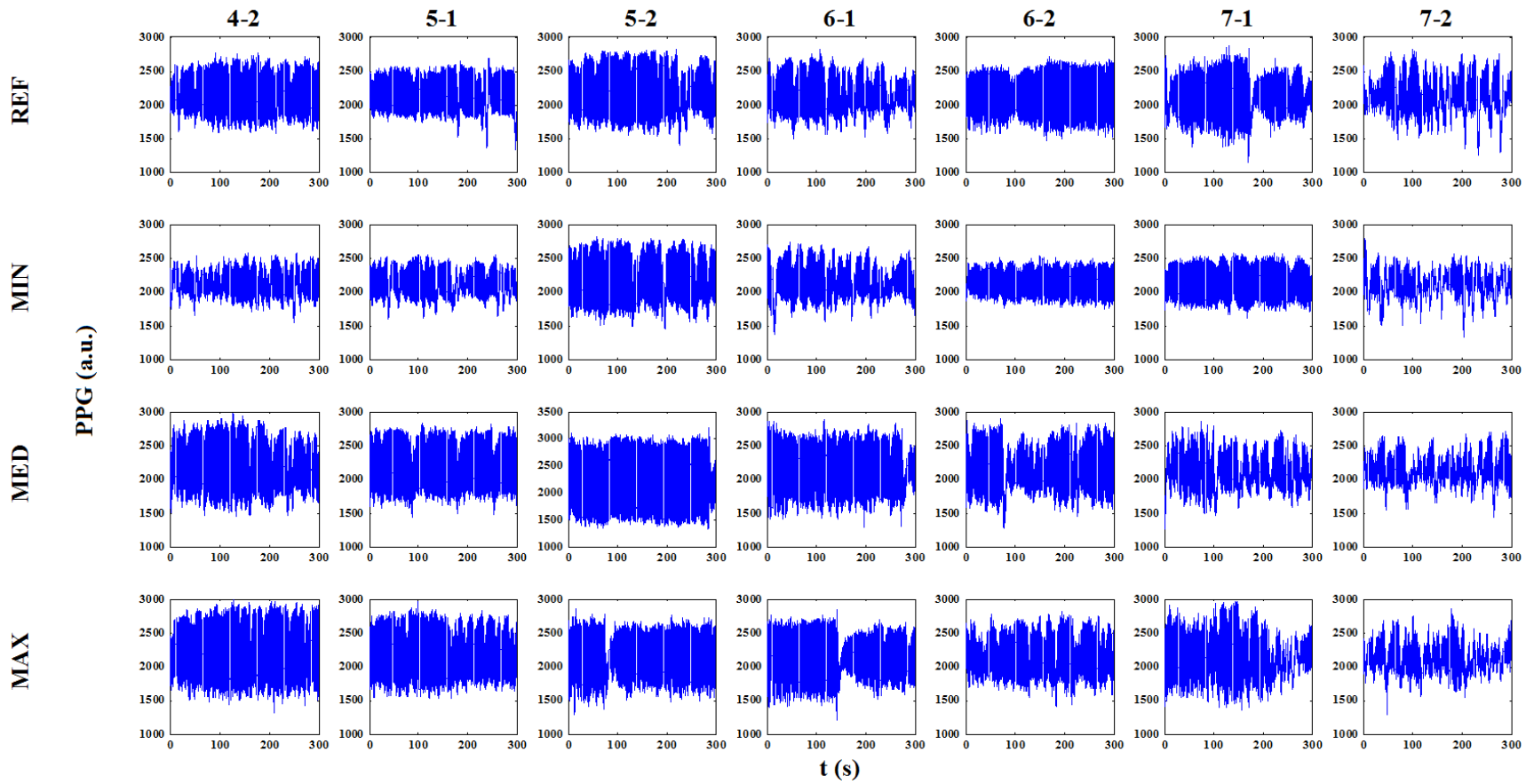

Fig. A. 32 *Experimentally obtained PPG time series of 2nd measurement repeat for subject 4 and two measurement repeats of subjects 5-7 and (columns) for reference, minimum, medium and maximum levels of noise (rows).*

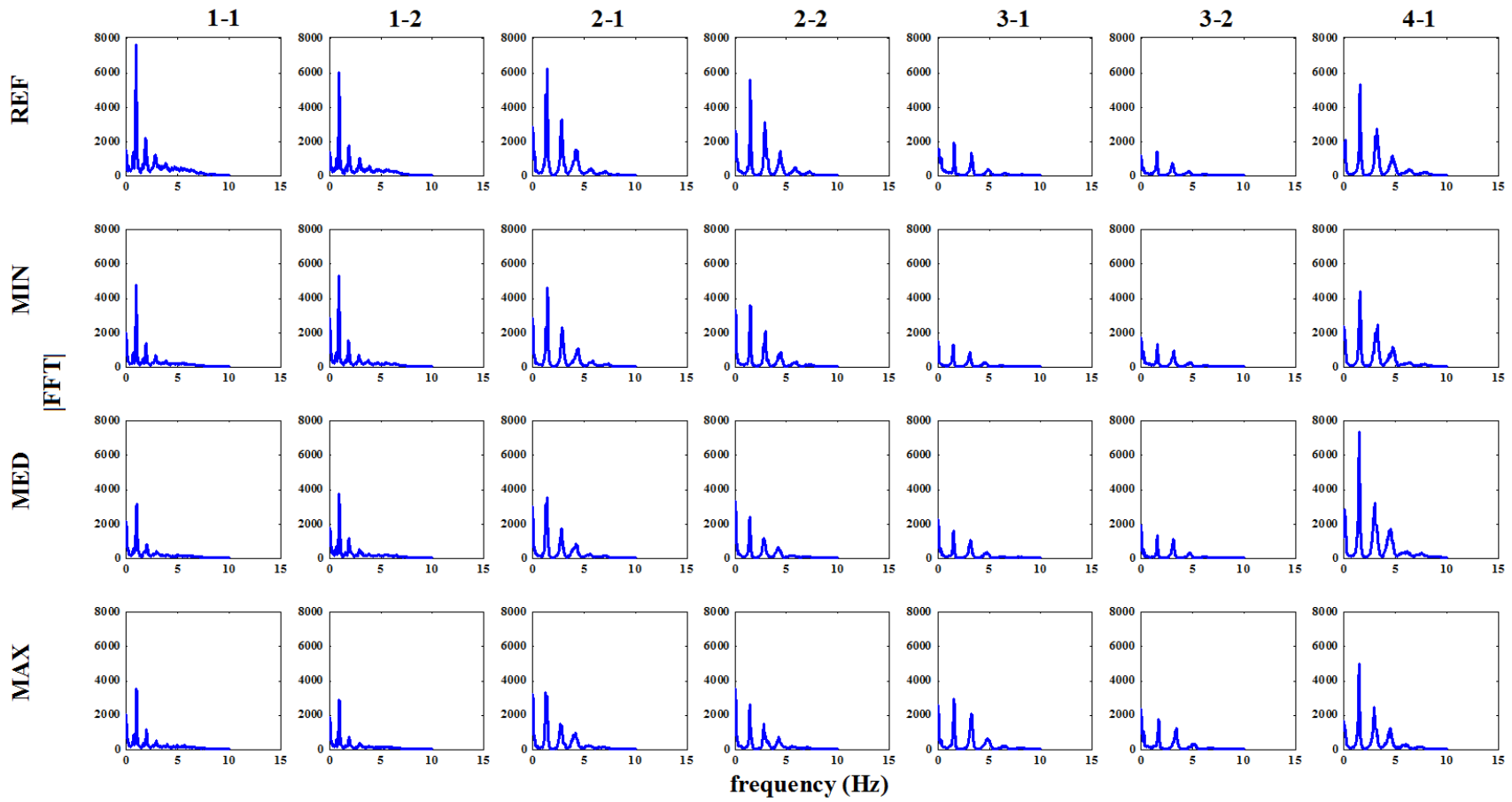

Fig. A. 33 *Fourier spectrum of PPG time series of two measurement repeats of subjects 1-3 and 1st measurement repeat for subject 4 (columns) for reference, minimum, medium and maximum levels of noise (rows).*

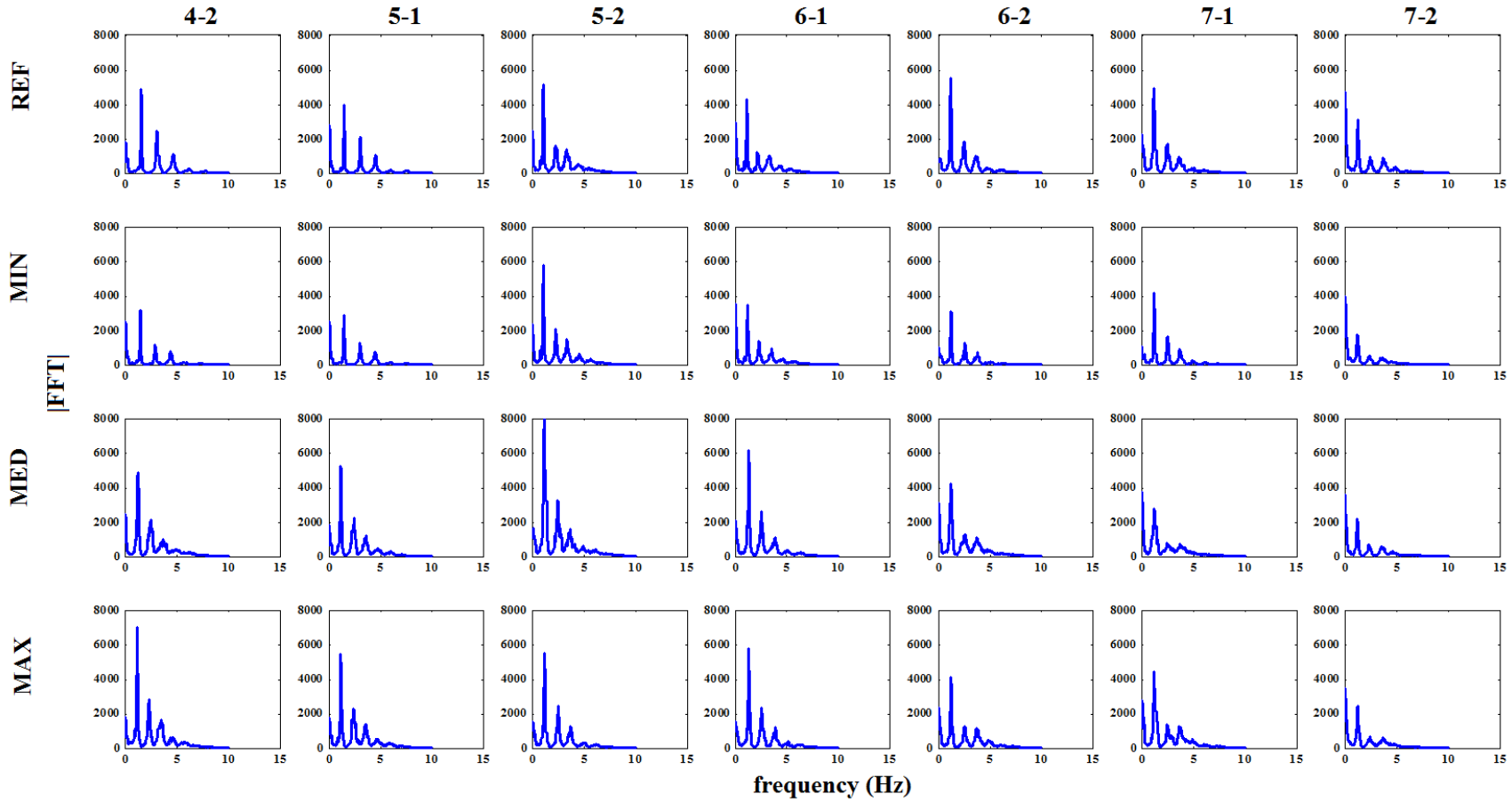

Fig. A. 34 *Fourier spectrum of PPG time series of 2nd measurement repeat for subject 4 and two measurement repeats of subjects 5-7 and (columns) for reference, minimum, medium and maximum levels of noise (rows).*

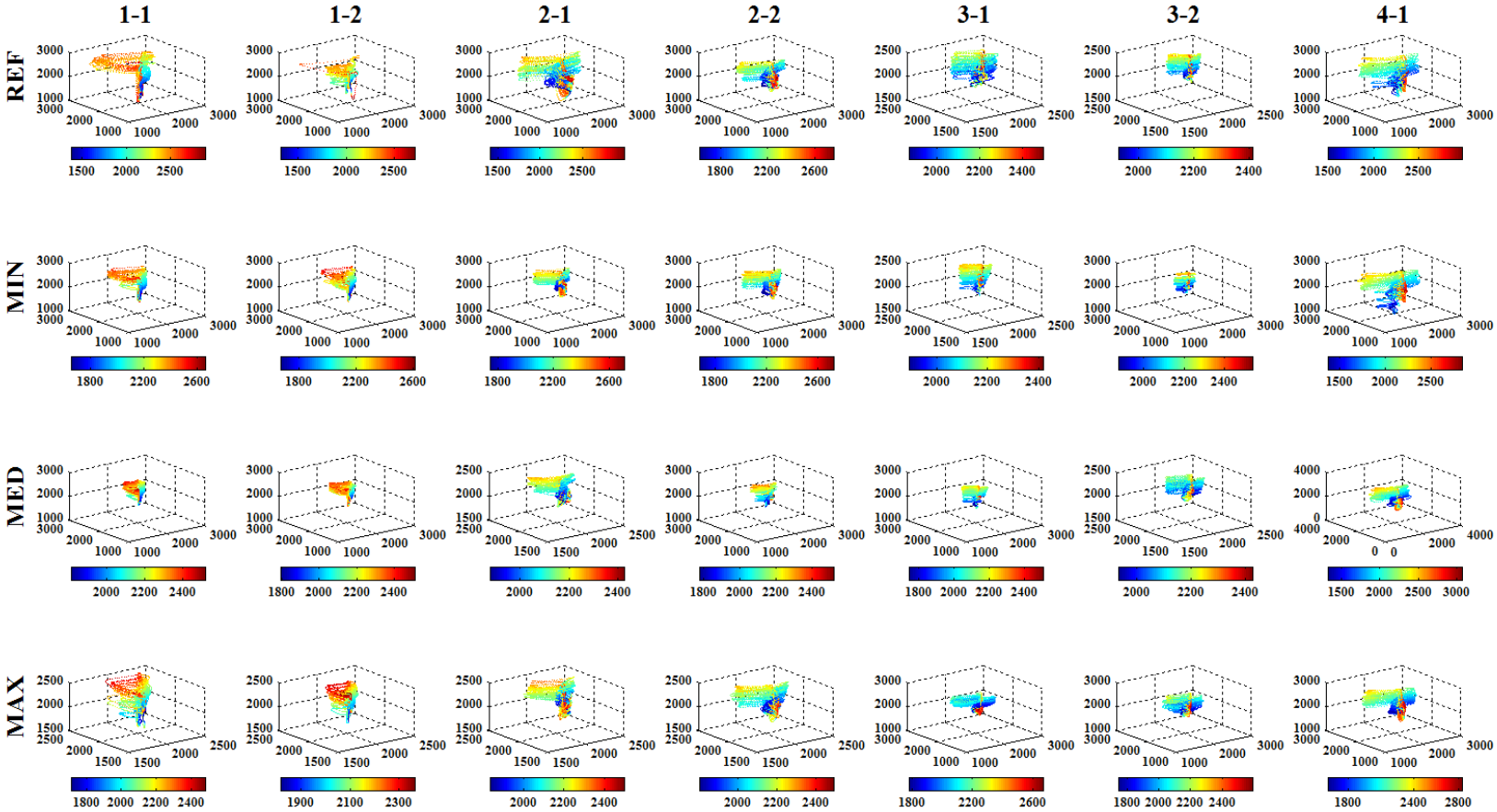

Fig. A. 35 *Reconstructed trajectory of PPG time series of two measurement repeats of subjects 1-3 and 1st measurement repeat for subject 4 (columns) for reference, minimum, medium and maximum levels of noise (rows); x-, y-, z-axis and color bar correspond to X(t), X(t+τ), X(t+2τ) and X(t+3τ) respectively.*

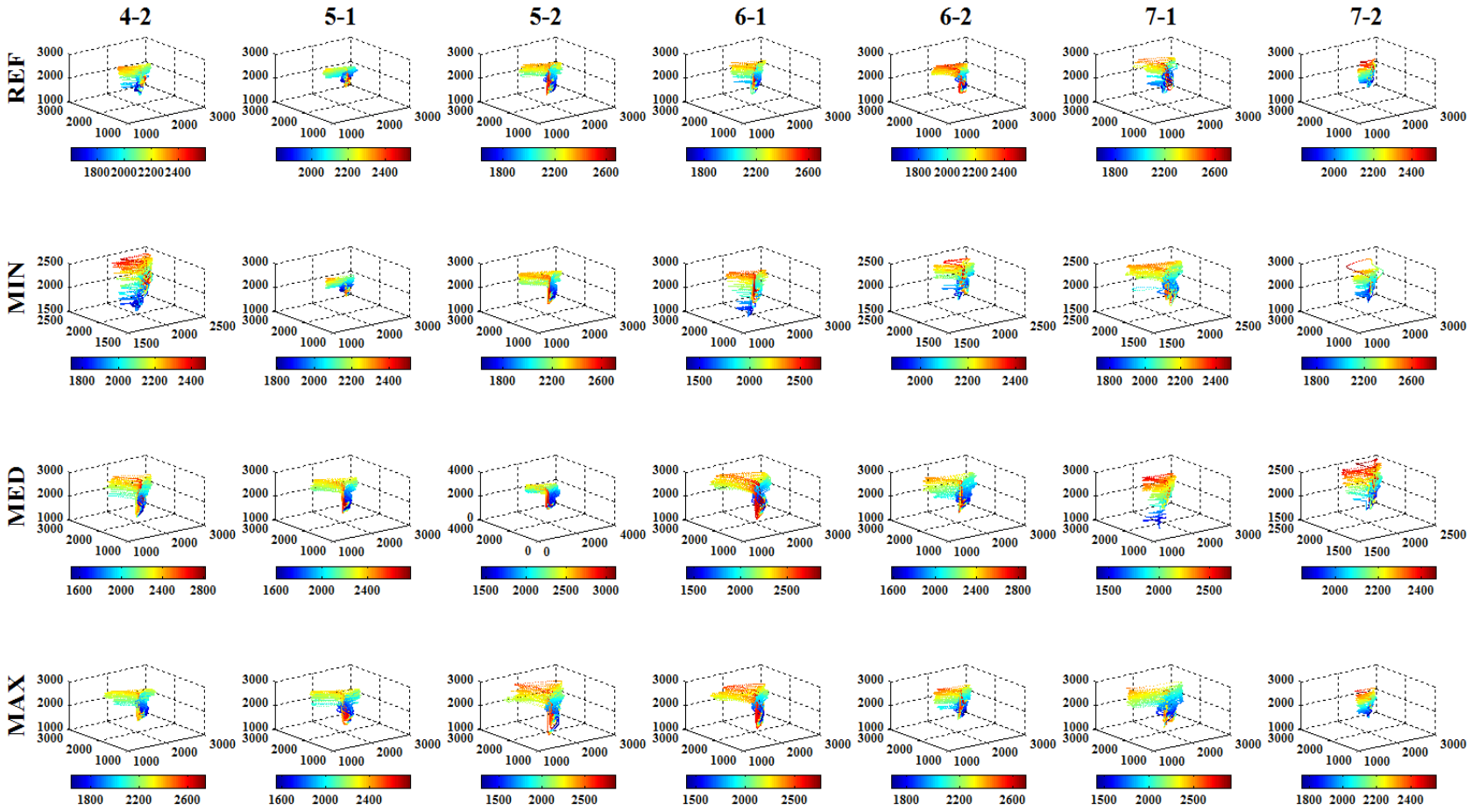

Fig. A. 36 *Reconstructed trajectory of PPG time series of 2nd measurement repeat for subject 4 and two measurement repeats of subjects 5-7 (columns) for reference, minimum, medium and maximum levels of noise (rows); x-, y-, z-axis and color bar correspond to X(t), X(t+τ), X(t+2τ) and X(t+3τ) respectively.*